APTD-0802

PB 204 385

RESEARCH REPORT

Battelle
Columbus Laboratories

Reproduced by
NATIONAL TECHNICAL
INFORMATION SERVICE
Springfield, Va. 22151

A

90

BATTELLE'S COLUMBUS LABORATORIES comprises the original research center of an international organization devoted to research and development.

Battelle is frequently described as a "bridge" between science and industry – a role it has performed in more than 90 countries. It conducts research encompassing virtually all facets of science and its application. It also undertakes programs in fundamental research and education.

Battelle-Columbus – with its staff of 2500 – serves industry and government through contract research. It pursues:

- research embracing the physical and life sciences, engineering, and selected social sciences
- design and development of materials, products, processes, and systems
- information analysis, socioeconomic and technical economic studies, and management planning research.

505 KING AVENUE • COLUMBUS, OHIO 43201

FINAL REPORT

on

INVESTIGATION OF THE REACTIVITY OF LIMESTONE AND DOLOMITE FOR CAPTURING SO_2 FROM FLUE GAS

Contract No. CPA 70-111

to

DIVISION OF CONTROL SYSTEMS
OFFICE OF AIR PROGRAMS
ENVIRONMENTAL PROTECTION AGENCY

October 1, 1971

by

R. W. Coutant, R. Simon,
B. Campbell, and R. E. Barrett

BATTELLE
Columbus Laboratories
505 King Avenue
Columbus, Ohio 43201
Franklin County

BIBLIOGRAPHIC DATA SHEET

1. Report No. APTD-0802

2.

3. Recipient's Accession No.

4. Title and Subtitle
Investigation of the Reactivity of Limestone and Dolomite for Capturing SO_2 From Flue Gas

5. Report Date
October 1, 1971

6.

7. Author(s) R. W. Coutant, R. Simon, B. Campbell, and R. E. Barrett

8. Performing Organization Rept. No.

9. Performing Organization Name and Address
BATTELLE
Columbus Laboratories
505 King Avenue
Columbus, Ohio 43201

10. Project/Task/Work Unit No.

11. Contract/Grant No.
CPA 70-111

12. Sponsoring Organization Name and Address
Division of Control Systems
Office of Air Programs
Environmental Protection Agency
Research Triangle Park, North Carolina 27711

13. Type of Report & Period Covered
Final

14.

15. Supplementary Notes DISCLAIMER - This report was furnished to the Office of Air Programs by Battelle, Columbus Laboratories, 505 King Avenue, Columbus, Ohio 43201 in fulfillment of Contract No. CPA 70-111

16. Abstracts

The results are presented of a study program which is closely related to work previously reported on the reaction between limestone and SO_2 as applied to the dry-limestone injection process for SO_2 control in conventional power-generating boilers. The primary emphasis of the current work has been on clarification of some of the features of the process and on the effect of physical parameters of the stones and limes etc., surface area, porosity, and particle size and of system variables such as temperature of injection, time-temperature profile, and SO_2 concentration on the reactivities of selected limestones and dolomites.

17. Key Words and Document Analysis. 17a. Descriptors

Desulfurization
Flue gases
Limestone
Dolomite
Sulfur dioxide
Reactivity

Areas
Surface properties
Porosities
Temperature gradients
Particle size

17b. Identifiers/Open-Ended Terms

17c. COSATI Field/Group 13B

18. Availability Statement Unlimited

19. Security Class (This Report) UNCLASSIFIED

20. Security Class (This Page) UNCLASSIFIED

21. No. of Pages 85

22. Price

FORM NTIS-35 (10-70)

USCOMM-DC 40329-P71

c

INVESTIGATION OF THE REACTIVITY OF LIMESTONE AND DOLOMITE FOR CAPTURING SO_2 FROM FLUE GAS

MANAGEMENT SUMMARY

The objective of this research program was to develop a better understanding of the reaction between limestone and SO_2 as applied to the dry-limestone injection process for SO_2 control in conventional power-generating boilers. This has been accomplished through study of some of the fundamental characteristics of this reaction under laboratory conditions simulating the time-temperature profile of the superheater/economizer section of a boiler. This work is an extension of earlier efforts conducted under Contract No. PH 86-67-115, "Investigation of the Reactivity of Limestone and Dolomite for Capturing SO_2 from Flue Gas".

During this contract period of June, 1970, through July, 1971:

- An empirical model was developed for the limestone-SO_2 reaction, and this model was used for correlation of previous data as well as in discussion of current data.
- Changes in reactivity caused by variation in time-temperature profile were shown to be predominantly related to residence time.
- It was shown that the maximum utilization of a limestone is proportional to the square root of the SO_2 concentration, which is consistent with observations of other workers studying the reaction under simulated boiler conditions.
- It was shown that calcination under simulated boiler conditions leads to generation of relatively small pores and high surface areas, and that the reactivity of a particular limestone is directly proportional to the surface area developed by a given reaction condition, provided that other factors, such as particle size, are taken into account.
- The theoretical model of the calcination process, previously developed under Contract No. PH 86-67-115, was extended to enable prediction of calcination rates, particle temperatures, circumferential stresses, and pressures within a limestone particle during calcination under simulated boiler conditions.

TABLE OF CONTENTS

Page

INTRODUCTION 1

SUMMARY 3

Experimental Work 3

Conclusions 5

EXPERIMENTAL METHODS AND MATERIALS 6

Dispersed-Phase Reactor 6

Limestones. 7

Chemical Analyses 7

Surface Areas and Porosities. 11

EXPERIMENTAL RESULTS AND DISCUSSION 12

Reaction of Limestone with SO_2 12
Correlation of Previous Data. 12
Effect of Temperature Gradient. 16
Effect of Particle Size 18
Effect of SO_2 Concentration 21

Surface Areas and Porosities 27
Effect of Time and Temperature on Pore Structure. 28
Surface Area and Reactivity 33

Calcination of Limestone 42
Application of the Model. 43

REFERENCES. 54

APPENDIX A - STONE ANALYSIS

APPENDIX B - REACTOR DATA

APPENDIX C - PORE SIZE DISTRIBUTIONS

APPENDIX D - COMPUTER PROGRAM - CALNOW

INVESTIGATION OF THE REACTIVITY OF LIMESTONE AND DOLOMITE FOR CAPTURING SO_2 FROM FLUE GAS

to

DIVISION OF CONTROL SYSTEMS
OFFICE OF AIR PROGRAMS
ENVIRONMENTAL PROTECTION AGENCY

by

R. W. Coutant, R. Simon,
B. Campbell, and R. E. Barrett

October 1, 1971

INTRODUCTION

Emission of sulfur dioxide by power plants and process industries using coal and residual oil as fuels constitutes a major contribution to air pollution in the United States. Ideally, the most positive approach to control of these emissions is to burn low sulfur fuels. However, although this approach is being investigated and developed, the burning of low sulfur fuels is currently not technically or economically feasible in most cases. The other alternative is the development of processes to remove the sulfur dioxide from the flue gas before emission into the atmosphere. A large number of such processes have been suggested. One of the most attractive of these because of its relative simplicity and low cost is the dry-limestone injection process.

Use of the dry-limestone injection process involves the use of the boiler itself as a reaction chamber, and thus imposes certain limitations on temperature and residence time. Generally, residence times in a useful temperature zone are of the order of 2 seconds. Furthermore, injection of the limestone close to the fireball, for the purpose of obtaining maximum residence, involves the risk of overburning of the lime, which greatly reduces its reactivity. It is therefore highly important that the chemistry and kinetics of calcination of the limestone, overburning or sintering of the lime, and reaction of SO_2 with the lime be well understood in order to make optimum use of this process.

The current program is one of several sponsored by EPA for the purpose of elucidation of various aspects of the dry-limestone injection process. This program is closely related to work previously reported(1,2,3) under Contract No. PH 86-67-115, and has been directed at clarification of previous observations as well as towards development of new information relevant to the process. Using Stone No. 2061 (a limestone being used by TVA(4) in full-scale demonstration of the process) under simulated boiler conditions, previous work(3) showed that:

(1) Under standard conditions of 0.3 and 3 percent SO_2 and O_2, respectively, the maximum utilization of 90-micron particles of the limestone is about 20 percent.

(2) Maximum limestone utilization is achieved at mean gas temperatures of 1900-2000 F for 90-micron particles.

(3) The maximum utilization of CaO is proportional to the square root of the SO_2 concentration.

(4) The efficiency of utilization of the CaO is increased by increasing the excess air level.

(5) Precalcination of the limestone before injection into the flue gas generally results in lower overall utilization of the CaO.

(6) The kinetics of calcination of limestone under simulated boiler conditions can adequately be modeled in terms of the heat and mass transport characteristics of the system.

Primary emphasis of the current work has been on clarification of some of the features of the process and on the effect of physical parameters of the stones and limes, e.g., surface area, porosity, and particle size and of system variables such as temperature of injection, time-temperature profile, and SO_2 concentration on the reactivities of selected limestones and dolomites.

SUMMARY

Experimental Work

During the current contract period, it has been shown that:

(1) Maximum reactivity is also obtained at 1900-2000 F for 48-micron particles.

(2) The maximum utilization of CaO is proportional to the square root of the SO_2 concentration. This is equivalent to saying that the amount of SO_2 which can be removed from the flue gas is proportional to the 3/2 power of the SO_2 concentration.

(3) Steeper time-temperature profiles are beneficial in reducing the time spent by the limestone in higher temperature regions, but generally lead to lower overall CaO utilization because of reduced overall residence times.

(4) Calcination of limestone under the relatively short time (less than 2 seconds) conditions of exposure encountered with boiler simulation leads to much smaller pore sizes and much higher surface areas than are observed with the usually long-term calcination in kilns.

(5) The generally high rates of reaction observed under conditions of boiler simulation can be related to the higher surface areas generated under these conditions.

(6) The reactivities of limestones, in general, can be correlated with surface areas, providing other factors such as particle size remain constant.

(7) Reduction in particle size in situ, as occurs naturally upon rapid calcination of many stones, may lead to increased rates of calcination, SO_2 reaction, and overburning, which can result in high apparent reactivities per unit area when surface area is not measured until after the fact.

An empirical model has been developed which is consistent with these observations. This model can be expressed in the form of the equation

$$S = b(1-e^{-kt})$$

where S is the sulfur pickup in SO_3/g, b is associated with maximum value of S obtainable under boiler simulation conditions, k is a rate constant, and t is the residence time. For -140 + 200 mesh* Stone No. 2061 and SO_2 and O_2 concentrations of 0.3 and 3 percent, respectively,

$$k = \exp\ (14.563 - 18734/T_m)$$

and

$$b = \exp\ (-2.982 + 10139/T_m)$$

where T_m is the mean gas temperature in degrees Kelvin. These equations are valid over the range of mean gas temperatures from 1600 to 2148 F.

A theoretical model of the calcination process has been extended to permit calculation of calcination rates, particle temperature, circumferential stress, and pressure within a limestone particle during calcination under simulated boiler conditions. This model is based on nonsteady heat and mass transfer within a limestone particle. Results of application of this model indicate that:

(1) The rate of calcination is controlled primarily by two factors: the rate of heat transfer to the surface of the particle, and the rate of escape of CO_2 through the relatively small pores of the limestone.

(2) Particle temperatures are moderated somewhat by the thermal requirements of the calcination process with the result that use of the mean gas temperature in place of the true particle temperature is a reasonable approximation at residence times of about 1 to 1.5 seconds at a mean gas temperature of 1600 F. At higher mean gas temperatures and longer residence times, the mean gas temperature is less valid as an approximation to the true particle temperature.

---

* Average size of 90 microns.

(3) Pressure buildup within the calcining particle can be appreciable, especially during the initial portion of the process, with the result that circumferential stresses which exceed the tensile strength expected for the stone are predicted by the model. This must result either in opening of cracks or, as is observed in some cases, fragmentation of the stone.

Conclusions

As has been recognized in preliminary field testing of the dry-limestone injection process by TVA(4), this process is relatively inefficient for removal of SO_2 from flue gas. The fact that only a relatively short time period is available in a boiler at temperatures favorable for the reaction does not explain why the process is inefficient. Laboratory investigations of the process under simulated boiler conditions indicate high enough initial reaction rates that appreciably greater efficiencies would be obtainable if these high rates could be maintained. The reason for these low efficiencies lies in the fundamental nature of this heterogeneous reaction.

Results of this work, and that of Borgwardt(5), show that the rate of reaction is proportional to the amount of surface area generated as a result of calcination of the limestone. But surface is continuously formed by calcination and destroyed by sintering of the lime. This sintering is manifested through growth of the pores during the process. Very small pores, less than 0.01 micron, are associated with very high surface areas, and hence high rates of reaction. However, since the molar volume of the reaction product, calcium sulfate, is about twice that of the lime, the pores tend to fill upon reaction. Furthermore, small pores are associated with appreciable diffusional resistance so that reaction tends to take place near the pore mouth. The result is confinement of the reaction to the outer portion of large particles, and eventual sealing off of the pore mouth by reaction product. With larger pores, say 0.1-0.3 micron as found with many commercially burnt limes, the interior of a limestone particle is more accessible, but the reaction rate is lower because of smaller surface area.

For limes calcined under simulated boiler conditions, pore radii are of the order of 0.01 micron. Appreciable overburning of the lime takes place at injection temperatures above about 2200 F and it appears that the dynamics of this deactivating process are important even at lower temperatures. It might be expected that increased utilization could be obtained with smaller, say 5-micron particles, but smaller particles also calcine faster, and hence the true particle temperature can rise more rapidly to temperatures where the sintering process is important. There is therefore a compromise between the dynamics of calcination, sintering, and reaction with SO_2, with the net result that reduction of particle size below, say 45-microns, does not greatly increase utilization.

That the percentage of SO_2 removed is proportional to the 1/2 power of the initial SO_2 concentration implies that the dry-limestone process would be relatively more effective in application with flue gas containing high concentrations of SO_2.

EXPERIMENTAL METHODS AND MATERIALS

Experimental procedures used for this work have been described in detail in earlier reports.(1,2,3) Briefly, limestone is exposed to flue gas under conditions closely simulating the time and temperature history in the superheater/exonomizer section of a power-boiler. The partly calcined, partly reacted limestone is then analyzed for degree of calcination and extent of reaction with SO_2.

Dispersed-Phase Reactor

The basic design of the dispersed-phase reactor (DPR), and the evolution of techniques employed with this reactor have been described in detail previously.(1,2,3) Only relatively minor changes in the apparatus have been made during this contract period to enable more flexibility in controlling the time-temperature profile. Modifications consisted mainly of the addition of a water-cooled jacket to each section of the DPR. Each of the three sections can now be operated independently with walls either cooled or uncooled to obtain the desired time-temperature profile for the system.

A photograph of the DPR is shown in Figure 1, and a line drawing indicating the construction elements is given in Figure 2. Figure 3 shows the effect of addition of the cooling jackets. The net result of this increased flexibility is that average time-temperature profiles expected in a steam-generating boiler can be simulated reasonably well.

Limestones

The majority of experiments performed during both this contract period and the previous one involved the use of Stone No. 2061, the same stone which is being used in the TVA full-scale demonstration of the dry-limestone injection process. During the course of this work, at least three distinctly different batches of Stone No. 2061 have been examined at least briefly. Analyses for two of these are given in Table A-1 of Appendix A. The third material was found to decrepitate severely upon heating to about 690 F and was not considered to be representative of the general type of Stone No. 2061.

Ten other stones were also studied in this work. These stones were typical of distinctly different types of limestones and dolomites as classified by Richard Harvey(6) of the Illinois State Geological Survey. They ranged in type from Iceland Spar to magnesite. Analyses for these materials are listed in Table A-1 of Appendix A.

Chemical Analyses

This experimental work included exposure of stones in the DPR both with and without SO_2 in the flue gas. For those samples where no sulfur was present, the samples, as received, were composed of calcium oxide, calcium carbonate, some calcium hydroxide originating from partial

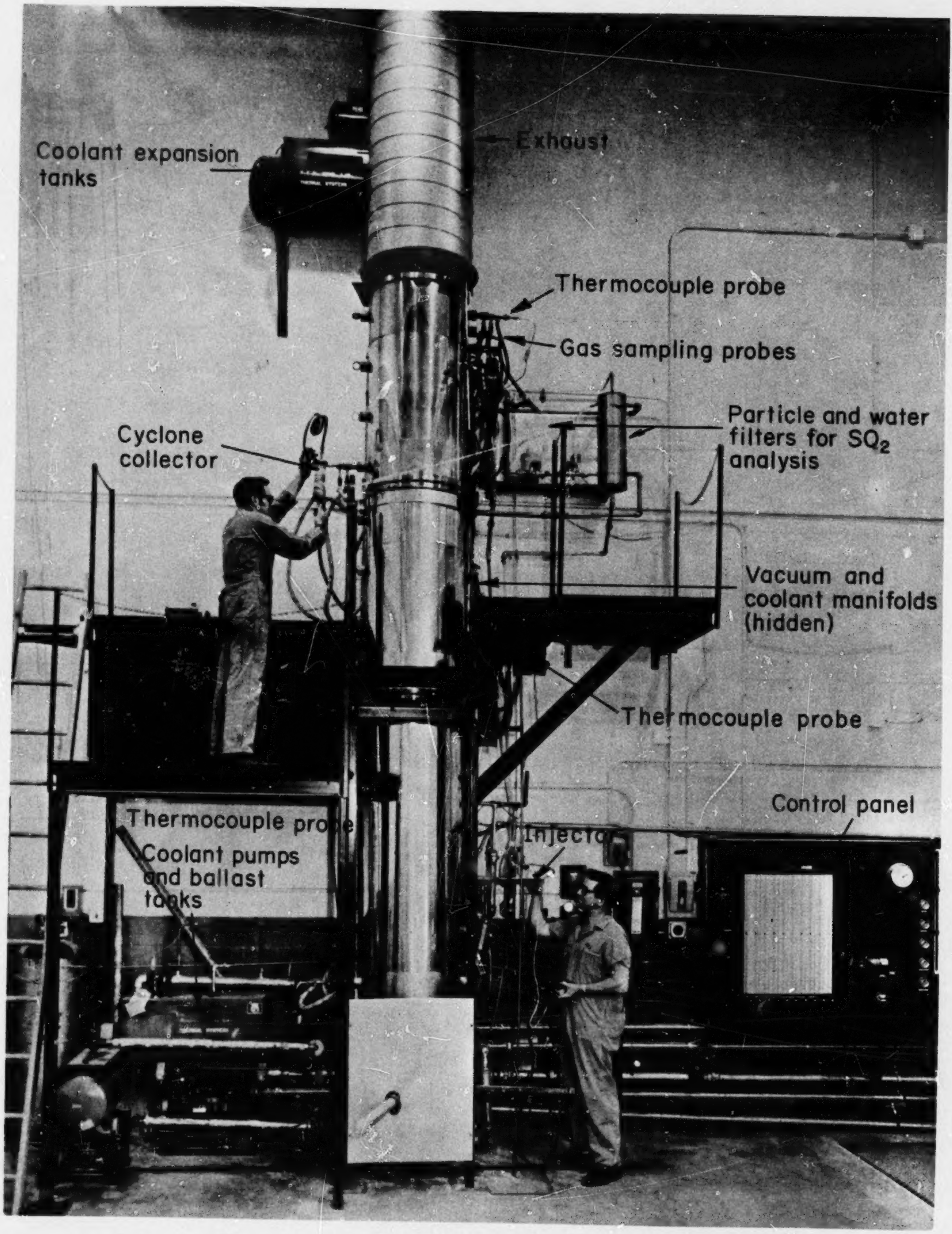

FIGURE 1. DISPERSED-PHASE REACTOR

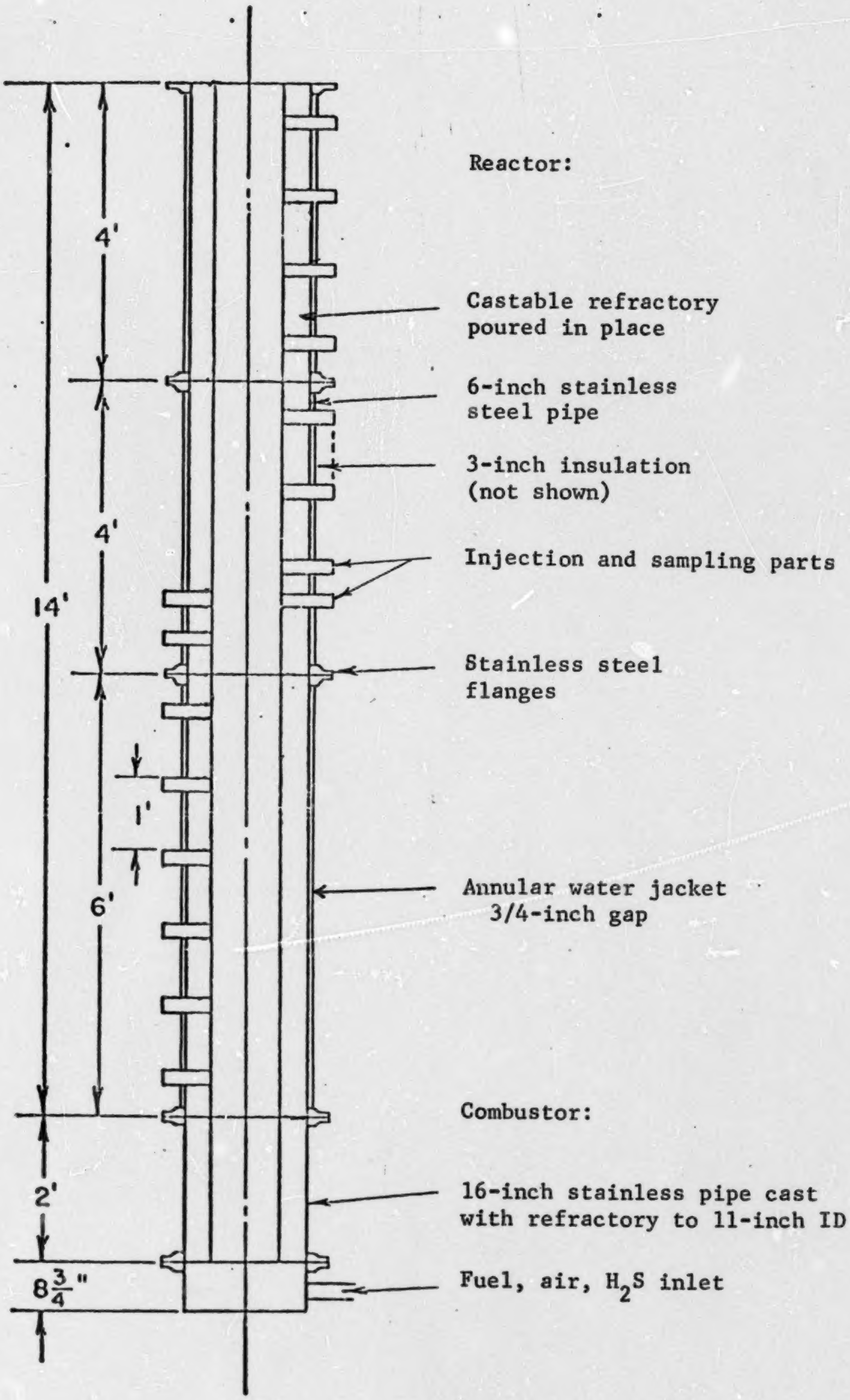
Reactor:
Castable refractory poured in place
6-inch stainless steel pipe
3-inch insulation (not shown)
Injection and sampling parts
Stainless steel flanges
Annular water jacket 3/4-inch gap
Combustor:
16-inch stainless pipe cast with refractory to 11-inch ID
Fuel, air, H_2S inlet
4'
4'
14'
1'
6'
2'
8 3/4"

Figure 2. REACTOR CONFIGURATION

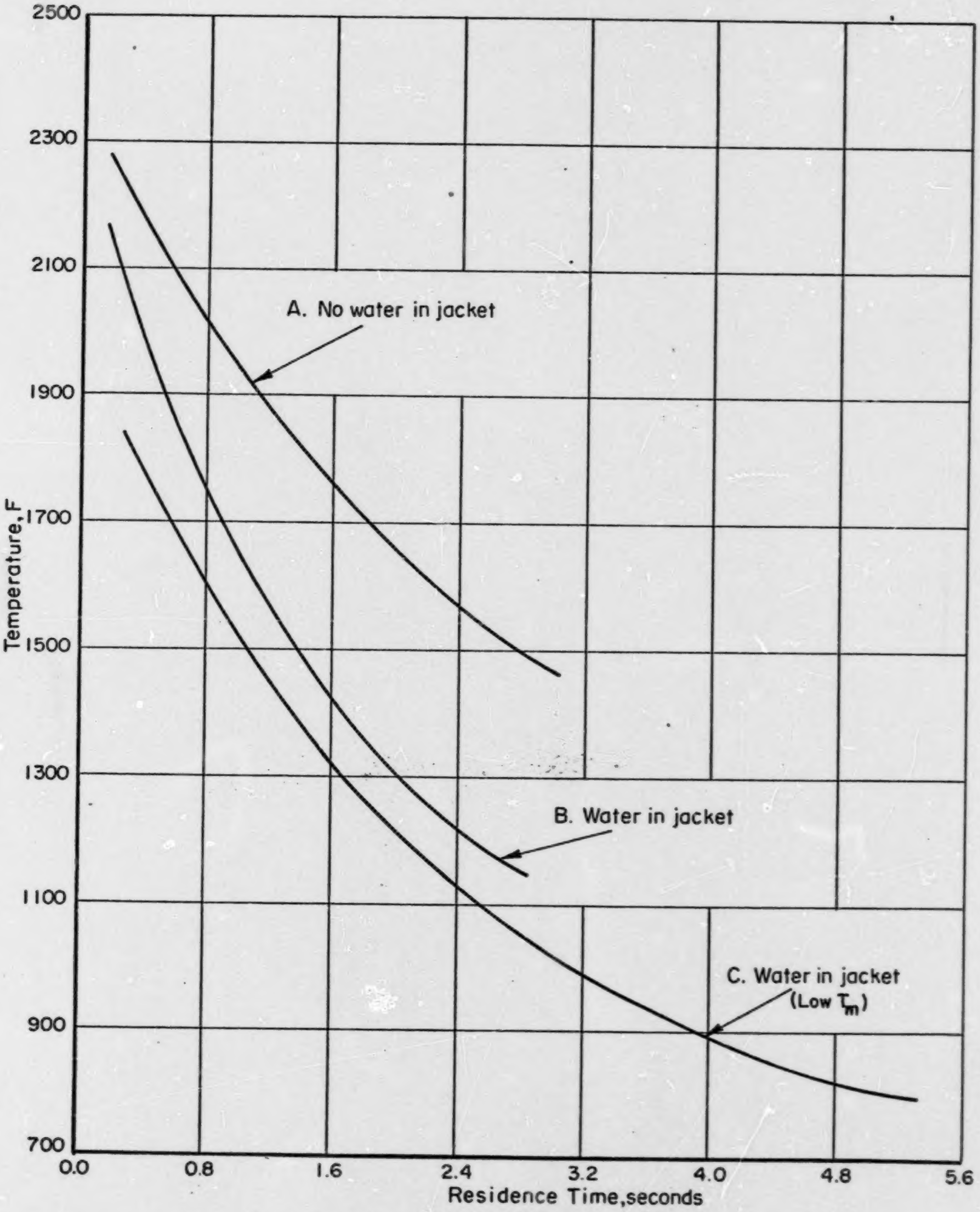

FIGURE 3. TIME-TEMPERATURE PROFILES IN MODIFIED REACTOR

hydration by water vapor in the flue gas, and various other non-reactive components depending on the composition of the original stone. These samples were first exposed to steam at approximately one atmosphere pressure and 250 F to convert the calcium oxide to calcium hydroxide and thereby simplify chemical analyses. Samples were then analyzed by a thermogravimetric method for hydroxide and carbonate content.

When samples had been exposed to SO_2 in the flue gas, a similar procedure of steam hydration and thermogravimetric analysis was followed. However, these samples also were analyzed for sulfate and, generally, for sulfite content. The procedure followed for sulfur analyses has been reported previously(3). Basically, this procedure consists of (1) digestion of sample using ion-exchange resin, followed by (2) colorimetric determination of sulfate using barium chloranilate as the reagent.

Surface Areas and Porosities

Surface area and porosity measurements were made on appropriate samples of both sulfurized and unsulfurized stones after exposure in the DPR. Area measurements were made using the dynamic BET method. Porosity measurements were made with a mercury porosimeter.

EXPERIMENTAL RESULTS AND DISCUSSION*

A considerable body of data has been developed relevant to the reaction of limestone with SO_2 in the dry-limestone injection process. The main purpose of this current work has been to organize and clarify previous data through correlation of data, development of supplemental information, and formulation of reaction models. Specifically, the following facets of the process have been considered and are discussed further below:

- The effect of time and temperature on reactivity
- The effect of SO_2 concentration on reactivity
- The effects of physical factors such as particle size, surface area, and pore size, on reactivity
- The effect of physical factors on calcination rates.

Reaction of Limestone with SO_2

Correlation of Previous Data

A number of different approaches can be taken to correlate the experimental data, and several empirical and theoretical models have been developed. However, the majority of the models have been based either on isothermal experimental data or on non-isothermal representations employing the time-temperature profile of the flue gas rather than that of the limestone. Either of these approaches is capable, in principle, of providing adequate representation of the limestone-SO_2 reaction if enough information concerning the effects of process variables is available. For example, it can be seen qualitatively from Figure 17 that the temperature of a limestone particle rises rather sharply upon injection into the flue gas to a temperature which is relatively stable for a considerable portion of its residence time in the flue gas. The particle temperature tends to follow the gas temperature after the initial heatup but at a slightly lower rate. Because of this, the process might be equally well represented either as an isothermal process at some intermediate temperature, or as a nonisothermal process using gas temperatures after the first half second or so. Departures from nonisothermal approximation are most serious with high injection temperatures, long residence times, and small particles.

---

* Details of reaction conditions and analytical results are listed in Appendix B under headings corresponding to appropriate sections of text.

Data gained with the DPR are expected to be more closely related to the process as it occurs in a boiler because of the similarities in time-temperature profile. It is therefore believed that empirical representation of DPR data may provide a slightly better representation of the limestone-SO_2 reaction in a boiler. Some work of this type was reported in the November, 1970, Summary Report(3), but the equations used were not developed to the point where any physical significance could be attached to the adjustable parameters used.

In general, the most outstanding characteristics of the reaction at any given temperature are the rapid decrease in reaction rate with increased loading and approach to some limiting extent of reaction which is dependent on temperature and particle size. This suggests that the rate equation should be expressed in terms of the loading, i.e., that the rate is a function of the amount of lime actually available for reaction. The correlation between reactivity and surface area as developed by Borgwardt(5) and as confirmed by other work also implies that the rate equation should be expressed in terms of loading.

Both the dependence of rate on loading and the concept of some limiting value of reactivity is expressed by

$$\frac{dS}{dt} = k(b-S) \tag{1}$$

where S is the loading (sulfur pickup in mg SO_3/g), k is a rate constant, and b is the maximum loading. Integration of Equation 1 yields

$$S = b(1-\exp(-kt)) \quad . \qquad (2)$$

If this equation is expanded in series form, the result is similar to the polynomial used to correlate data in the November 20, 1970 Summary Report(3), i.e.

$$S = b(kt - k^2t^2/2! + \ldots\ldots\ldots) \qquad (3)$$

It is expected therefore that Equation 2 would fit the experimental data at least as well as the truncated polynomial used in the Summary Report. Furthermore, use of Equation 2 permits attachment of some physical significance to the parameters b and k.

A least-squares fit of Equation 2 to the SO_2-limestone reaction data from the Summary Report consistently yielded smaller standard deviations than had been obtained in any previous attempts at correlation of this data. Furthermore, Equation 2 was applicable at mean reactor temperatures above 1845 F, where the maximum loading decreases with increasing temperature. All of the data can be organized in a relatively straightforward fashion using Equation 2. Figure 4 shows semi-log plots of b and k versus the reciprocal of the absolute mean reactor temperature for the data for -140+200 mesh Stone No. 2061 at C_{SO_2} = 3000 ppm and C_{O_2} = 3 percent. This plot shows that, within the limits of the experimental work, both k and b can be expressed in terms of Arrhenius-type functions of temperature

$$k = \exp(14.563 - 18734/T_m) \qquad (4)$$

and

$$b = \exp(-2.982 + 10139/T_m) \qquad (5)$$

where T_m is the mean reaction temperature in degrees Kelvin. These expressions for k and b are consistent with the fact that the amount of lime available for reaction decreases at the higher temperatures and that rate constants are normally expected to increase exponentially with temperature. It should be noted that Equation 5 cannot be used for b at temperatures below about 1500-1600 F because b is allowed to increase without limit. This is, of course, of little consequence in a practical sense since reaction rates are too low to be of practical value below these temperatures.

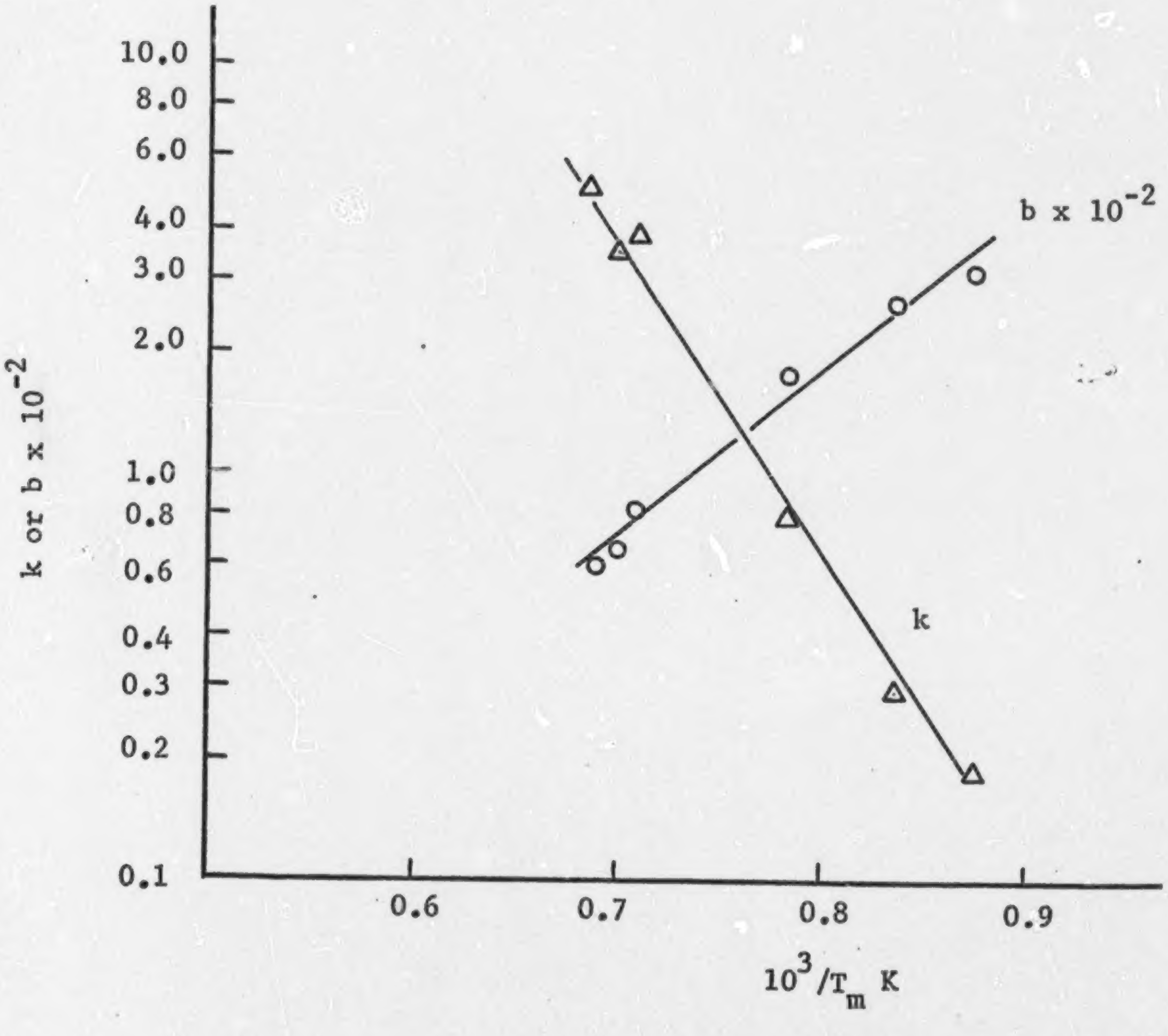

FIGURE 4. DEPENDENCE OF k AND b ON MEAN GAS TEMPERATURE

In the Summary Report(3), it was shown that the apparent order of reaction with respect to SO_2 concentration changes during the course of the reaction. Further examination of these data in terms of the expression given in Equation 2 reveals that k is independent of SO_2 concentration and the value of b is proportional to $C_{SO_2}^{1/2}$. Since the rate of reaction is proportional to (b-S), the apparent order of reaction, $(d \ln (dS/dt)/d \ln C_{SO_2})$, depends on loading. This square-root dependence of the maximum loading has been further confirmed by recent work which is discussed on Page 21.

According to Equation 4, the activation energy for the process is 37.2 kcal/mole. However, the apparent activation energy, $RT^2(d \ln(dS/dt)/dT)$, reflects both the temperature dependence of k and that of b, and is dependent on time. For example, at very short times, the apparent activation energy approaches 17.1 kcal/mole at all temperatures, but at $t = 0.1$ sec at 1950 F, the apparent activation energy is 10.5 kcal/mole. At higher temperatures and longer residence times, the apparent activation energy can even become negative, reflecting the decreased overall reactivity with increased temperature due to loss of surface area by overburning.

Effect of Temperature Gradient

The average time-temperature profile of a boiler is dependent on the specific design and size of the unit, so that different boilers are apt to be characterized by different time-temperature profiles. Furthermore, the time-temperature profile in any given boiler will vary depending upon load. Therefore, there is some need to know how the performance of a given limestone may vary with a change in temperature gradient.

Two series of injections in the DPR were made with -270+325 mesh Stone No. 2061 operating the reactor with two different time-temperature profiles. Profiles for these series are shown in Figure 5. Results

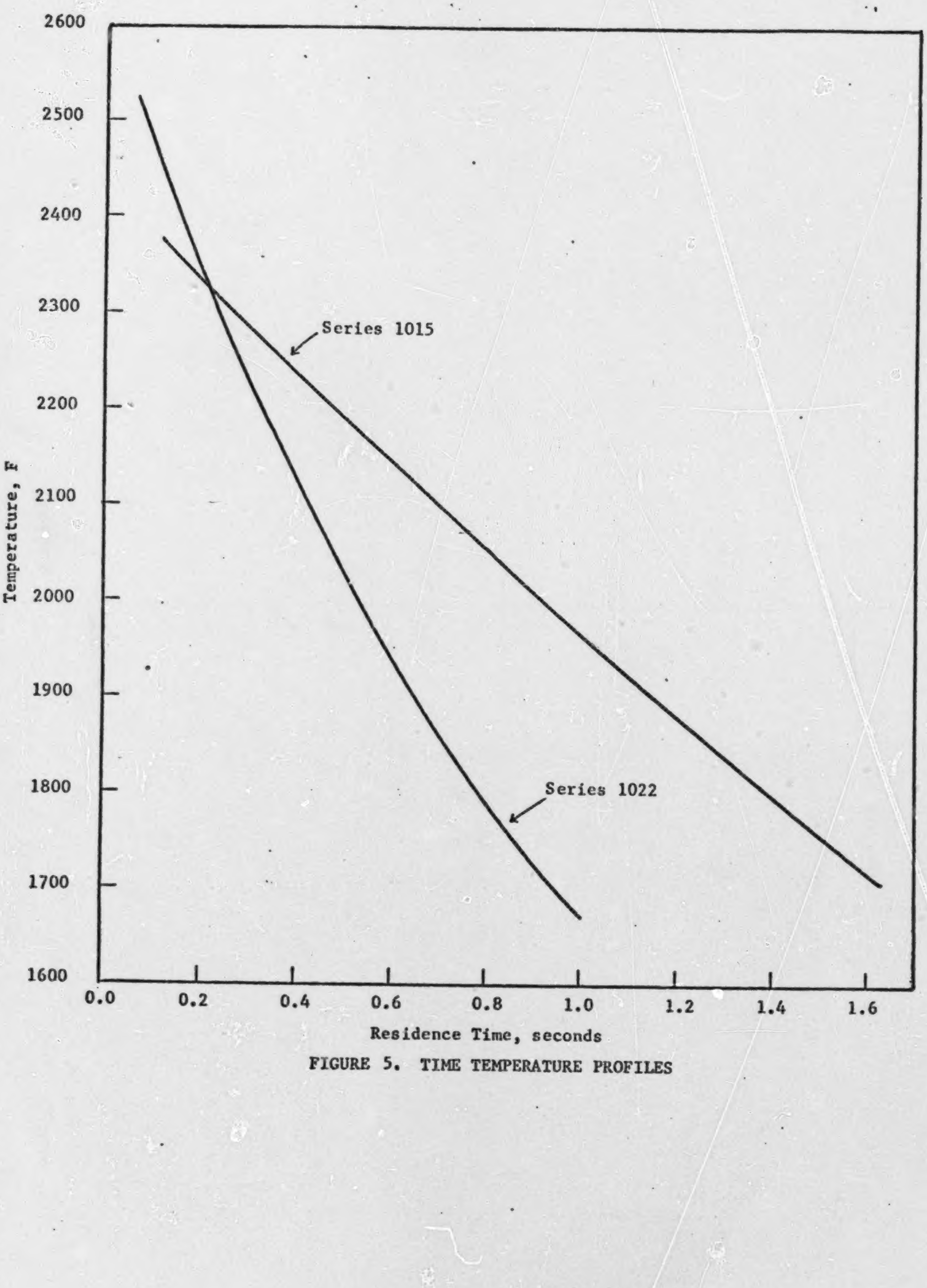

FIGURE 5. TIME TEMPERATURE PROFILES

of these runs are summarized in Table 1. For each series, a maximum in reactivity was found for injection at 2100-2200 F (mean temperature = 1950 F) as indicated in Figure 6. However, with the steeper time-temperature profile (Series 1022), higher injection temperatures appear less detrimental, possibly because of the reduced time of exposure at these high temperatures.

The most serious effect of increasing the temperature gradient is of course a decrease in the time available for reaction at favorable temperatures. This shows up in comparison of the results obtained for these two series. However, if comparisons are made between pairs of samples having approximately common mean temperatures and residence times, little difference in reactivity is seen beyond that which might be attributed to the slight differences in residence time.

In principle, the response curves shown in Figure 6 could be calculated from Equation 2 of the previous section of this report providing adequate knowledge of the dependence of b and k on particle size were available. Equation 2 predicts a maximum reactivity at temperatures in agreement with Figure 6, but the dependence of b and k on particle size is not fully known. Furthermore, the particular batch of Stone No. 2061 used in these experiments was slightly different in composition from that used in the previous work, and it is not known how strongly this factor influences the reactivity.

Effect of Particle Size

To obtain some idea of the effect of particle size on the factors b and k of Equation 2, a single series of runs was made in the DPR at constant mean temperature (1930 F). For this series, the particle size was -270+325* mesh, and the batch of Stone No. 2061 used was similar in composition to that used previously for the -140+200 mesh material.

---

* Average size 48 microns.

TABLE 1. EFFECT OF TIME-TEMPERATURE PROFILE

Run No.	Temperature, F Injection	Temperature, F Collection	Residence Time, seconds	Sulfur Pickup, mg SO_3/g Sample
1015-B	2402	2179	0.45	55
1015-C	2402	2014	0.82	87
1015-E	2179	2014	0.37	124
1015-G	2345	1730	1.38	136
1015-K	2179	1730	1.04	175
1015-L	2070	1730	0.80	175
1015-N	2014	1730	0.67	163
1015-P	1901	1730	0.41	156
1015-S	1843	1730	0.28	142
1022-A	2565	2216	0.27	96
1022-C	2565	1996	0.49	89
1022-E	2216	1996	0.22	154
1022-G	2565	1693	0.91	115
1022-J	2216	1693	0.64	167
1022-L	2138	1693	0.57	150
1022-N	1996	1693	0.42	150
1022-P	1865	1693	0.26	122
1022-R	1805	1693	0.17	79

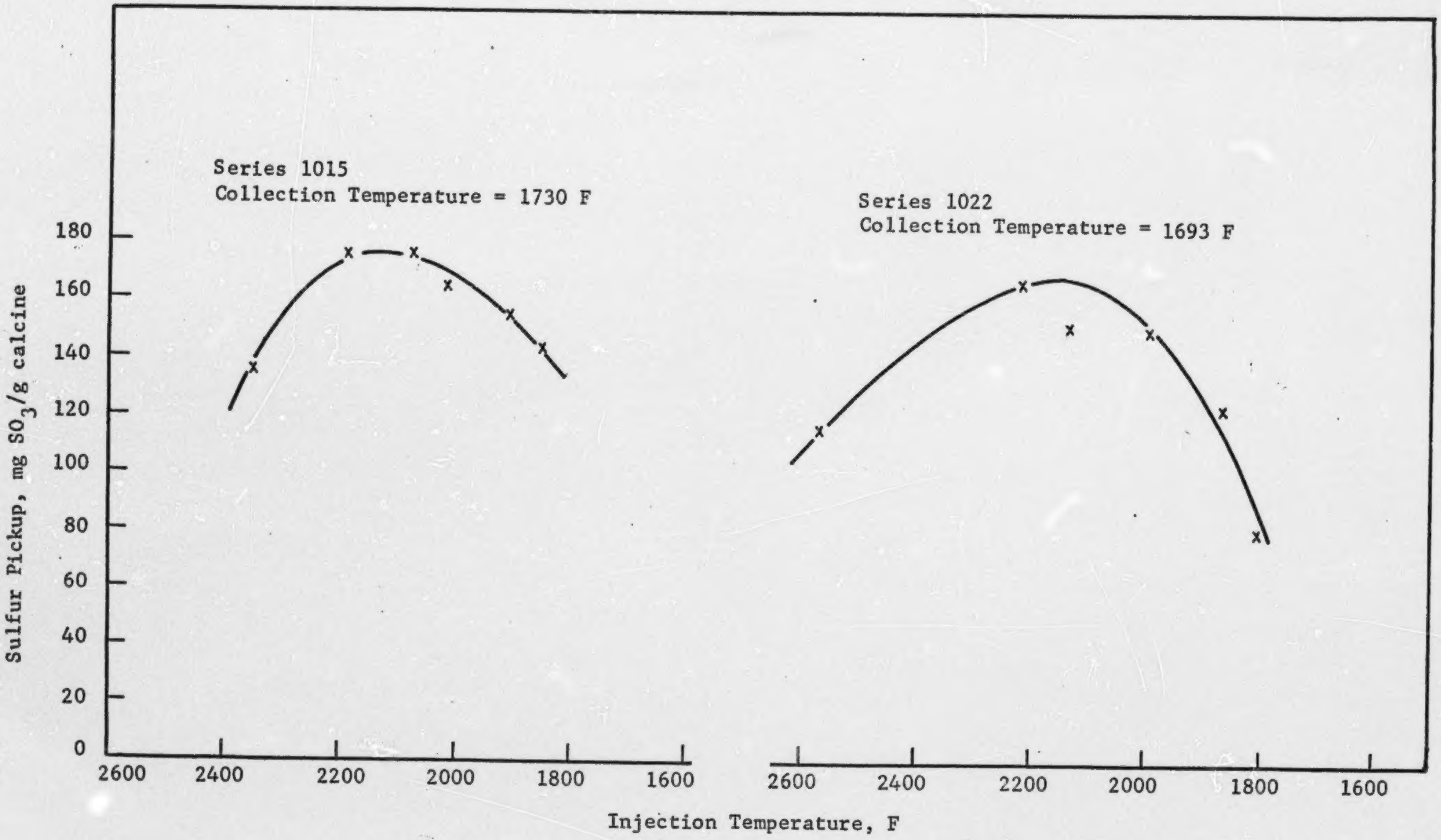

FIGURE 6. EFFECT OF TIME-TEMPERATURE PROFILE ON REACTIVITY

A least-squares fit of the data to Equation 2 yields values of b and k of 135 mg SO_3/g and 3.09 sec^{-1} respectively. These may be compared with calculated values of b = 105 and k = 1.56 for the larger particle size at the same temperature. Thus, approximate halving of the particle size had only a minor effect on b, the maximum loading, but the rate constant was approximately doubled. This is consistent with the observations made in the previous section of this report, but, again, because of the potential differences between the two batches of stone, no quantitative comparison seems warranted. These data are also consistent with observations of Ishihara(7) whose work indicated higher initial rates of reaction for smaller particles but only a relatively minor effect of particle size on overall utilization.

Effect of SO_2 Concentration

Reaction Rates. Rate data summarized in the Summary Report of November 20, 1970(3) indicated that the rate of reaction of Limestone No. 2061 with SO_2 in flue gas was proportional to the square root of the SO_2 concentration during the initial stages of the reaction, and that the apparent order of reaction increased to unity or greater as the reaction proceeded. Further work has now been done to clarify this seemingly complex behavior.

Firstly, the previous data have been treated in terms of Equation 2 given above to determine the specific dependencies of k and b on concentration. This treatment of the previous data reveals that the rate constant, k, is essentially independent of the SO_2 concentration at a mean reactor temperature of 1770 F. However, the maximum loading, b, depends on the square root of the concentration. Inspection of the form of Equation 2 shows that comparison of rates at common values of S along the response curves for various concentrations, will lead to a complex and varying apparent order. However, if the rates are compared at constant times, the apparent order is constant at one-half.

A second clarification of apparent reaction order was made through a series of additional runs in the reactor at concentrations of 125, 255, 650, 1600, 3980, and 9900 ppm. These runs included injection and collection of samples under various temperature and residence conditions, but most of the data were taken in the plateau region of the response curve so that the data more generally represent b.

In each of these runs limestone injection rates were approximately 1 gram per minute. This means that, with the lowest SO_2 concentration, the effective stoichiometry of the system was about one, i.e., the molar throughputs of limestone and SO_2 were approximately equal. However, the maximum lime utilization observed was only 3 percent, and, for all practical purposes, the SO_2 concentration can be considered constant. At higher concentrations, the effective stoichiometric ratios were less than one and the net SO_2 removal achieved in each case was less than 3 percent. This means that these data can be considered as valid tests of reactivity at the stated concentrations.

It will be noted from the data cited in Table B-3 of Appendix B that similar time and temperature conditions were used for corresponding samples at each SO_2 concentration. Comparison can thus be made on a point-by-point basis. Also, since most of the data were taken in the plateau region of the reaction trajectory, averages of the results at each concentration can be used to represent the effect of concentration on overall reactivity. Either the point-by-point comparison or the comparison of average reactivities leads to the same conclusion, as indicated in Figure 7.

Figure 7 shows clearly that the overall reactivity is proportional to the square root of the SO_2 concentration, which is entirely in agreement with data of the Summary Report(3). This fact is seemingly in conflict with results obtained by Babcock & Wilcox(8). It must be recognized, however, that the B&W data represent a different type of experimental

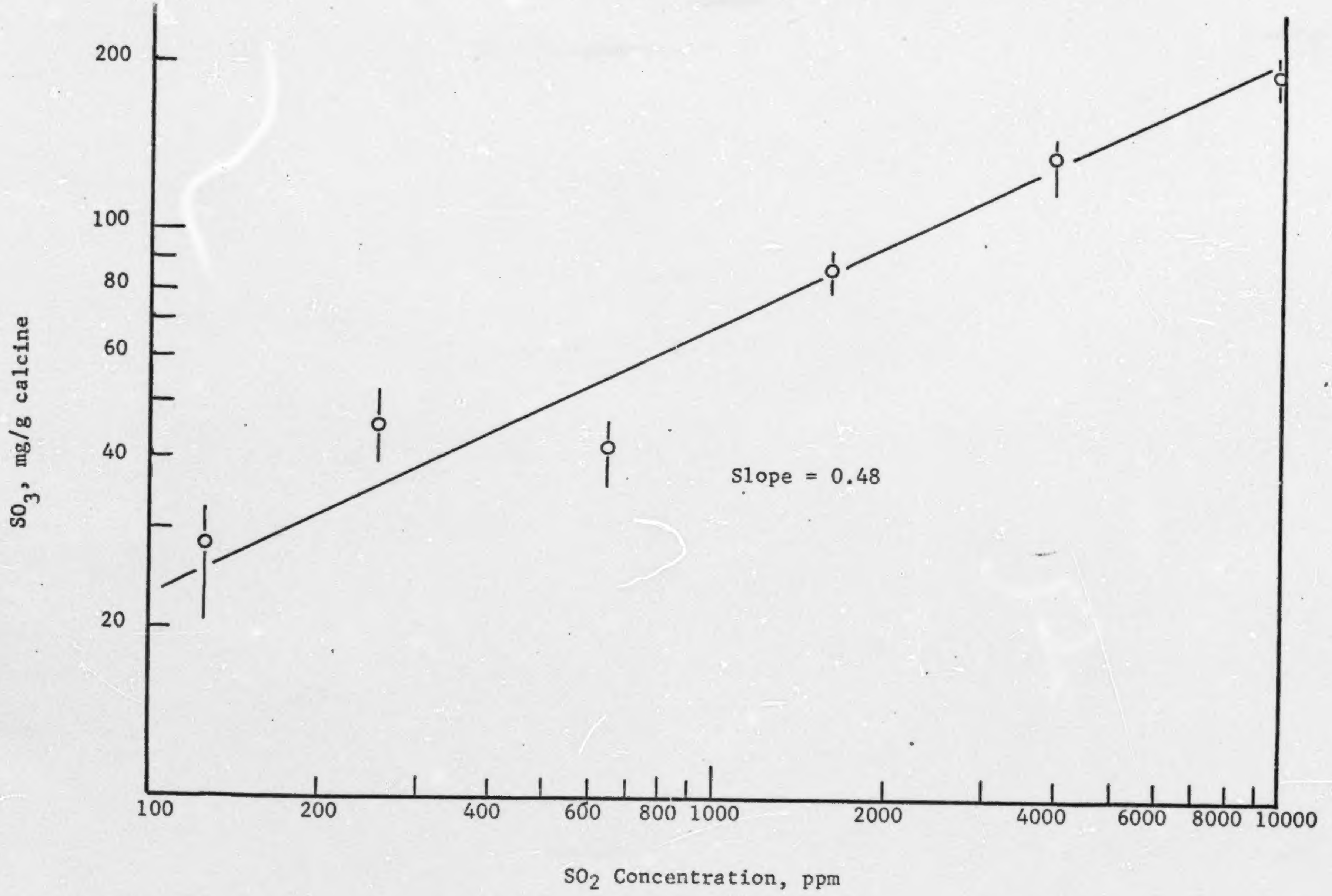

FIGURE 7. EFFECT OF SO_2 CONCENTRATION OF OVERALL SULFUR PICKUP

approach. Their data show the amount of SO_2 removed from the flue gas stream as a function of initial SO_2 concentration. The current data can be transformed into this form by multiplying the percentage SO_2 removal* at unit stoichiometry by the SO_2 concentration, in which case the apparent order of the concentration dependence should be 1.5. It can be readily seen from Figure 8 that when the data are represented in this fashion the apparent order is 1.5. Although the B&W report cites an apparent order of about 1 for their data, a least squares treatment of the B&W data reveals an apparent order of 1.4. Hence these two pieces of work are in agreement.

Equilibria. Some comment is warranted on the effect of the SO_2 concentration on the dissociation of calcium sulfate and the relation of this process to the observed maximum in reactivity. Consider the following reaction

$$CaO + SO_2 + 1/2 \text{ or } 1/2\ O_2 \underset{k_r}{\overset{k_f}{\rightleftarrows}} CaSO_4 \ .$$

Although this expression may not necessarily represent the actual chemical reaction mechanisms, it does represent the essential chemistry involved in the dry-limestone injection process. Here, k_f and k_r are the forward and reverse rate constants. Taking constant oxygen partial pressure of 0.03 atm, a typical value for boiler operation, the equilibrium partial pressure of SO_2 over pure calcium sulfate can be calculated as shown in Table 2 from the thermodynamic data of Reid, et al.(9). It can be seen from this Table that at particle temperatures above about 2150 F, the driving force for reaction of lime with SO_2 will be decreased appreciably by virtue of the increasing instability of the sulfate.

In a boiler, particle temperatures could conceivably reach this value momentarily if the stone were injected at temperatures above about 2350 F, but since the temperature gradients in a boiler are rather steep it is unlikely that this temperature would persist in the stone particles

---

* Assumed to be equal to the CaO utilization.

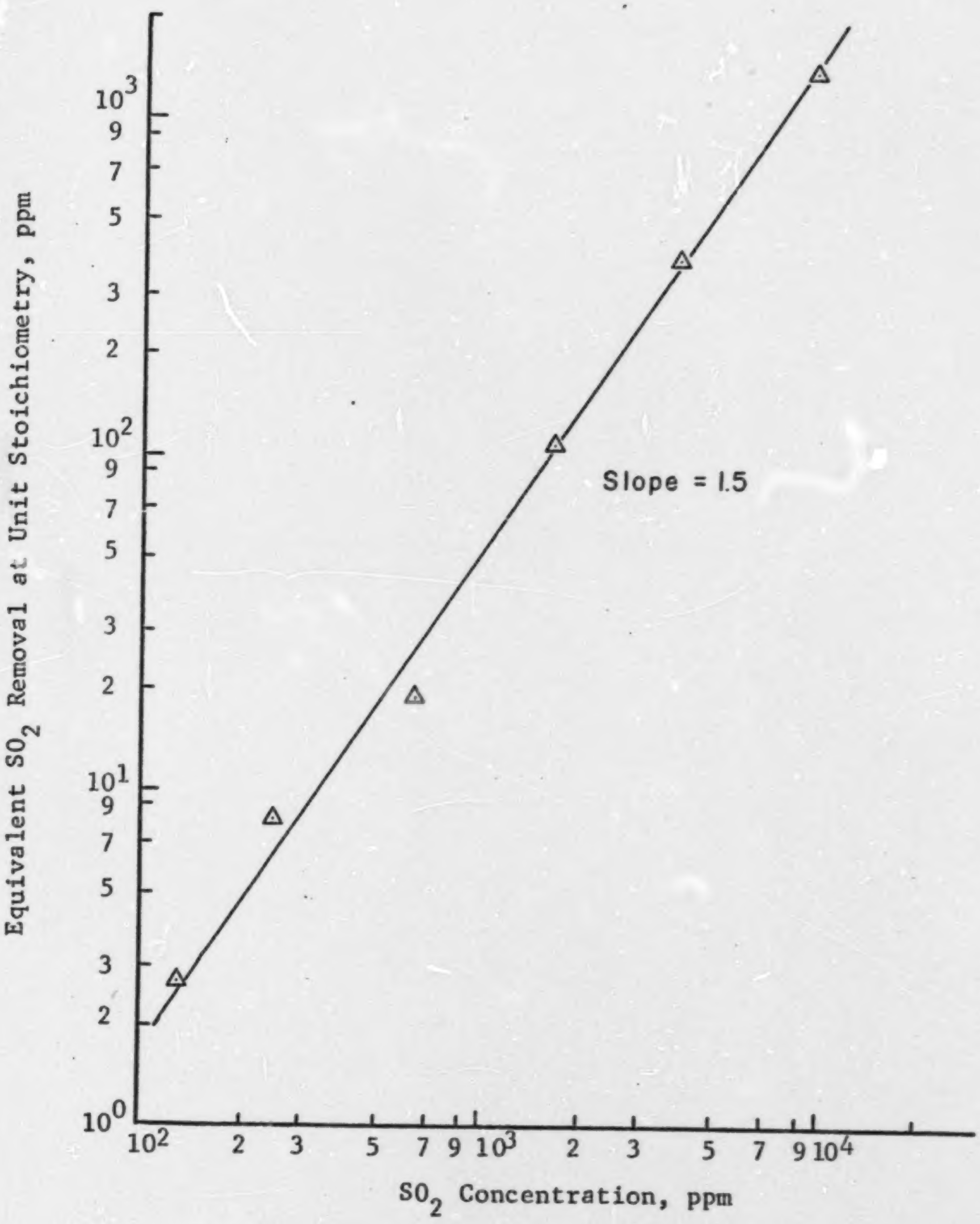

FIGURE 8. EFFECT OF SO_2 CONCENTRATION ON SO_2 REMOVAL

TABLE 2. EQUILIBRIUM PARTIAL PRESSURE OF SO_2

$CaSO_4 = CaO + 1/2\ O_2 + SO_2\ (O_2 = 0.03\ \text{atm})$
$P\ (\text{torr}) = \exp\ (37.4556 - 55440/T^{o}K)$

$T^{o}F$	P, torr	P, ppm
1600	1.67×10^{-5}	2.20×10^{-2}
1650	5.26×10^{-5}	6.92×10^{-2}
1700	1.57×10^{-4}	2.07×10^{-1}
1750	4.48×10^{-4}	5.89×10^{-1}
1800	1.22×10^{-3}	1.61
1850	3.17×10^{-3}	4.17
1900	1.90×10^{-3}	10.4
1950	1.90×10^{-2}	25.0
2000	4.42×10^{-2}	58.2
2050	9.91×10^{-2}	130
2100	2.16×10^{-1}	284
2150	4.55×10^{-1}	599
2200	9.34×10^{-1}	12.3×10^{2}
2250	1.87	24.6×10^{2}
2300	3.64	47.9×10^{2}
2350	6.92	91.1×10^{2}
2400	12.9	17.0×10^{3}
2500	41.9	55.1×10^{3}
2600	126.	16.6×10^{4}

for very long. Even if it is assumed that the particle temperature precisely follows the gas temperature, there is a maximum in reactivity predicted by rate equations implied by the chemical equation above, but the decreased reactivity above 2100 F does not compare with that observed experimentally. It is therefore unlikely that the instability of the sulfate can be blamed for decreased reactivity at high injection temperatures.

Surface Areas and Porosities

The results of Borgwardt(5) have indicated that the most important factors in determining the reactivity of a given limestone are the surface area and porosity developed during the course of calcination. These factors directly determine the availability of lime for reaction,the accessibility of the lime, and the space which is available within a given particle for occupancy by reaction products. The surface area and porosity are determined by calcination rate and sintering rate, of which the latter is apparently more important in determining the decreased reactivity of limestones at high temperatures. Sintering itself is a complex process, depending on grain size, impurity content, and temperature of the lime and time. Kuczynski(10) has identified at least four distinct mechanisms for the sintering process, and, in view of this complexity, it is necessary to rely upon direct measurements of surface area and porosity and empirical correlation with reactivity as a means of identifying reaction conditions and particular limestones which could be of interest in the dry-limestone injection process or related limestone-SO_2 removal schemes.

Surface areas of kiln-calcined limes are generally of the order of a few square meters per gram or less depending on the degree of overburning of the lime. Average pore diameters in these same materials are generally of the order of a few tenths of microns. Borgwardt(5) has shown that the isothermal reaction rates of such kiln-calcined limes are directly proportional to surface areas.

The process of pore formation during calcination involves continuous growth of the pores from essentially molecular dimensions to some final state which is determined largely by temperature, when calcination times are of the order of minutes to hours. But insufficient information is available to determine how important the dynamics of the process may be at short times, say seconds or less, which are important in consideration of the calcination and reaction of limestone either in a boiler or in the DPR. If the dynamics of the process are important on this time scale, the use of a correlation of reactivity with surface area measured after completion of the process could be subject to question.

To clarify this point, two series of experiments were run using the DPR. The first series was directed at examining the time and temperature dependence of surface area in the DPR. The second series was concerned with the question of correlating surface area with reactivity in the DPR.

Effect of Time and Temperature on Pore Structure

Data shown in Table 3 summarize the results of surface area and porosimetry measurements made on Stone No. 2061 calcined in the DPR under a variety of temperature and residence time conditions. A typical pore distribution for DPR-calcined Stone No. 2061 is shown in Figure 9. Note that most of the apparent pore volume at pore diameters greater than 10 μ is probably interparticle space rather than true pore volume. Complete pore distribution data for these samples are given in Appendix C. Series 925 was run with -140+200 mesh stone and series 106 was run using -270+325 mesh stone.

Pore volumes and surface areas cited in Table 3 are listed relative to the weight of CaO formed during the partial calcination. Pore diameters listed are calculated from the surface area and pore

TABLE 3. POROSITY AND SURFACE AREA DATA

Sample[(a)] Number	Temperature, F		Residence Time, seconds	Percentage Calcination	Pore Volume,[(b)] cc/g CaO	Surface Area m^2/g CaO	Average Pore Diameter, microns
	Injection	Collection					
925-B	2224	1440	2.86	86	0.187	21.3	0.044
925-A	2224	1765	1.27	83	0.203	21.5	0.048
925-D	1830	1440	1.82	73	0.337	61.3	0.028
925-C	1830	1765	0.23	19	0.575	44.2	0.066
106-A	2243	2156	0.15	40	0.133	52.9	0.013
106-B	2156	2073	0.16	45	0.226	66.7	0.017
106-C	1996	1920	0.17	28	0.411	67.8	0.030
106-F	1920	1500	1.35	78	0.164	36.6	0.022
106-E	1849	1782	0.18	45	0.166	42.9	0.019
106-D	2243	1500	0.99	85	0.100	7.6	0.066

(a) Series 925 is -140+200 mesh, Series 106 is -270+325 mesh.

(b) For pores with $d < 2\ \mu$.

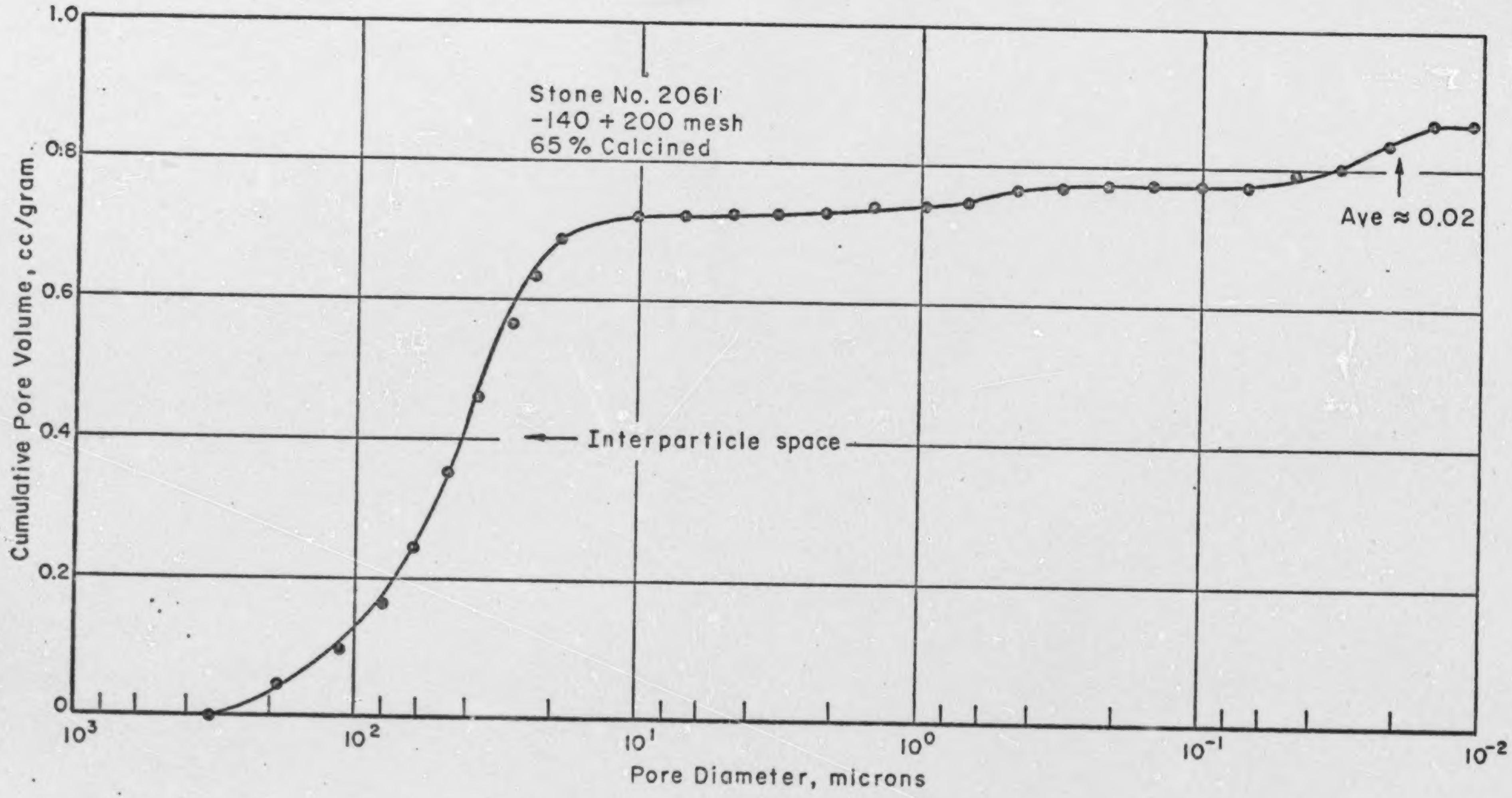

FIGURE 9. PORE SIZE DISTRIBUTION

volume data using the equation

$$\bar{d} = 5V_p/A,$$

where V_p and A are the pore volume and surface area respectively. This equation is only an approximation; the actual relationship between volume and area depends on the specific pore shape. However, the calculated values can serve to determine whether any significant contribution to the surface area is made by pores smaller than those observed in the porosimetry measurements. With these samples, the calculated diameters agree well with the pore size distribution shown in Appendix C, indicating that no significant pore structure exists at diameters less than about 0.01 micron.

The porosity data indicate a bidisperse system of pores with a minor pore distribution having diameters of the order of a few tenths of microns. This second pore distribution is especially evident in samples having larger pore volumes than might be expected for a soft-burned lime, 0.36 cc/gCaO. This may indicate that the second pore distribution is due to cracks in the lime caused by the violent nature of the calcination process, or it may be caused by pore inclusion in the original limestone sample. It should be noted also that many of the samples have pore volumes smaller than 0.36 cc/gCaO, implying that a significant amount of sintering has already taken place in the relatively short time of exposure.

Maximum surface areas in these runs appear to be developed with injection temperatures in the neighborhood of 1900-2000 F, implying the overburning of the lime is significant at higher temperatures.

The surface area data also reflect the importance of the dynamics of the sintering process. Comparing sample 106-A with Sample 106-F, it can be seen that although the injection temperatures were the same for these two samples, the longer exposure of Sample F resulted in a much lower surface area. This is also evident in comparison of Samples 106-C and 106-D. Although the injection temperature for Sample C was slightly higher than that for Sample D, the shorter exposure time for C resulted in a higher surface area per unit weight of CaO formed.

Some additional experiments with other stones were performed to determine the effect of temperature on surface area development. This involved use of three selected members of a set of ten stones provided by APCO, all ten of which were used in tests of the correlation between area and reactivity, discussed below. The results of study of the effect of temperature on area of these materials is shown in Table 4. These results clearly show that the surface area developed during a given residence time decreases with increasing temperature.

TABLE 4. EFFECT OF TEMPERATURE ON SURFACE AREA

Run	Stone Type(a)	Temperature		Residence Time, sec	Percentage Calcination	Area, m^2/g(b)
		Injection	Collection			
318-A	Mich.Marl	2006	1712	1.03	52	13.6
318-B	IGS-4	2006	1712	1.03	72	24.8
318-C	No. 1336	2006	1712	1.03	71	26.4
317-A	Mich.Marl	2155	1785	1.17	66	7.5
317-B	IGS-4	2155	1785	1.17	80	16.3
317-C	No. 1336	2155	1785	1.17	83	23.7
318-D	Mich.Marl	2263	1828	1.14	74	5.9
318-E	IGS-4	2263	1828	1.14	81	8.2
318-F	No. 1336	2263	1828	1.14	84	14.1

(a) -140+200 mesh.

(b) Area per gram of sample.

Surface Area and Reactivity

In a further attempt to clarify the validity of correlation of surface area with reactivity, ten stones selected by APCO as representative of the spectrum of limestone classes were tested in the DPR both for surface area development and reactivity. The mineralogical characteristics of these ten stones have been examined in detail by Harvey$^{(6)}$, and identification numbers used in discussing the data refer to Harvey's classification. All of the stones were -270+325 U.S. Standard mesh.

The type of data obtained in this series of tests must be distinguished from the area-reactivity data of Borgwardt.$^{(5)}$ Borgwardt showed that the isothermal reaction rates of precalcined limes were proportional to their surface areas. Because of the nature of the DPR experiments, however, it was not possible to determine actual surface areas existing during the course of reaction with SO_2. In these experiments, only the terminal surface area, i.e., that area existing after completion of calcination and sintering, could be determined. It is recognized that the SO_2 reaction occurs simultaneously with calcination and sintering in the DPR. Hence correlation between SO_2 pickup and terminal surface area is not necessarily expected. The purpose of this work was therefore to explore the possibility of correlation of reactivity with terminal surface area.

Table 5 shows a summary of terminal area data for samples of the ten stones calcined in the DPR in the absence of SO_2. Table 6 shows the reactivities of these same materials exposed in the DPR under similar temperature and residence time conditions with an SO_2 concentration of 3000 ppm. Also indicated in Table 6 is the effect of reaction on lowering the area due to filling of pore space during reaction.

TABLE 5. SURFACE AREAS OF TEN CALCINES

Run	Stone Type[(a)]	Temperature Injection	Temperature Collection	Residence Time, sec	Percentage Calcination	Terminal Area, m^2/g[(b)]
226-A	Mich. Marl	2140	1495	2.08	67	5.4
226-B	No. 1336	2140	1495	2.08	83	14.2
226-C	IGS-1	2140	1495	2.08	83	18.4
226-D	IGS-2	2140	1495	2.08	81	11.0
226-E	IGS-3	2140	1495	2.08	81	18.3
32-A	IGS-4	2140	1495	2.08	82	8.6
32-B	IGS-5	2140	1495	2.08	(c)	21.9
32-C	IGS-6	2140	1495	2.08	(c)	14.7
32-D	IGS-7	2140	1495	2.08	(c)	23.6
32-E	IGS-8	2140	1495	2.08	76	15.1

(a) -270+325 mesh.
(b) Area per gram of sample.
(c) Approximately 80 percent calcination.

TABLE 6. REACTIVITY AND SURFACE AREA

Stone	Terminal Area, m^2/g	Sulfur Pickup mg SO_3/g-calcine(a)
Marl	5.4	260
1336	14.2	126
IGS 1	18.4	115
IGS 2	11.0	132
IGS 3	18.3 (6.7)(b)	178 (179)(c)
IGS 4	8.6 (2.5)(b)	274 (260)(c)
IGS 5	21.9	259
IGS 6	14.7	246
IGS 7	23.6	85
IGS 8	15.1	168

(a) Reaction temperatures and times similar to those given in Table 5.

(b) Area of sample after reaction.

(c) Repeat values on separately injected samples.

It is readily apparent from Figure 10 that no linear correlation exists between reactivity and terminal surface area for these samples. Five of the test stones (IGS-2,8,3,5, and No. 1336) could conceivably display a linear correlation. IGS-7 is almost pure magnesite, and since MgO is relatively unreactive, this material probably should not be included in the correlation. However, the very high reactivities of the two materials showing the lowest terminal surface areas, IGS-4 and Michigan Marl, strongly mitigates against the general validity of a correlation, unless other factors are taken into consideration.

Although all of the ten stones were initially sieved to -270+325 mesh, microscopic examination of samples recovered from the DPR indicates severe disintegration of particles for some of the stones. Figures 11 a-J show photomicrographs of these ten stones before and after injection into the DPR. It is readily apparent from these photos that five of the stones, IGS-4,5,6,7 and Michigan Marl underwent severe size reduction in the reactor. With Michigan Marl even those few large particles remaining are really agglomerates of fine particles. Reexamination of Figure 10 reveals that these are all materials for which the reactivity was higher than that expected from the terminal surface area. This is especially true for IGS-5, 6, and 7 because of the fact that these stones contain relatively little CaO per gram of calcine; IGS-5 and 6 are dolomites and IGS-7 is a magnesite having about 3 percent $CaCO_3$ as an impurity. In each case, the reactivity of these three materials is greater than the 10-15 percent utilization of the CaO usually observed with other -270+325 mesh limestones. Since $MgSO_4$ is not thermodynamically stable under the conditions of these experiments, little of the increased reactivity can be attributed to reaction with MgO.

There is therefore some reason to believe that the reactivity-terminal area correlation may be valid, providing all other factors are equal. By the same token, a low-terminal surface area does not necessarily imply low reactivity if the stone is one which does undergo decrepitation upon exposure to the severe thermal stresses imposed in the DPR or in a boiler.

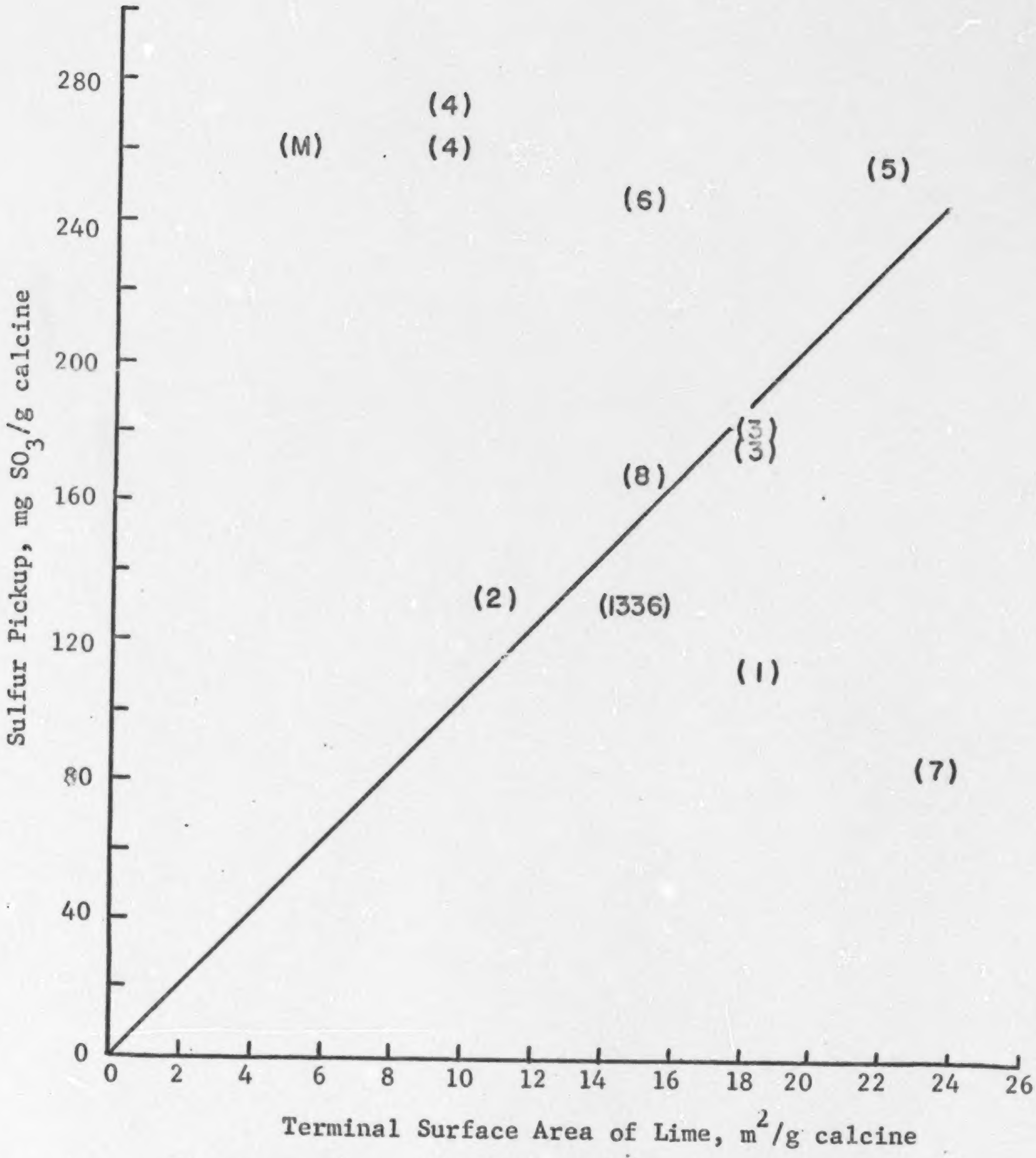

FIGURE 10. REACTIVITY vs SURFACE AREA

Scale: 1 in. = 435 μ

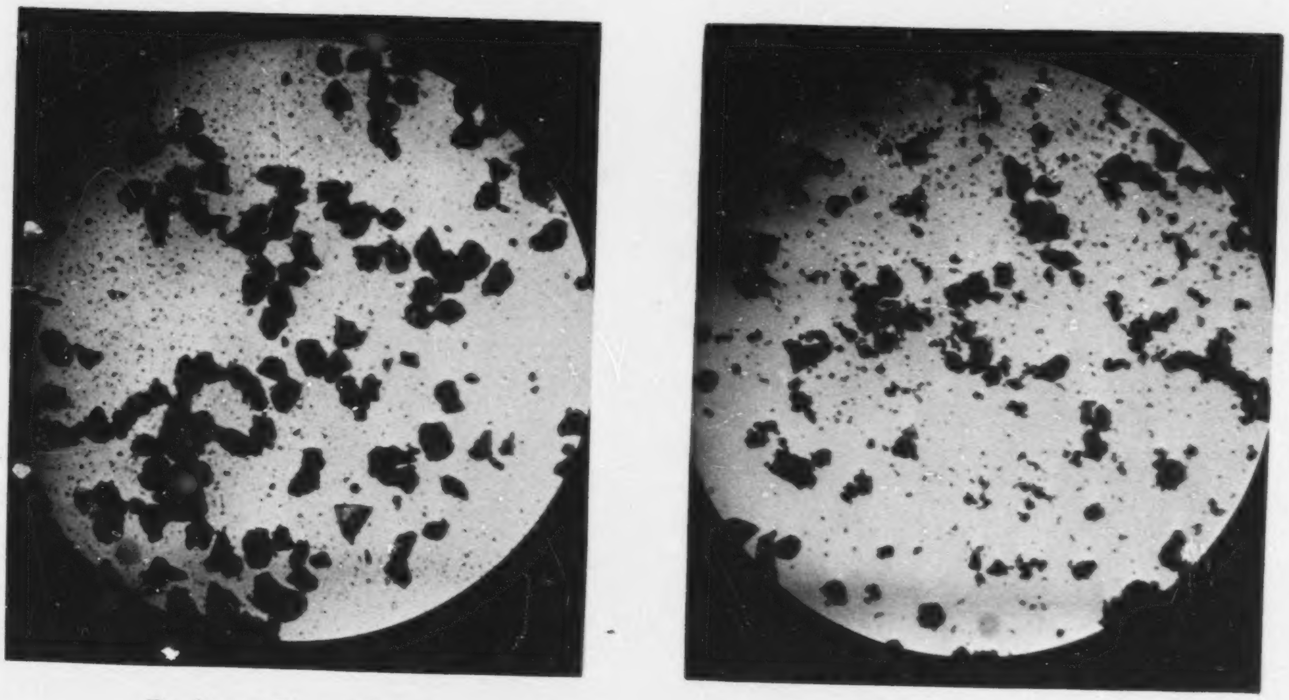

Before Reaction

After Reaction

a. Michigan Marl

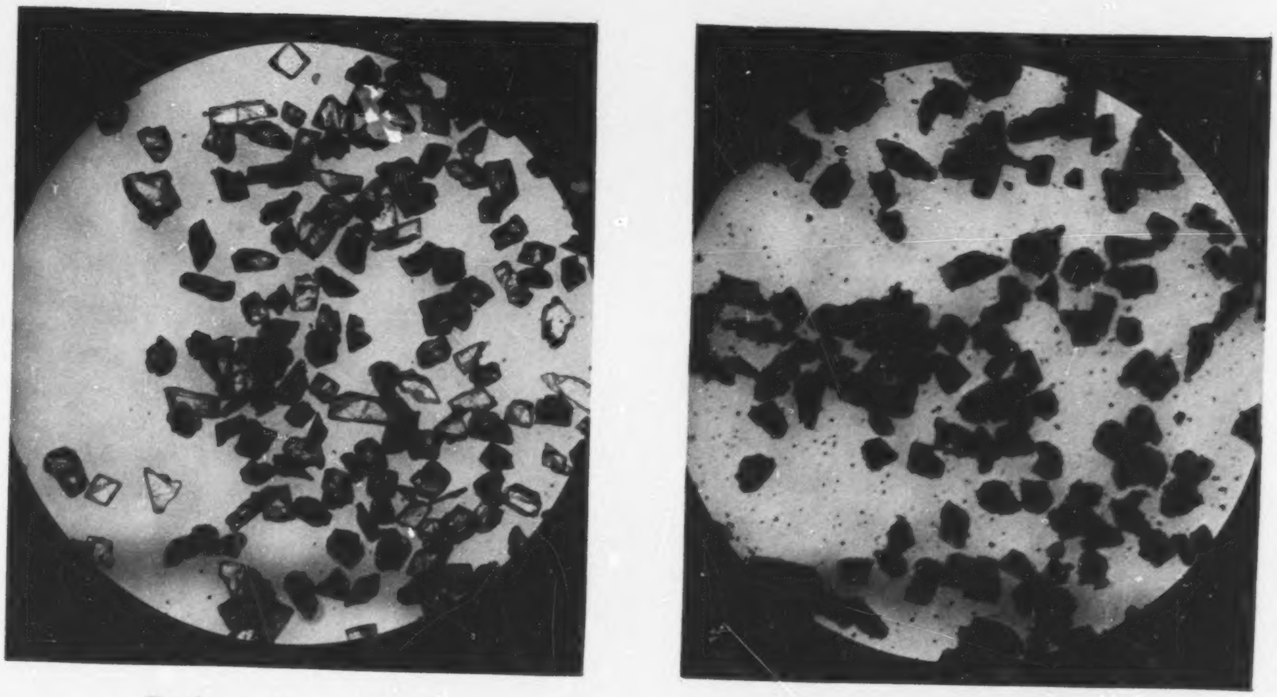

Before Reaction

After Reaction

b. No. 1336

FIGURE 11. PHOTOMICROGRAPHS OF TEN STONES BEFORE AND AFTER REACTION

Scale: 1 in. = 435 μ

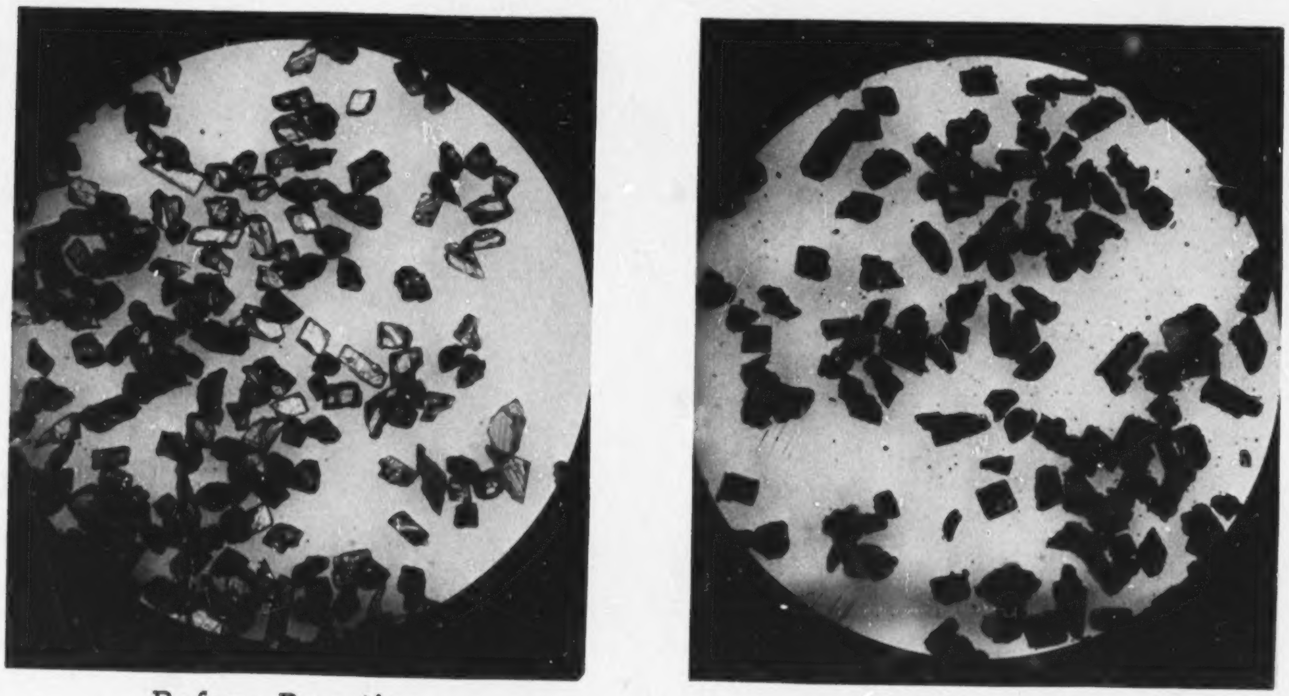

Before Reaction

After Reaction

c. IGS 1

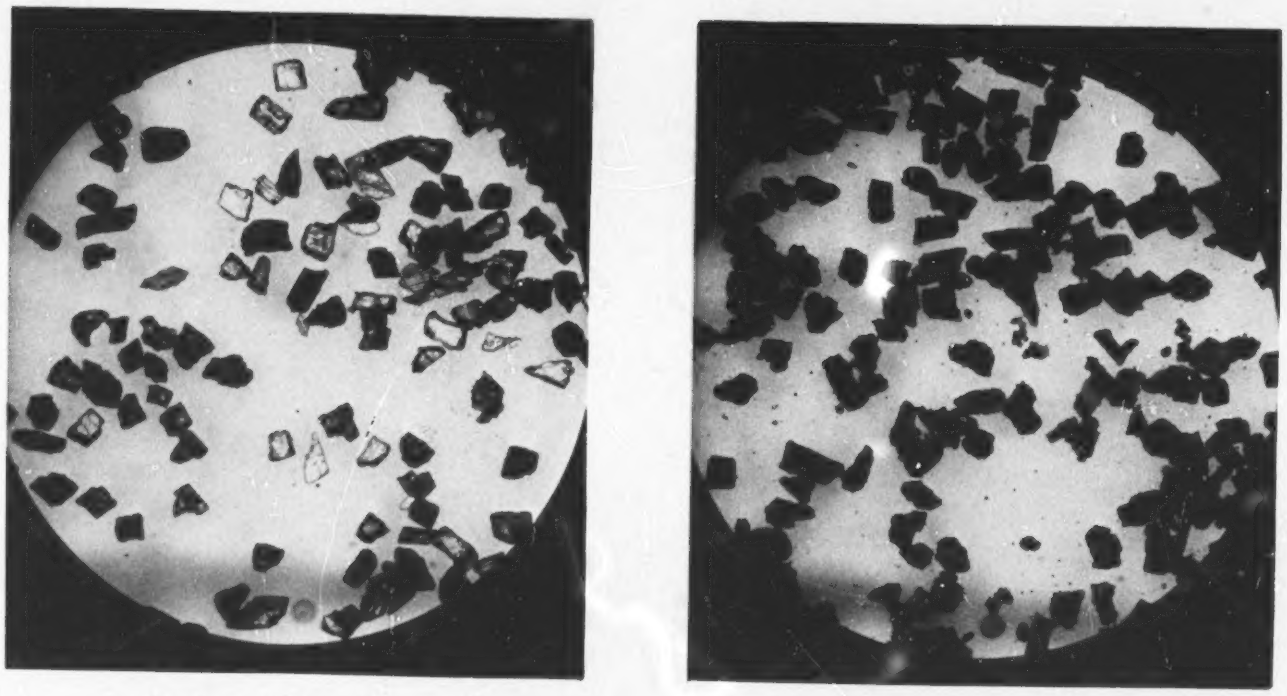

Before Reaction

After Reaction

d. IGS 2

FIGURE 11. (Continued)

Scale: 1 in. = 435 μ

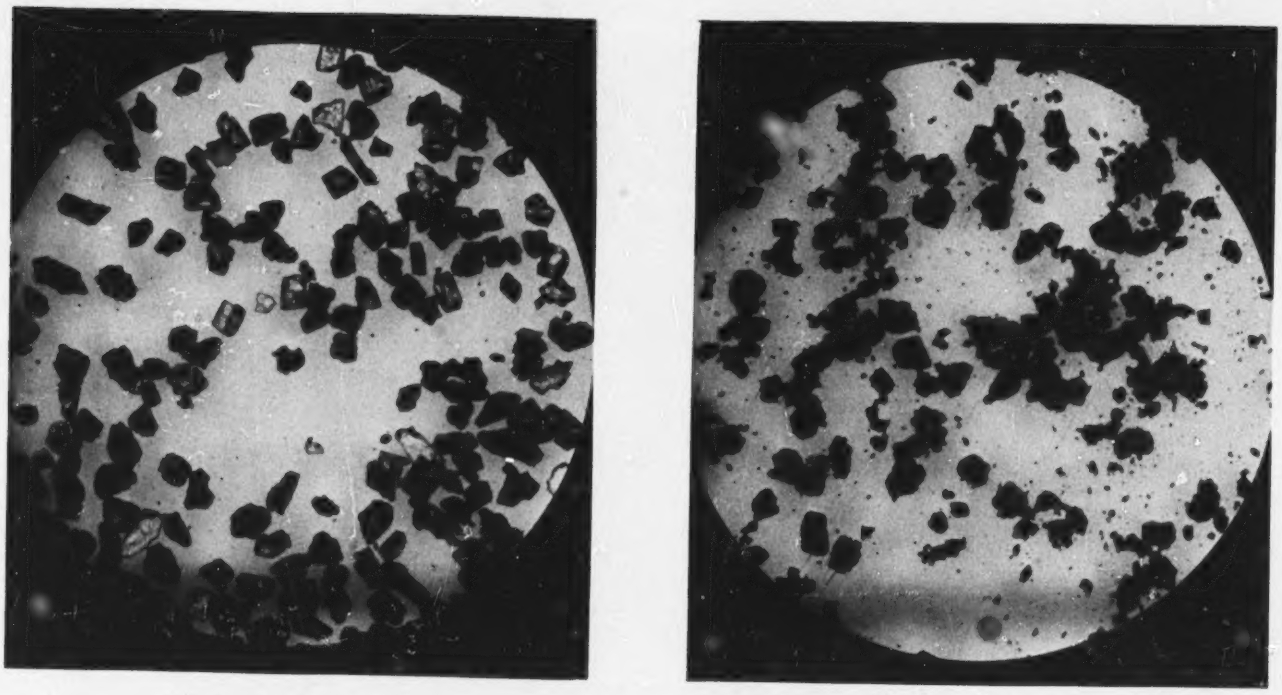

Before Reaction

After Reaction

e. IGS 3

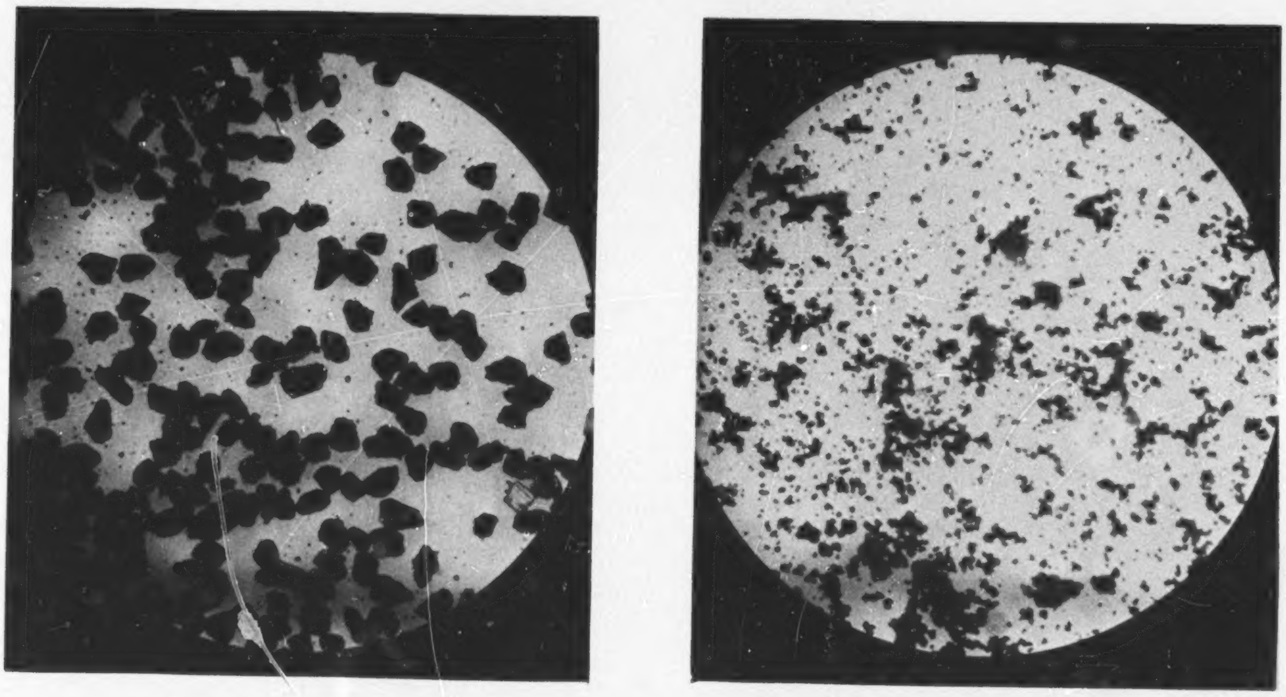

Before Reaction

After Reaction

f. IGS 4

FIGURE 11. (Continued)

Scale: 1 in. = 435 μ

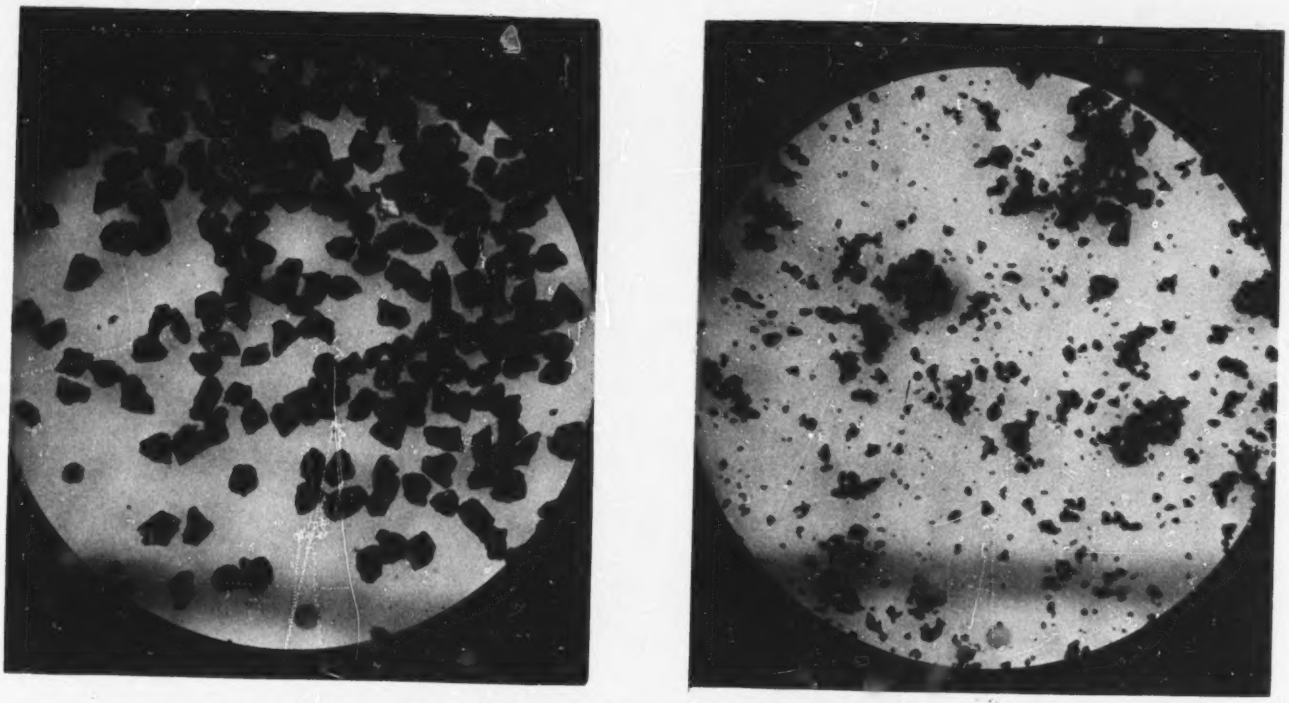

Before Reaction

After Reaction

g. IGS 5

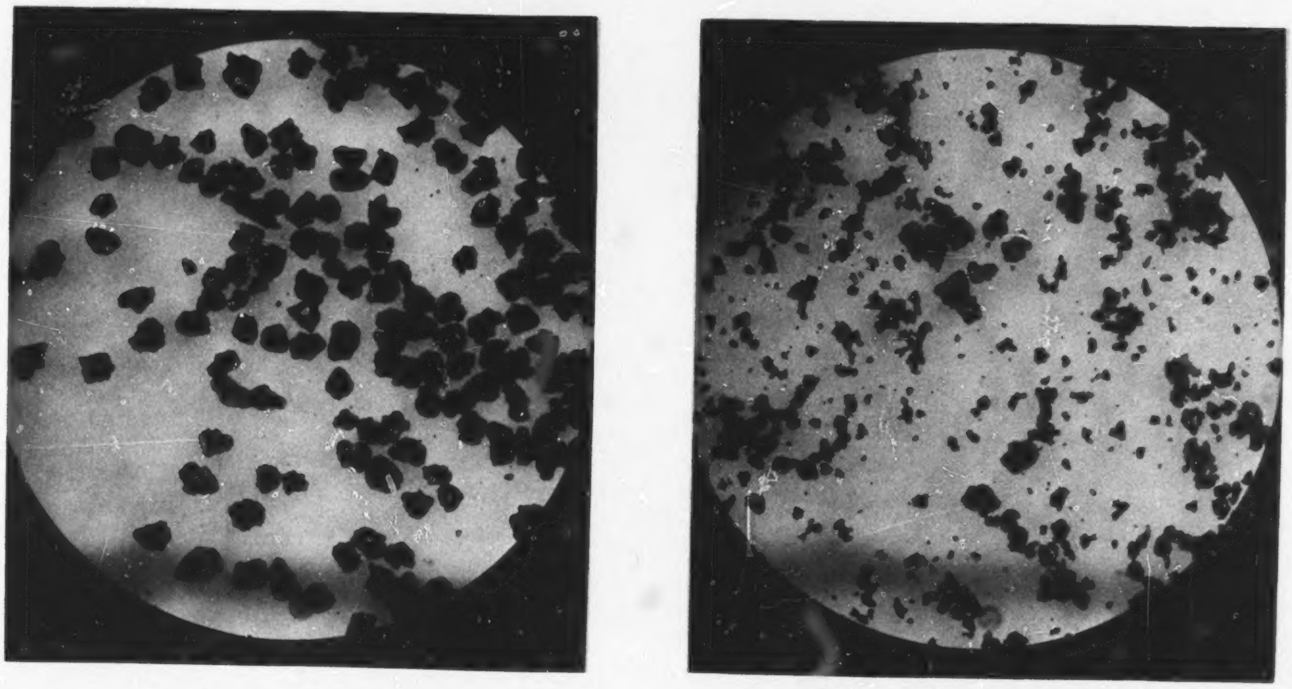

Before Reaction

After Reaction

h. IGS 6

FIGURE 11. (Continued)

Scale: 1 in. = 435 μ

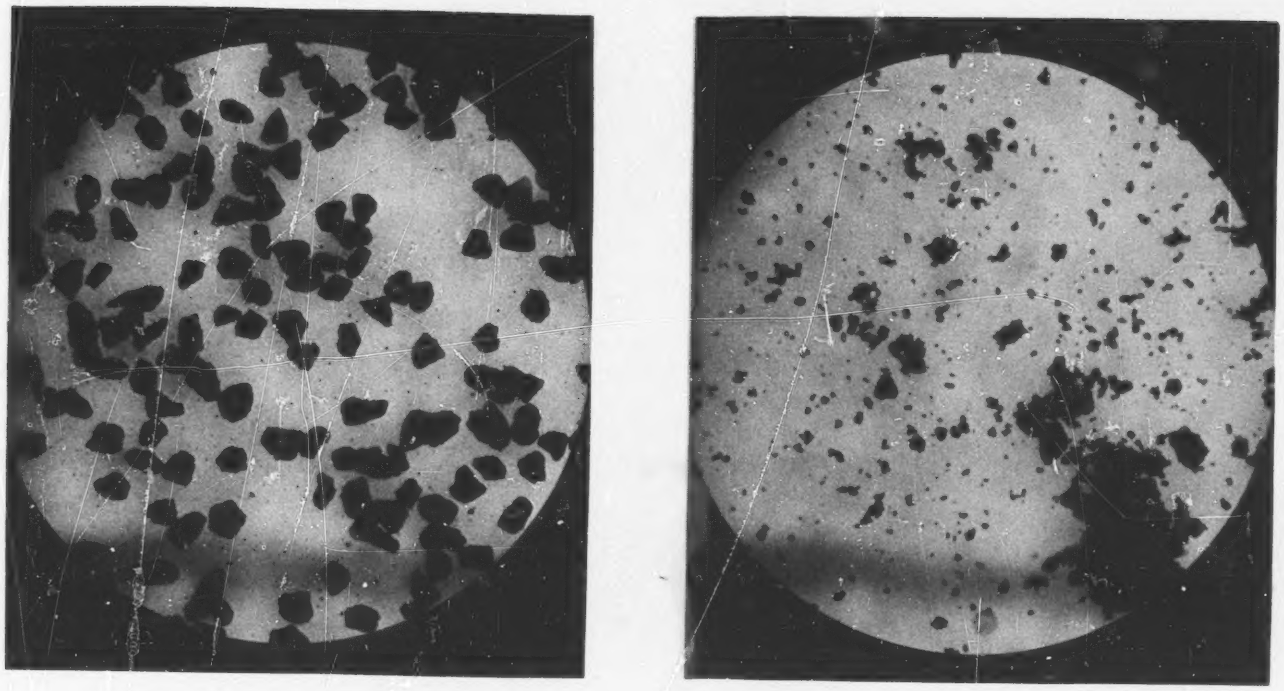

Before Reaction

After Reaction

i. IGS 7

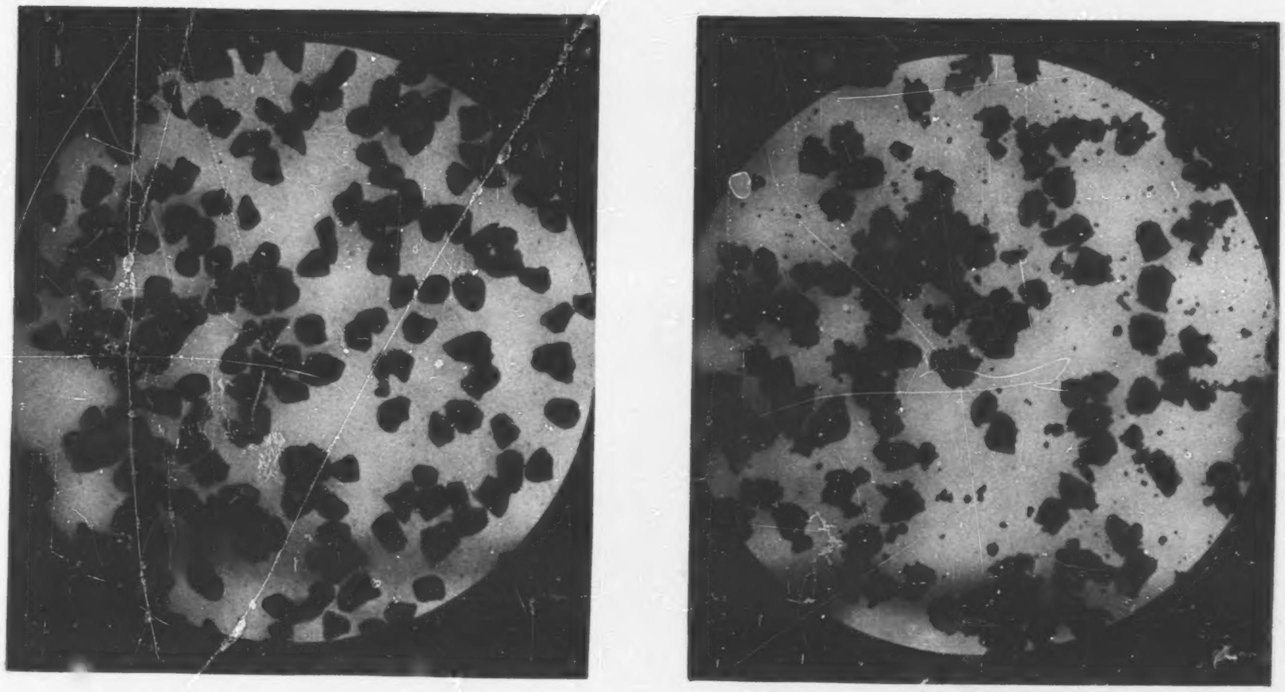

Before Reaction

After Reaction

j. IGS 8

FIGURE 11. (Continued)

These data could also be taken as a reflection of the importance of the relative dynamics of the calcination, sintering and reaction processes. The calcination process does act as a thermal buffer in protecting the particles from reaching too high a temperature (see Figure 17). The smaller the particles, the more rapid the calcination process, and hence the higher will be the maximum particle temperature. Thus the rate of sintering is also expected to be greater for small particles. At the same time, the rate of reaction is also greater for small particles*, but most of the reaction takes place while calcination is still occurring. That is, most of the reaction with SO_2 occurs before high temperatures and hence rapid sintering is encountered. It is therefore highly probable that additional sintering of small particles, such as those produced by fragmentation in the DPR, took place after essentially all of the SO_2 reaction had occurred. In other words, the measured terminal surface areas are not representative of areas available during the actual course of reaction. This is also shown by comparison of data in Tables 4 and 5 where it is indicated that surface areas depend on the time of exposure in the DPR.

Calcination of Limestone

A theoretical model of the calcination of limestone was presented in the November 20, 1970, Summary Report.(3) This model was based on a representation of the heat and mass transfer processes occurring during calcination. The model has now been extended to permit simulation of the calcination process under non-isothermal conditions similar to those encountered in the DPR or a boiler. To accomplish this, the original computer program given in the Summary Report has been modified in several ways:

---

* As indicated on Page 21 the maximum loading, b, is influenced only slightly by decreased particle size, but the rate constant, k, is approximately inversely proportional to particle size.

(1) The model now takes into account the effects of the actual variation in gas temperature from the injection point to the collection point in the DPR. This replaces the previous approximation of constant gas temperature at some mean value. This change has made an appreciable difference in the results, particularly for the longer residence times. The percentage calcination was found to be much more sensitive to the higher rates of calcination obtained for gas temperatures near the injection point.

(2) The computer output format was modified from that given in Appendix D of the Summary Report to show the position of the particle between points and the gas temperature at this position as functions of time. In addition, the following information is printed out regarding the calcination front at each time: calcination front radius, calcination temperature, calcination pressure, and circumferential tensile stress. When the particle has reached the sampling point, the profile of temperature, pressure and stress as functions of radial position are also printed out.

(3) The model was made completely dynamic by including the effects of the time rate of change in gas density in the gas flow continuity equation and also of the inertia term in the gas-diffusion equation. Closer attention was also given to more accurate representations of the effects of porosity and also of the boundary conditions at the calcination front. A listing of the modified program is given in Appendix D.

Application of the Model

Comparison With Experimental Work. Comparison of the computed results of the extended model has been made with experimental results cited in the Summary Report. In doing this, more realistic values of pore radii have been used based on the porosimetry results cited earlier in this report.

The encircled points on Figure 12 are the computed values of percentage calcination as a function of residence time for the central port (nominal) gas temperature of 1600 F, assuming values of 100 Å for the pore radius and 90 μ for the particle diameter. These computed points are seen to alternate in vertical position about some average curve, which is not drawn, probably because the extent of calcination is more sensitive to the value of the initial port temperature than to the final port temperature. Lower lying points correspond to the same initial port temperature, but to a lower final port temperature than those for their neighboring points to the left.

The smooth curve on Figure 12 is drawn through the experimental data for the nominal gas temperature of 1604 F. Except for the initial point, there is considerable disagreement between the experimental and computed results.

Variation of Pore Radius and Particle Diameter. Figure 13 shows the effects of altering the values of either the pore radius or particle diameter alone on the computed calcination percentage values. Here again, the smooth curve represents the experimental data. Although best agreement is obtained for the pore radius value of 400 Å, all computed variations of calcination percentage with residence time exhibit a much more gradual decrease in slope with increased residence time than is obtained experimentally.

Figure 14 indicates that a reasonably good agreement can be obtained by adjusting both the pore radius and particle diameter. It is difficult to justify the combination of 16 times the nominal pore radius and the 50 percent increase over the nominal particle diameter. An effective particle diameter that is somewhat smaller than actual can be justified in terms of the increased ratio of surface area to volume characteristic of departures of the particle shapes from the perfect sphericity assumed for the computations.

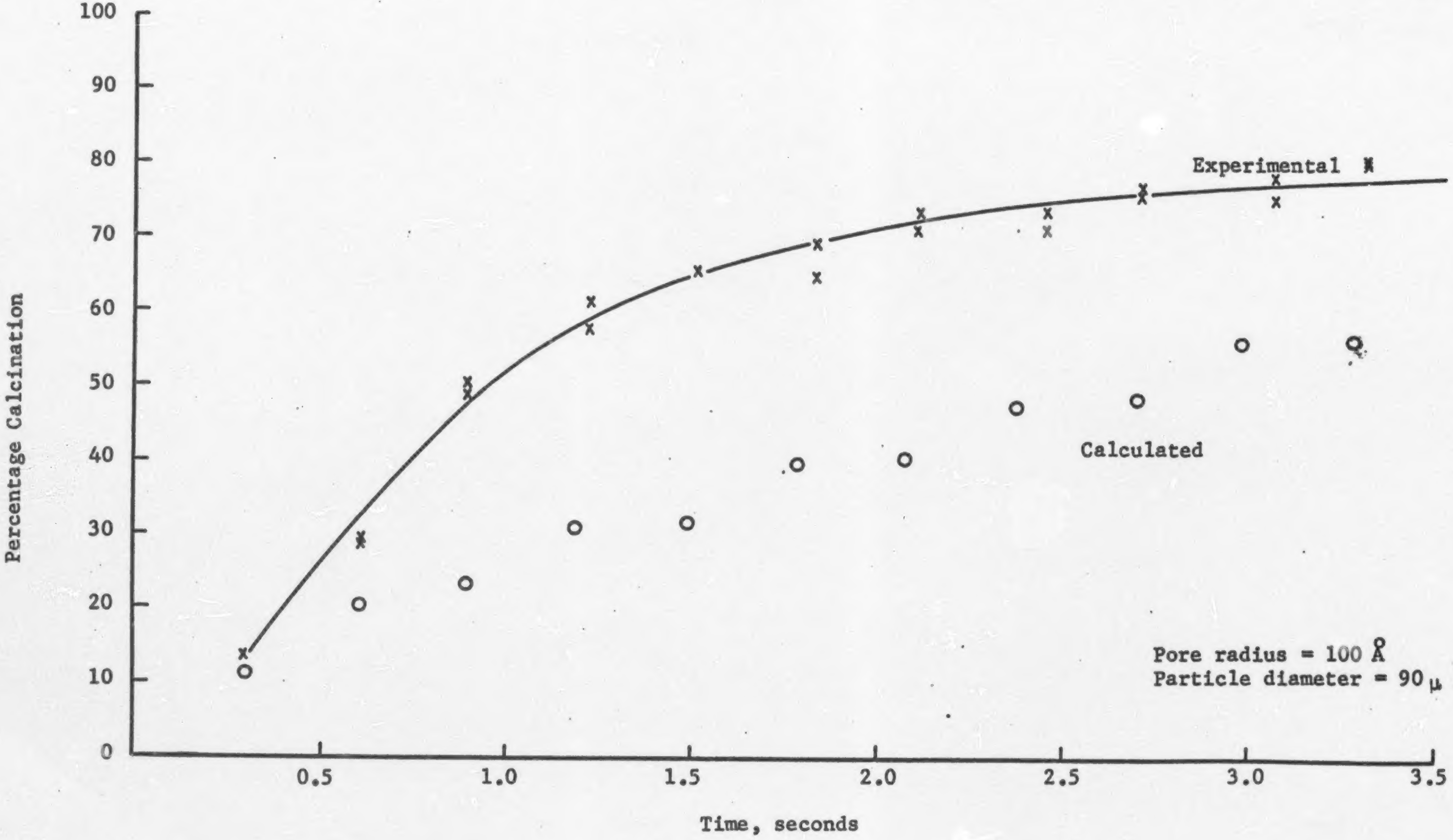

FIGURE 12. CALCINATION OF LIMESTONE AT 1600 F

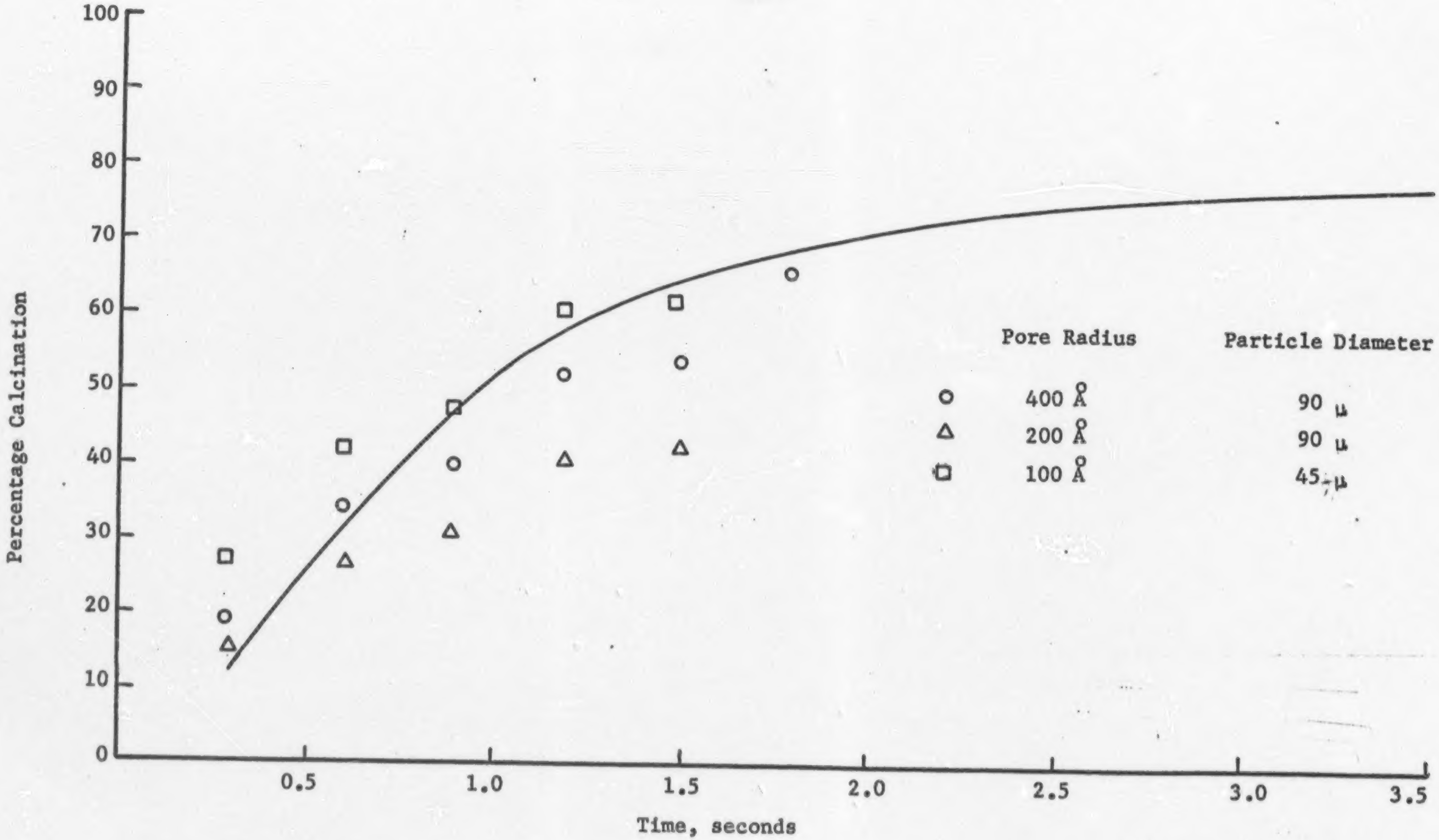

FIGURE 13. EFFECT OF VARIATION OF PORE RADIUS AND PARTICLE SIZE ON CALCINATION AT 1600 F

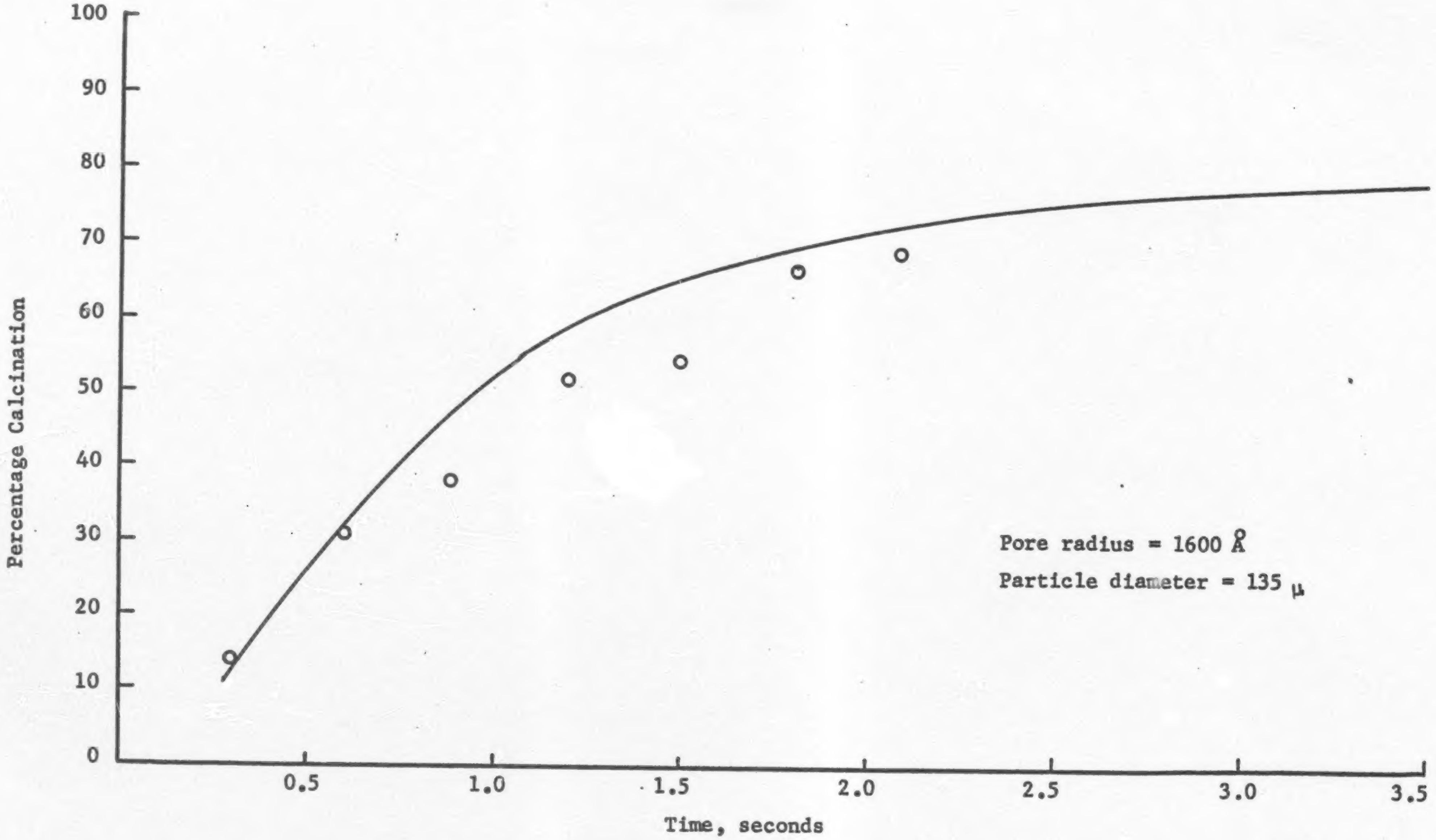

FIGURE 14. PARTICLE SIZE AND PORE RADIUS FOR FORCED FIT TO EXPERIMENT

The encircled points on Figure 15 are for the case of the nominal value of 90 μ for the particle diameter in combination with 8 times the nominal pore radius. Except for the two uppermost points at somewhat over 80 percent calcination, it is evident that agreement with the experimental curve would be good if the experimental curve were shifted about 0.2 second to the left. A time delay in the onset of calcination of this amount would account for the discrepancy, such as could possibly correspond to the time required to inject the particles into the gas stream and for the injection gas to disperse.

Variation of Heat Transfer Coefficient. Another possible cause of the discrepancy is an actual value for the heat transfer coefficient for the boundary layer between flue gas and particle surface that is smaller than the theoretical one because of departures from the assumed sphericity. The points enclosed by triangles on Figure 15 are computed values for which the heat transfer coefficient has been reduced by 50 percent. Agreement with the experimental curve is good, except for the two uppermost curves which predict about 10 percent more calcination than is actually observed.

The true situation may well correspond to an effective particle diameter near the nominal average particle diameter, an effective pore size between 4 to 8 times the nominal pore size, and some combination of a reduced value of the boundary-layer heat-transfer coefficient and delay in the onset of calcination. The effective value of the pore radius may well be several times that of the observed pore size because of the presence of cracks in the particle. Even a few small cracks extending partially in the radial direction could reduce greatly the effective value of the diffusion constant. The circumferential stresses produced in the particle by the radial pressure gradient, to be discussed later, are such as to tend to open radial cracks.

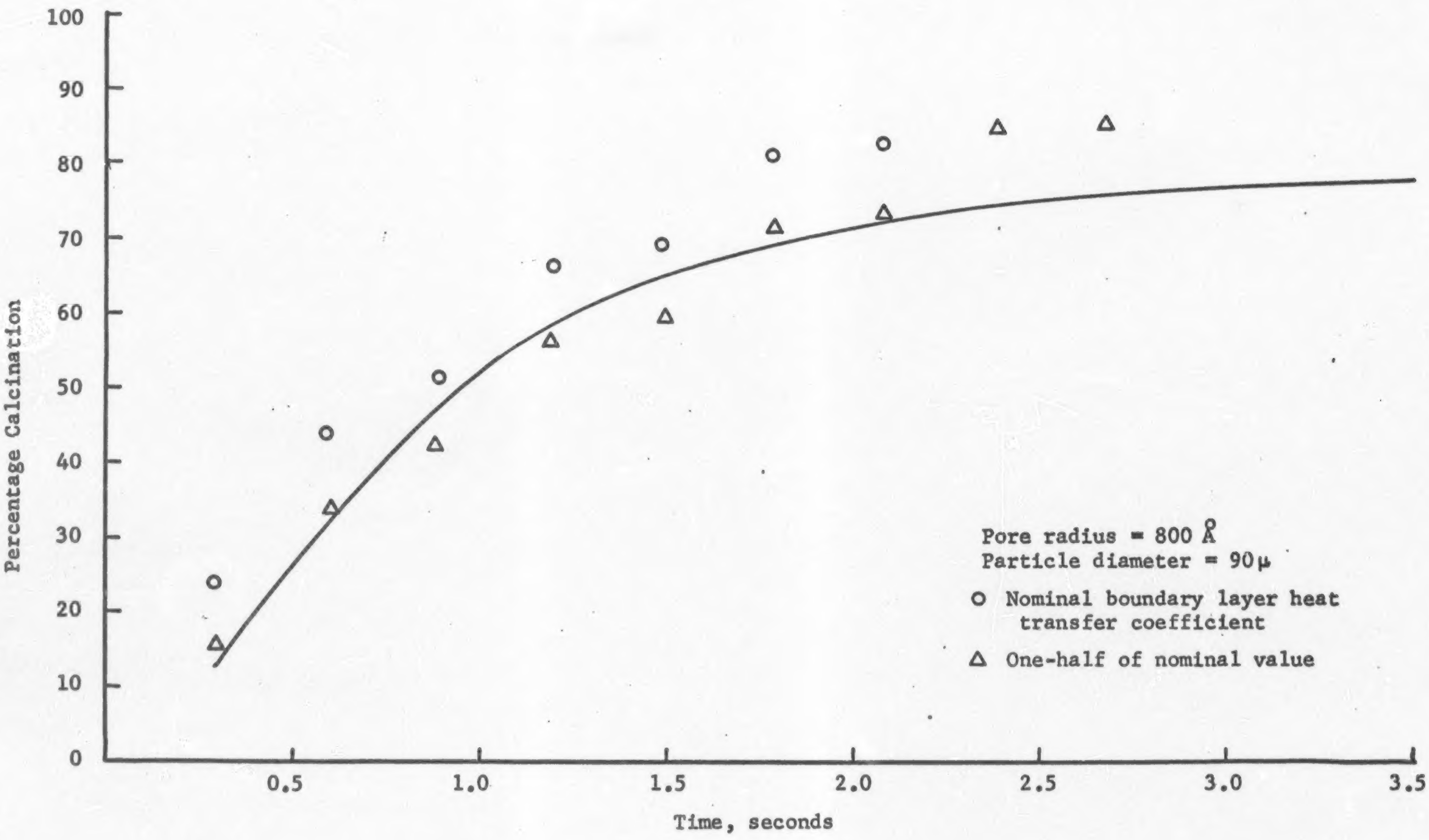

FIGURE 15. VARIATION OF HEAT TRANSFER COEFFICIENT

Variation of Other Parameters. Several additional computations were made to ascertain the effects of altering other parameters whose assumed valued could be questioned. Changing the thermal conductivity value for the limestone by as much as a factor of two had little effect on the computed calcination values. Also, little effect was obtained by varying the specific heats of the calcined or uncalcined portions of the limestone particle. Likewise, altering the assumed initial particle temperature had little effect. Thus, the transfer of heat into the particle is largely controlled by the thermal conductance of the boundary layer.

Calcination at Higher Temperature. Figure 16 shows the results of computations for the 1770 F nominal temperature case, using 800 Å for the pore radius, for both the nominal and reduced values of the boundary layer heat transfer coefficient. The latter yields good agreement with experiment except for the prediction of about 10 percent more calcination for the uppermost points, as was also obtained at the lower nominal temperature.

Particle Temperature, Pressure, and Stress. Figure 17 shows a typical set of computed points for the nominal gas temperature of 1600 F. The gas temperature, Curve (a), is assumed to decrease linearly with time from 1825 F at the injection port to 1425 F at the particle sampling port. Curve (b) shows the particle temperature at the calcination front. The temperature on the outer surface of the particle never differs from this value by more than a fraction of a degree. Calcination begins at 0.064 second after injection, when the particle temperature is 1383 F, the calcination temperature corresponding to the 76 torr partial pressure of CO_2. The particle temperature quickly reaches a flat maximum value of 1643 F and then slowly declines, approaching the gas temperature asymptotically. Near the removal port, at 2.12 sec after injection, Curves (a) and (b) cross. At removal, the particle temperature is actually 2.6 F above the gas temperature.

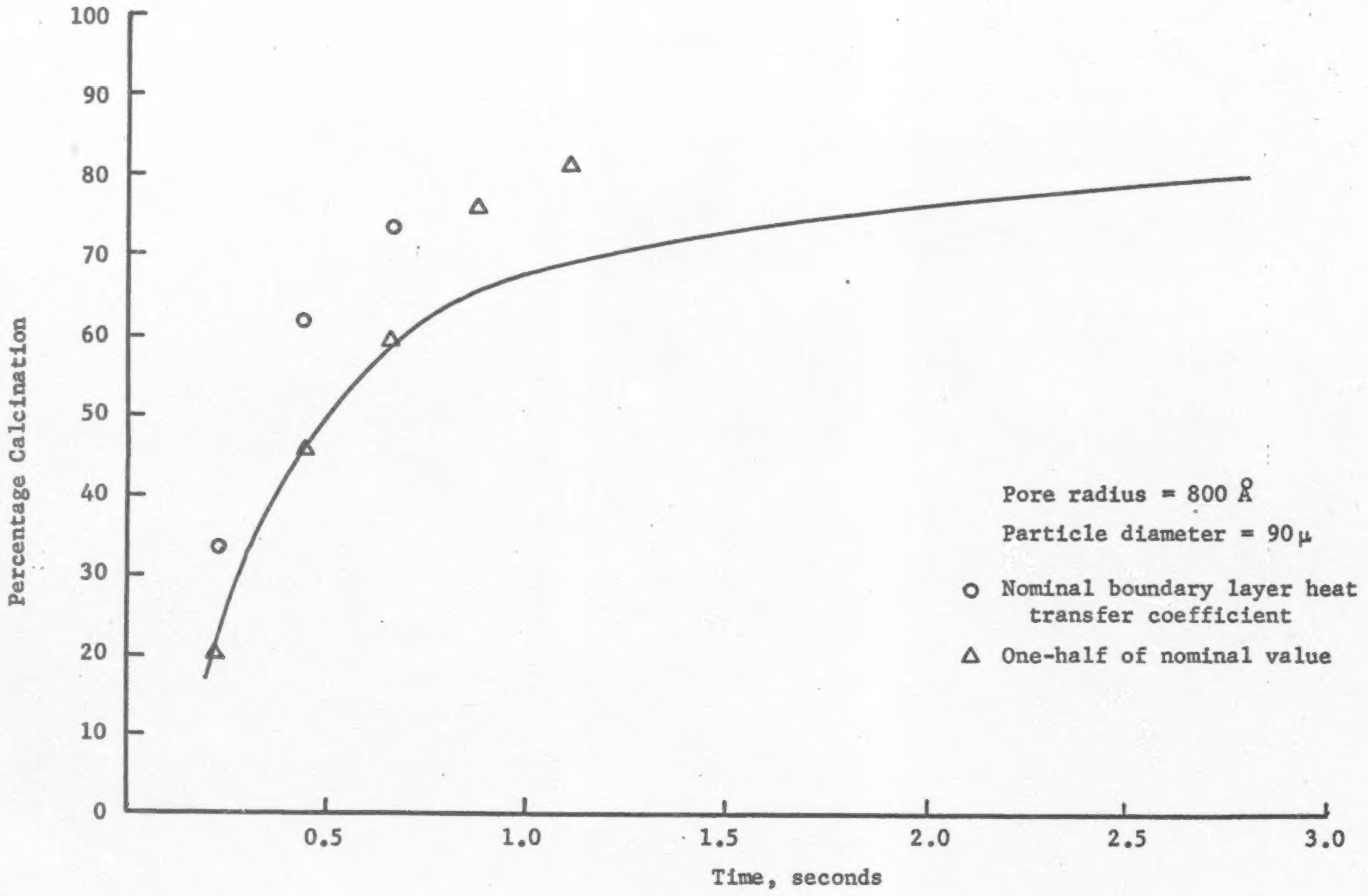

FIGURE 16. CALCINATION AT 1770 F

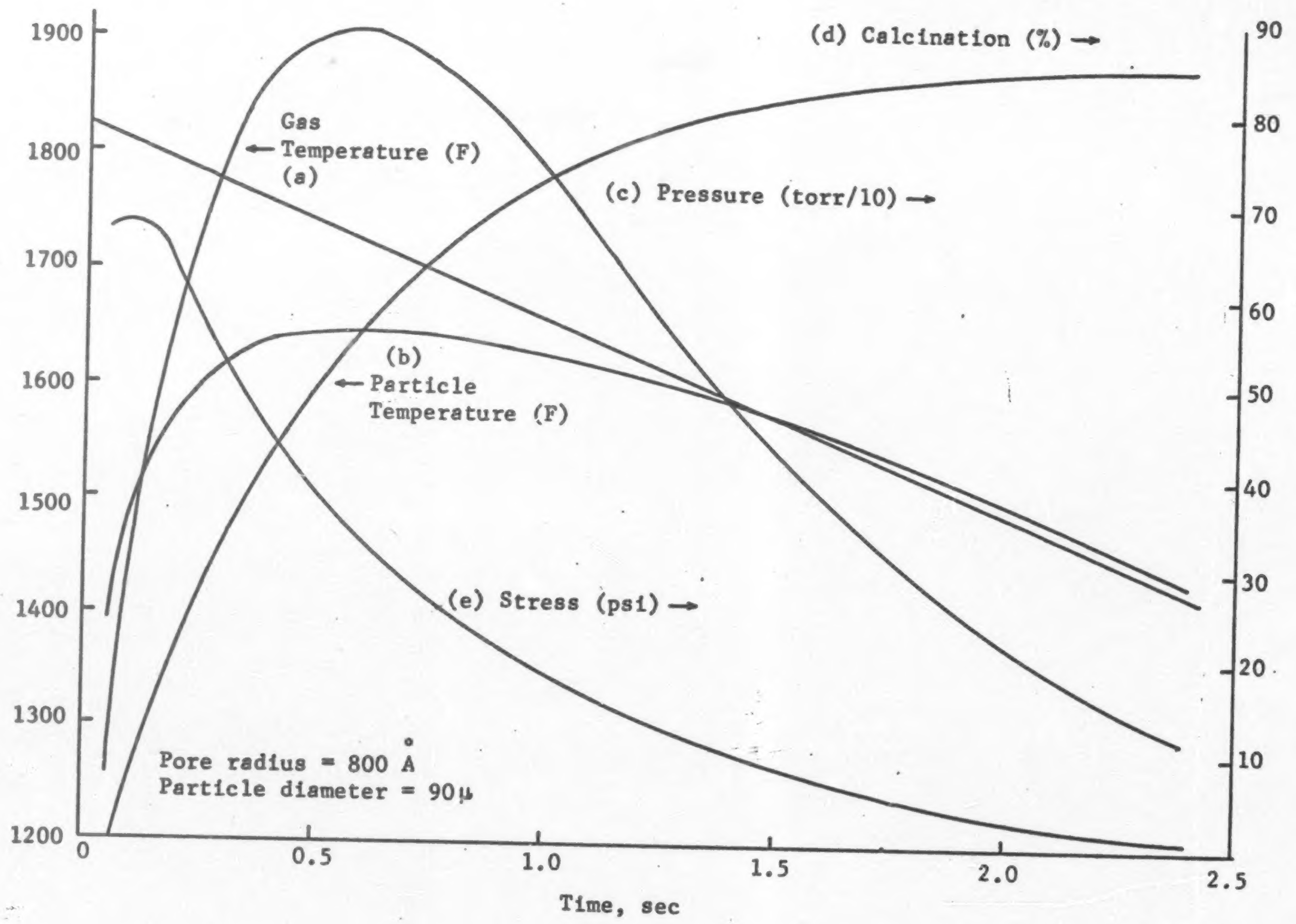

FIGURE 17. CALCINATION VARIABLES

Curve (c) of Figure 16 shows the variation in gas pressure at the calcination front. This gas pressure rises to a maximum value of 885 torr when the particle temperature reaches its maximum. The ordinates of Curves (b) and (c) are functionally related, since the calcination temperature is a function of pressure. Curve (d), the percentage calcination, increases rapidly with time at first and then slows down considerably as the particle temperature approaches gas temperature. The calcination process does not stop, but continues at a low rate, as the gas temperature drops below particle temperature. A portion of the outward flowing heat then also contributes to advancing the calcination front. Calcination does not cease altogether until the particle temperature has dropped below 1383 F, the calcination temperature at 76 torr.

Curve (e) of Figure 16 shows the circumferential stress in psi at the calcination front as a function of time. This is a tensile stress resulting from the high pressure gradient. Its value at any radial position is given by

$$\sigma = -\frac{1}{2} r \left(\frac{\partial p}{\partial r}\right)$$

where r is the radius and $(\partial p/\partial r)$ is the pressure gradient. The maximum tensile stress of almost 68 psi is reached soon after calcination begins. Later, it declines rapidly even though the pressure is increasing, because of the decreasing value of the pressure gradient resulting from the increasing distance between the calcination fraction and the outer surface of the particle. This more than compensates for the increasing pressure. Since the tensile strength of limestone is several hundred psi, the maximum circumferential stress is nowhere near great enough to rupture the limestone particle in this case. However, it would affect significantly the degree of opening of radial cracks, and hence the effective value of the diffusion constant. Closing of these radial cracks as this stress decreases may account for the lower calcination percentages obtained experimentally for the higher residence times than are predicted theoretically in Figures 14 and 15 for assumed effective pore radii of 800 Å. In other words, the theory should be modified to incorporate a decreasing value of effective pore radius, corresponding to a decreasing diffusion coefficient as the circumferential tensile stress decreases.

REFERENCES

(1) R. Coutant, R. E. Barrett, and E. H. Lougher, Summary Report on "Investigation of the Reactivity of Limestone and Dolomite for Capturing SO_2 From Flue Gas", to NAPCA, August 30, 1968, Contract No. PH 86-67-115.

(2) R. Coutant, R. E. Barrett, and E. H. Lougher, Summary Report on "Investigation of the Reactivity of Limestone and Dolomite for Capturing SO_2 From Flue Gas", to NAPCA, June 27, 1969, Contract No. PH 86-67-115.

(3) R. Coutant, R. E. Barrett, and E. H. Lougher, Summary Report on "Investigation of the Reactivity of Limestone and Dolomite for Capturing SO_2 From Flue Gas", to NAPCA, November 20, 1970, Contract No. PH 86-67-115.

(4) T. D. Womble, et al., "Presentation of Full-Scale Dry Limestone Injection Project at Shawnee Steam Plant", paper presented at the Dry Limestone Injection Process Symposium, Gilbertsville, Ky., June 22-26, 1970.

(5) R. H. Borgwardt, et al., "Alkaline Additives for Sulfur Dioxide Control", Annual Report from Division of Control Systems to APCO, EPA, March 29, 1971.

(6) R. D. Harvey, "Petrographic and Mineralogical Characteristics of Carbonate Rocks Related to Sorption of Sulfur Oxides in Flue Gases", Interim Report to NAPCA, June 22, 1970.

(7) Y. Ishihara, "Kinetics of the Reaction of Calcined Limestone with Sulfur Dioxide in Combustion Gases", paper presented at the Dry Limestone Injection Process Symposium, Gilbertsville, Ky. June 22-26, 1970.

(8) R. C. Attig and P. Sedor, "Additive Injection for Sulfur Dioxide Control, A Pilot Plant Study", Research Center Report 5460 from The Babcock & Wilcox Company to NAPCA, March 27, 1970.

(9) W. T. Reid, et al., "Fundamental Study of Sulfur Fixation by Lime and Magnesia", Final Report to Robert A. Taft Engineering Center, PHS, June 30, 1966.

(10) G. C. Kuczynski, Trans. AIME, 185, 169 (1949).

RWC:RS:ao

APPENDIX A

STONE ANALYSES

TABLE 1. CHEMICAL ANALYSES DATA

Stone No.	Percentage $MgCO_3$	Percentage $CaCO_3$	Weight Loss Percentage Calculated	Weight Loss Percentage Measured	ρ g/cc
IGS 1	0.16	99.9	44.04	44.17	2.57±0.03
IGS 2	0.70	99.3	43.94	43.80	2.64±0.01
IGS 3	7.89	92.4	44.49	44.76	2.71±0.01
IGS 4	0.45	99.0	43.78	44.23	2.73±0.01
IGS 5	44.2	55.7	46.56	48.88	2.86
IGS 6	41.3	49.9	42.52	42.48	2.77±0.1
IGS 7	97.8 98.3	3.08 3.00	50.02	48.10	2.82±0.01
IGS 8	2.66 2.58	94.8 94.6	42.95	41.03	2.48±0.02
BCR 1336	3.72 2.57	97.4 98.8	44.65	42.95	2.70
Michigan Marl	4.00	80.7	37.46	37.95	2.05±0.1
2061(new)	1.87	99.0	44.49	43.68	2.67±0.04
2061(old)	0.75	93.9	41.6	41.5	2.58

APPENDIX B

REACTOR DATA

- Effect of Time-Temperature Profile
- Effect of Particle Size
- Effect of SO_2 Concentration
- Effect of Time and Temperature on Pore Structure
- Reactivities of Ten Stones

TABLE B-1. EFFECT OF TIME-TEMPERATURE PROFILE

Run No.	Gas Temperature F		Residence Time, sec	Product Analysis					Percentage Utilization		mg SO_3 Per Gram Calcine	Percentage Calcination	Gas Analysis,$^{(e)}$ volume percent		
	Injection	Collection		Weight mg	Total$^{(a)}$ Sulfur	$SO_4^=$$^{(a)}$	$CO_2$$^{(b)}$ mg	$H_2O$$^{(b)}$ mg	Actual$^{(c)}$	Apparent$^{(d)}$			SO_2	CO_2	O_2
1015-B	2402	2179	0.45	10.08	7.0	5.4	0.20	1.75	4.1	3.9	54.9	96.2	0.306	10.0	3.0
1015-C	2402	2114	0.82	10.00	11.3	9.1	0.15	1.75	6.3	6.1	86.8	97.1	0.306	10.0	3.0
1015-E	2179	2114	0.37	10.09	16.1	13.2	0.19	1.69	9.1	8.8	124	96.4	0.306	10.0	3.0
1015-G	2345	1730	1.38	10.07	18.0	16.9	0.15	1.73	9.9	9.6	136	97.1	0.306	10.0	3.0
1015-K	2179	1730	1.04	10.10	22.4	19.6	0.20	1.60	12.9	12.3	175	96.1	0.306	10.0	3.0
1015-L	2070	1730	0.80	10.62	21.6	19.8	0.36	1.56	13.3	12.3	175	93.2	0.306	10.0	3.0
1015-N	2014	1730	0.67	10.03	20.9	17.2	0.20	1.61	12.0	11.5	163	96.1	0.306	10.0	3.0
1015-P	1901	1730	0.41	10.12	19.7	15.5	0.55	1.46	12.5	11.0	156	89.1	0.306	10.0	3.0
1015-S	1843	1730	0.28	10.02	18.0	12.8	1.00	1.28	12.9	10.1	142	79.8	0.306	10.0	3.0
1022-A	2565	2216	0.27	9.97	12.0	10.8	0.14	1.63	7.1	6.9	95.8	97.3	0.294	10.0	3.0
1022-C	2565	1996	0.49	9.90	11.7	10.1	0.15	1.71	6.6	6.4	88.8	97.1	0.294	10.0	3.0
1022-E	2216	1996	0.30	10.03	19.3	17.1	0.41	1.45	12.3	11.1	154	91.6	0.294	10.0	3.0
1022-G	2565	1693	0.91	10.78	15.0	13.8	0.55	1.65	9.3	8.3	115	89.9	0.294	10.0	3.0
1022-J	2216	1693	0.64	10.06	21.4	19.9	0.35	1.50	13.1	12.1	167	93.0	0.294	10.0	3.0
1022-L	2138	1693	0.57	11.60	19.5	18.4	0.38	1.80	11.6	10.8	150	93.5	0.294	10.0	3.0
1022-N	1996	1693	0.42	10.19	19.4	17.5	0.54	1.48	12.3	10.9	150	89.3	0.294	10.0	3.0
1022-P	1865	1693	0.26	10.23	15.5	11.4	1.06	1.28	11.5	8.8	122	78.8	0.294	10.0	3.0
1022-R	1805	1693	0.17	10.01	9.6	7.3	2.34	0.71	12.4	5.7	78.7	49.4	0.294	10.0	3.0

(a) Weight percent as $CaSO_4 \cdot 2H_2O$.

(b) Thermogravimetric weight losses.

(c) Based on actual amount of CaO formed.

(d) Based on total CaO content of sample.

(e) Dry basis.

TABLE B-2 EFFECT OF PARTICLE SIZE
(-270+325 mesh No.2061)

Run No.	Gas Temperature F Inject	Gas Temperature F Collect	Residence Time, sec	Product Analysis Weight, mg	Product Analysis Total Sulfur[(a)]	Product Analysis CO_2[(b)] mg	Product Analysis H_2O[(b)] mg	Percentage Utilization Actual[(c)]	Percentage Utilization Apparent[(d)]	mg SO_3 Per Gram Calcine	Percentage Calcination	Gas Analysis,[(e)] volume percent SO_2	Gas Analysis, volume percent CO_2	Gas Analysis, volume percent O_2
421-A	1967	1906	0.15	9.98	6.5	2.23	0.76	8.20	3.90	54.1	47.6	0.303	10.0	3.0
421-B	1967	1843	0.31	9.93	10.6	0.70	1.66	6.22	5.36	74.2	86.1	0.303	10.0	3.0
421-C	2030	1843	0.45	10.08	15.2	0.30	1.71	8.57	8.04	111	93.8	0.303	10.0	3.0
421-D	2030	1776	0.61	10.20	14.3	0.26	1.70	8.24	7.79	108	94.6	0.303	10.0	3.0
421-E	2095	1776	0.75	10.14	16.4	0.20	1.75	9.05	8.68	120	95.9	0.303	10.0	3.0
421-F	2095	1712	0.92	10.09	18.2	0.33	1.66	10.38	9.67	134	93.2	0.303	10.0	3.0
421-G	2157	1712	1.06	10.04	17.2	0.20	1.80	9.12	8.76	121	96.0	0.303	10.0	3.0
421-H	2157	1646	1.23	9.80	20.1	0.20	1.65	11.11	10.64	147	95.8	0.303	10.0	3.0
421-J	2220	1645	1.36	10.25	18.2	0.16	1.83	9.64	9.34	129	96.9	0.303	10.0	3.0
421-K	2220	1582	1.54	10.04	17.8	0.25	1.75	9.66	9.17	127	95.0	0.303	10.0	3.0

(a) Weight percent as $CaSO_4 \cdot 2H_2O$.

(b) Thermogravimetric weight losses.

(c) Based on actual amount of CaO formed.

(d) Based on total CaO content of sample.

(e) Dry basis.

TABLE B-3 EFFECT OF SO_2 CONCENTRATION

Run No.	Gas Temperature F Injection	Gas Temperature F Collection	Residence Time sec	Product Analysis Weight, mg	Product Analysis Total Sulfur[a]	Product Analysis $SO_4^=$[a]	Product Analysis CO_2[b] mg	Product Analysis H_2O[b] mg	Percentage Utilization Actual[c]	Percentage Utilization Apparent[d]	mg SO_3 Per Gram Calcine	Percentage Calcination	Gas Analysis[e] volume percent SO_2	Gas Analysis[e] volume percent CO_2	Gas Analysis[e] volume percent O_2
111-A	2341	1908	0.74	10.04	3.0	3.0	0.28	1.90	1.63	1.54	21.4	94.8	0.013	10.0	3.0
111-C	2341	1844	0.88	9.99	6.3	6.3	0.39	1.70	3.73	3.42	47.4	92.5	0.013	10.0	3.0
111-E	2341	1780	1.02	10.04	3.0	2.3	0.20	1.83	1.69	1.62	22.5	96.2	0.013	10.0	3.0
111-G	2341	1715	1.16	10.00	2.6	1.9	0.45	1.80	1.49	1.35	18.7	91.6	0.013	10.0	3.0
111-J	2341	1654	1.31	10.01	2.8	2.4	0.40	1.73	1.67	1.53	21.1	92.4	0.013	10.0	3.0
111-L	2341	1593	1.47	10.07	4.4	4.4	0.25	1.83	2.47	2.34	32.5	95.3	0.013	10.0	3.0
111-P	2263	1780	0.90	10.01	2.6	2.4	0.50	1.79	1.50	1.35	18.7	90.6	0.013	10.0	3.0
111-T	2263	1654	1.20	10.04	3.3	3.1	0.60	1.75	1.94	1.71	23.7	88.7	0.013	10.0	3.0
111-V	2263	1593	1.35	10.04	3.8	3.7	0.36	1.85	2.11	1.96	27.2	93.2	0.013	10.0	3.0
111-X	2191	1780	0.79	10.03	3.6	3.2	0.61	1.68	2.20	1.92	26.6	88.4	0.013	10.0	3.0
111-AA	2191	1715	0.93	10.03	5.0	4.3	0.35	1.85	2.76	2.57	35.6	93.5	0.013	10.0	3.0
111-CC	2191	1654	1.08	10.08	4.7	4.3	0.70	1.61	2.99	2.55	35.3	86.6	0.013	10.0	3.0
111-DD	2191	1593	1.23	10.09	5.1	4.5	0.53	1.71	3.05	2.72	37.7	90.0	0.013	10.0	3.0
123-A	2321	1928	0.71	9.99	4.9	4.5	0.33	1.85	2.69	2.52	34.9	93.8	0.025	10.0	3.0
123-C	2321	1866	0.84	10.08	5.5	5.4	0.51	1.73	3.24	2.91	40.3	90.4	0.025	10.0	3.0
123-E	2321	1804	0.97	9.93	6.8	4.7	0.40	1.84	3.70	3.41	47.2	92.5	0.025	10.0	3.0
123-G	2321	1744	1.10	10.00	5.1	3.8	0.60	1.79	2.90	2.56	35.4	88.8	0.025	10.0	3.0
123-J	2321	1684	1.24	10.07	6.6	4.8	0.54	1.76	3.80	3.39	47.0	89.9	0.025	10.0	3.0
123-L	2321	1626	1.39	9.96	6.4	5.9	0.65	1.66	3.86	3.35	46.4	87.5	0.025	10.0	3.0

TABLE B-3 EFFECT OF SO_2 CONCENTRATION (continued)

Run No.	Gas Temperature, F Injection	Gas Temperature, F Collection	Residence Time sec	Product Analysis Weight mg	Product Analysis Total Sulfur[(a)]	Product Analysis $SO_4^=$[(a)]	Product Analysis CO_2 mg[(b)]	Product Analysis H_2O mg[(b)]	Percentage Utilization Actual[(c)]	Percentage Utilization Apparent[(d)]	mg SO_3 Per Gram Calcine	Percentage Calcination	Gas Analysis[(e)] volume percent SO_2	Gas Analysis volume percent CO_2	Gas Analysis volume percent O_2
123-N	2253	1866	0.73	10.01	6.6	5.0	0.31	1.83	3.64	3.41	47.3	94.2	0.025	10.0	3.0
123-P	2253	1904	0.86	9.94	6.2	5.8	0.30	1.85	3.37	3.17	43.9	94.4	0.025	10.0	3.0
123-R	2253	1744	0.99	10.09	6.3	5.5	0.75	1.63	3.92	3.32	46.0	85.7	0.025	10.0	3.0
123-T	2253	1684	1.13	10.04	7.0	6.1	0.63	1.68	4.19	3.66	50.7	88.0	0.025	10.0	3.0
123-V	2253	1626	1.28	9.93	7.7	6.9	0.40	1.74	4.40	4.03	55.9	92.4	0.025	10.0	3.0
123-X	2186	1804	0.75	10.04	5.1	5.0	0.70	1.66	3.13	2.68	37.1	86.7	0.025	10.0	3.0
123-AA	2186	1744	0.88	10.04	6.5	6.0	0.48	1.80	3.66	3.31	45.8	91.0	0.025	10.0	3.0
123-CC	2186	1684	1.02	10.00	6.6	5.8	0.43	1.74	3.82	3.48	48.2	91.8	0.025	10.0	3.0
123-EE	2186	1626	1.17	10.00	9.4	7.9	0.55	1.70	5.47	4.86	67.4	89.5	0.025	10.0	3.0
121-A	2350	1971	0.76	9.96	5.1	4.0	0.51	1.79	2.88	2.59	35.9	90.4	0.065	10.2	2.8
121-C	2350	1912	0.90	10.01	4.6	4.0	0.60	1.66	2.82	2.47	34.2	88.5	0.065	10.2	2.8
121-E	2350	1854	1.04	9.93	5.0	4.3	0.39	1.85	2.73	2.52	34.9	92.7	0.065	10.2	2.8
121-G	2350	1796	1.19	10.04	5.1	4.1	0.55	1.75	2.97	2.64	36.6	89.7	0.065	10.2	2.8
121-J	2350	1739	1.34	10.01	5.5	4.3	0.70	1.64	3,39	2.90	40.2	86.6	0.065	10.2	2.8
121-L	2350	1684	1.49	10.00	5.5	4.9	0.58	1.70	3.27	2.89	40.0	89.0	0.065	10.2	2.8
121-N	2284	1912	0.78	9.97	4.8	5.2	0.65	1.70	2.86	2.48	34.4	87.6	0.065	10.2	2.8
121-P	2284	1854	0.92	10.06	5.2	5.0	0.35	1.85	2.87	2.67	37.0	93.5	0.065	10.2	2.8
121-R	2284	1796	1.07	9.98	5.5	5.4	0.56	1.70	3.27	2.89	40.1	89.3	0.065	10.2	2.8
121-T	2284	1739	1.22	10.04	6.3	5.9	0.56	1.68	3.79	3.35	46.4	89.3	0.065	10.2	2.8

TABLE B-3 EFFECT OF SO_2 CONCENTRATION
(continued)

Run No.	Gas Temperature F		Residence Time sec	Product Analysis					Percentagw Utilization		mg SO_3 Per Gram Calcine	Percentage Calcination	Gas Analysis[(e)] volume percent		
	Injec-tion	Collec-tion		Weight mg	Total Sulfur[(a)]	$SO_4^=$[(a)]	CO_2[(b)] mg	H_2O[(b)] mg	Actual[(c)]	Apparent[(d)]			SO_2	CO_2	O_2
121-V	2284	1684	1.37	10.01	6.0	5.7	0.61	1.73	3.51	3.08	42.6	88.5	0.065	10.2	2.8
121-X	2220	1854	0.80	10.06	6.3	5.8	0.70	1.69	3.78	3.25	45.0	86.8	0.065	10.2	2.8
121-AA	2220	1796	0.95	10.01	7.0	5.6	0.65	1.61	4.36	3.76	52.1	87.5	0.065	10.2	2.8
121-CC	2220	1739	1.09	9.95	7.5	6.7	0.40	1.76	4.25	3.90	54.1	92.4	0.065	10.2	2.8
121-EE	2220	1684	1.25	10.01	7.1	6.0	0.43	1.76	4.05	3.70	51.3	91.9	0.065	10.2	2.8

TABLE B-3 EFFECT OF SO_2 CONCENTRATION (continued)

Run No	Gas Temperature F Injection	Gas Temperature F Collection	Residence Time sec	Product Analysis Weight, mg	Product Analysis Total Sulfur	Product Analysis $SO_4^{=(a)}$	Product Analysis $CO_2^{(b)}$ mg	Product Analysis $H_2O^{(b)}$ mg	Percentage Utilization Actual[(c)]	Percentage Utilization Apparent[(d)]	mg SO_3 Per Gram Calcine	Percentage Calcination	Gas Analysis[(e)] volume percent SO_2	Gas Analysis[(e)] volume percent CO_2	Gas Analysis[(e)] volume percent O_2
1210-A	2329	1990	0.72	10.80	21.3	17.7	0.19	1.81	11.7	11.3	157	96.4	0.398	10.0	3.0
1210-C	2329	1936	0.85	10.21	16.6	14.8	0.24	1.68	9.6	9.1	126	95.0	0.398	10.0	3.0
1210-E	2329	1884	0.98	10.08	15.7	14.1	0.31	1.66	9.1	8.5	118	93.5	0.398	10.0	3.0
1210-G	2329	1832	1.12	9.94	17.9	15.3	0.34	1.75	9.6	9.0	124	93.3	0.398	10.0	3.0
1210-J	2329	1781	1.26	10.03	18.2	17.0	0.26	1.70	10.1	9.6	133	94.7	0.398	10.0	3.0
1210-L	2329	1731	1.40	10.06	19.0	17.1	0.49	1.55	11.4	10.3	142	89.7	0.398	10.0	3.0
1210-N	2271	1936	0.74	9.96	18.4	14.9	0.33	1.68	10.3	9.6	132	93.3	0.398	10.0	3.0
1210-P	2271	1884	0.87	10.40	19.5	17.8	0.36	1.65	11.4	10.6	146	92.7	0.398	10.0	3.0
1210-R	2271	1832	1.01	10.20	19.6	17.0	0.25	1.74	10.7	10.2	141	95.0	0.398	10.0	3.0
1210-T	2271	1781	1.14	10.28	18.2	16.9	0.15	1.81	9.8	9.5	131	97.0	0.398	10.0	3.0
1210-V	2271	1731	1.29	10.20	19.3	18.3	0.24	1.70	10.8	10.3	142	95.1	0.398	10.0	3.0
1210-X	2213	1884	0.75	10.00	18.4	18.0	0.25	1.69	10.2	9.7	134	94.9	0.398	10.0	3.0
1210-AA	2213	1832	0.89	10.44	18.7	18.2	0.28	1.73	10.6	10.0	138	94.4	0.398	10.0	3.0
1210-CC	2213	1781	1.03	9.97	21.6	20.1	0.46	1.50	13.1	11.8	163	90.2	0.398	10.0	3.0
1210-EE	2213	1731	1.17	10.09	19.4	17.6	0.30	1.65	11.0	10.4	144	93.8	0.398	10.0	3.0
1202-A	2368	1979	0.69	10.02	10.5	8.7	0.45	1.70	6.08	5.52	76.5	90.8	0.160	10.0	3.0
1202-C	2368	1921	0.71	10.35	10.7	9.1	0.26	1.84	5.93	5.62	77.9	94.8	0.160	10.0	3.0
1202-E	2368	1864	0.84	10.03	11.4	9.5	0.29	1.78	6.30	5.93	88.2	94.1	0.160	10.0	3.0
1202-G	2368	1809	0.97	9.94	11.6	10.3	0.25	1.73	6.52	6.18	85.6	94.8	0.160	10.0	3.0

TABLE B-3 EFFECT OF SO_2 CONCENTRATION
(continued)

Run No.	Gas Temperature F Injec-tion	Gas Temperature F Collec-tion	Residence Time, sec	Product Analysis Weight, mg	Product Analysis Total Sulfur$^{(a)}$	Product Analysis $SO_4^{=}$$^{(a)}$	Product Analysis $CO_2$$^{(b)}$ mg	Product Analysis $H_2O$$^{(b)}$ mg	Percentage Utilization Actual$^{(c)}$	Percentage Utilization Apparent$^{(d)}$	mg SO_3 Per Gram Calcine	Percentage Calcination	Gas Analysis,$^{(e)}$ volume percent SO_2	Gas Analysis,$^{(e)}$ volume percent CO_2	Gas Analysis,$^{(e)}$ volume percent O_2
1202-J	2368	1756	1.11	10.05	11.7	10.6	0.18	1.83	6.30	6.07	84.1	96.4	0.160	10.0	3.0
1202-L	2368	1705	1.25	10.02	14.4	13.2	0.55	1.55	8.88	7.84	108.6	88.3	0.160	10.0	3.0
1202-N	2299	1921	0.71	10.00	11.4	9.6	0.19	1.81	6.18	5.94	82.4	96.1	0.160	10.0	3.0
1202-P	2299	1864	0.83	9.99	12.2	9.2	0.20	1.78	6.69	6.41	88.8	95.9	0.160	10.0	3.0
1202-R	2299	1809	0.97	10.00	11.7	9.8	0.29	1.78	6.44	6.06	83.9	94.1	0.160	10.0	3.0
1202-T	2299	1756	1.10	9.98	12.6	10.4	0.30	1.75	6.99	6.57	91.0	93.9	0.160	10.0	3.0
1202-V	2299	1705	1.24	9.95	13.6	10.8	0.24	1.75	7.49	7.12	98.6	95.1	0.160	10.0	3.0
1202-X	2231	1864	0.72	9.98	11.6	9.2	0.24	1.75	6.47	6.15	85.2	95.0	0.160	10.0	3.0
1202-AA	2231	1809	0.86	9.94	11.5	10.8	0.25	1.75	6.40	6.07	84.1	94.8	0.160	10.0	3.0
1202-CC	2231	1756	0.99	10.00	12.1	11.0	0.21	1.80	6.57	6.29	87.2	95.7	0.160	10.0	3.0
1202-EE	2231	1705	1.13	10.00	13.1	12.0	0.21	1.75	7.26	6.95	96.3	95.7	0.160	10.0	3.0
1208-A	2320	1909	0.74	10.02	20.2	18.6	0.18	1.65	11.38	10.94	152	96.2	0.990	10.0	3.0
1208-C	2320	1850	0.88	10.04	22.4	21.1	0.16	1.63	12.62	12.19	169	96.6	0.990	10.0	3.0
1208-E	2320	1793	1.02	9.98	24.0	22.6	0.15	1.55	13.92	13.46	187	96.7	0.990	10.0	3.0
1208-G	2320	1738	1.16	10.03	24.8	23.2	0.28	1.50	14.79	13.88	192	93.9	0.990	10.0	3.0
1208-J	2320	1686	1.31	9.99	25.6	24.3	0.20	1.56	14.64	14.02	194	95.7	0.990	10.0	3.0
1208-L	2320	1637	1.46	10.00	26.4	25.4	0.25	1.48	15.73	14.87	206	94.5	0.990	10.0	3.0
1208-N	2245	1850	0.76	9.97	25.2	23.2	0.25	1.53	14.66	13.87	192	94.6	0.990	10.0	3.0
1208-P	2245	1793	0.90	10.03	24.9	24.2	0.21	1.59	14.12	13.49	187	95.9	0.990	10.0	3.0

TABLE B-3 EFFECT OF SO_2 CONCENTRATION
(continued)

Run No.	Gas Temperature F		Residence Time sec	Product Analysis					Percentage Utilization		mg SO_3 Per Gram Calcine	Percentage Calcination	Gas Analysis,[e] volume percent		
	Injection	Collection		Weight, mg	Total Sulfur	$SO_4^{=}$[a]	CO_2[b] mg	H_2O[b] mg	Actual[c]	Apparent[d]			SO_2	CO_2	O_2
1208-R	2245	1738	1.05	10.03	27.1	23.9	0.34	1.45	16.40	15.18	210	92.6	0.990	10.0	3.0
1208-T	2245	1686	1.19	10.28	27.5	25.6	0.25	1.50	16.47	15.59	216	94.6	0.990	10.0	3.0
1208-V	2245	1637	1.34	10.16	27.8	25.6	0.44	1.46	16.84	15.27	212	90.7	0.990	10.0	3.0
1208-X	2173	1793	0.78	10.37	23.3	22.1	0.50	1.50	14.43	12.92	179	89.6	0.990	10.0	3.0
1208-AA	2173	1738	0.93	10.45	26.1	24.9	0.34	1.58	15.30	14.24	197	93.1	0.990	10.0	3.0
1208-CC	2173	1686	1.07	10.36	26.4	25.2	0.49	1.44	16.58	14.86	206	89.6	0.990	10.0	3.0
1208-EE	2173	1637	1.23	10.22	29.5	27.2	0.33	1.51	17.29	16.09	223	93.1	0.990	10.0	3.0

(a) Weight percent as $CaSO_4 \cdot 2H_2O$.

(b) Thermogravimetric weight losses.

(c) Based on actual amount of CaO formed.

(d) Based on total CaO content of sample.

(e) Dry basis.

TABLE B-4 REACTOR DATA - EFFECT OF TIME AND TEMPERATURE ON PORE STRUCTURE

Run No.	Gas Temperature F		Residence Time, sec	Product Analysis[(a)]			Percentage Calcination	Gas Analysis,[(b)] volume percent		
	Injection	Collection		Weight, mg	CO_2, mg	H_2O, mg		SO_2	CO_2	O_2
925-A	2224	1440	2.86	10.53	0.88	1.73	85.8	0	10.0	3.0
925-B	2224	1765	1.27	8.05	0.81	1.25	82.6	0	10.0	3.0
925-C	1830	1440	1.82	10.19	1.54	1.35	73.0	0	10.0	3.0
925-D	1830	1765	0.23	9.36	3.55	0.19	19.0	0	10.0	3.0
106-A	2245	2156	0.15	10.55	3.08	0.73	40.0	0	10.0	3.0
106-B	2156	2073	0.16	11.60	3.15	0.90	45.1	0	10.0	3.0
106-C	1996	1920	0.17	10.67	3.58	0.54	28.3	0	10.0	3.0
106-D	1920	1500	1.35	10.00	1.18	1.45	79.0	0	10.0	3.0
106-E	1849	1782	0.18	10.49	2.85	0.75	45.5	0	10.0	3.0
106-F	2243	1500	1.99	10.35	0.83	1.83	85.8	0	10.0	3.0

(a) Termogravimetric analysis data.

(b) Dry basis.

TABLE B-5 REACTIVITIES OF TEN STONES

Run No.	Stone Type	Gas Temperature, F		Residence Time, Sec	Product Analysis				Percentage Utilization		mg SO_3 Per Gram Calcine	Percentage Calcination	Gas Analysis,[e] volume percent		
		Inject	Collect		Weight, mg	Total Sulfur[a]	CO_2,[b] mg	H_2O,[b] mg	Actual[c]	Apparent[d]			SO_2	CO_2	O_2
56-A	Marl	2136	1475	2.27	10.16	31.2	0.33	0.85	28.07	25.19	260	89.8	0.299	10.0	3.0
56-B	1336	2136	1475	2.27	10.04	15.8	0.26	1.58	9.51	8.96	126	94.3	0.299	10.0	3.0
56-C	IGS1	2136	1475	2.27	10.21	15.0	0.21	1.75	8.39	8.03	115	95.7	0.299	10.0	3.0
56-D	IGS2	2136	1475	2.27	9.99	15.8	0.26	1.50	9.93	9.32	132	94.0	0.299	10.0	3.0
56-E	IGS3	2136	1475	2.27	10.47	23.5	0.[illegible]	1.63	13.66	13.37	178	97.9	0.299	10.0	3.0
56-F	IGS4	2136	1475	2.27	10.60	31.6	0.[illegible]	1.34	20.74	19.42	274	93.7	0.299	10.0	3.0
56-G	IGS5	2136	1475	2.27	10.81	38.4	0.20	0.89	32.80	30.89	259	94.2	0.299	10.0	3.0
56-H	IGS6	2136	1475	2.27	9.16	37.6	0.14	0.60	37.53	35.42	246	94.4	0.299	10.0	3.0
56-J	IGS7	2136	1475	2.27	9.92	15.7	0.0	0.58	--	--[f]	85	~100.	0.299	10.0	3.0
56-K	IGS8	2136	1475	2.27	10.35	23.0	0.40	1.56	13.77	12.63	168	91.7	0.299	10.0	3.0
56-L	IGS4	2136	1475	2.27	10.27	31.7	0.25	1.40	19.57	18.49	260	94.5	0.299	10.0	3.0
56-M	IGS3	2136	1475	2.27	10.32	24.8	0.18	1.65	13.97	13.45	179	96.3	0.299	10.0	3.0

(a) Weight percent as $CaSO_4 \cdot 2H_2O$.

(b) Thermogravimetric weight losses.

(c) Based on actural amount of CaO formed.

(d) Based on total CaO content of sample.

(e) Dry basis.

(f) Utilization of CaO ≈ 100 percent, utilization of MgO ≈ 1.4 percent.

APPENDIX C

PORE SIZE DISTRIBUTIONS

Sample No. - 925-A

Surface Area - 13.7 m^2/g sample

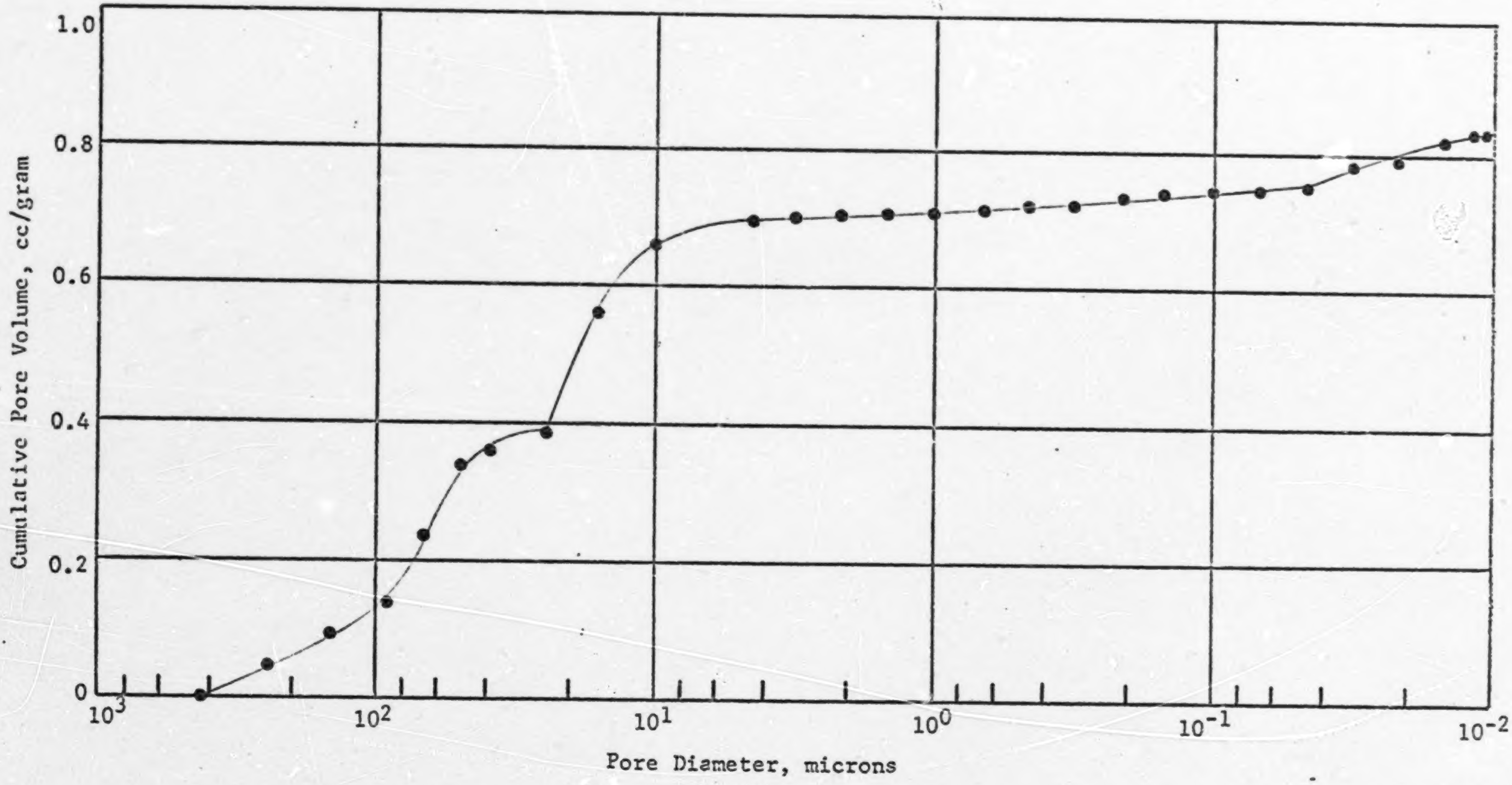

FIGURE C-1. PORE SIZE DISTRIBUTION

Sample No. - 925-B

Surface Area - 13.1 m^2/g sample

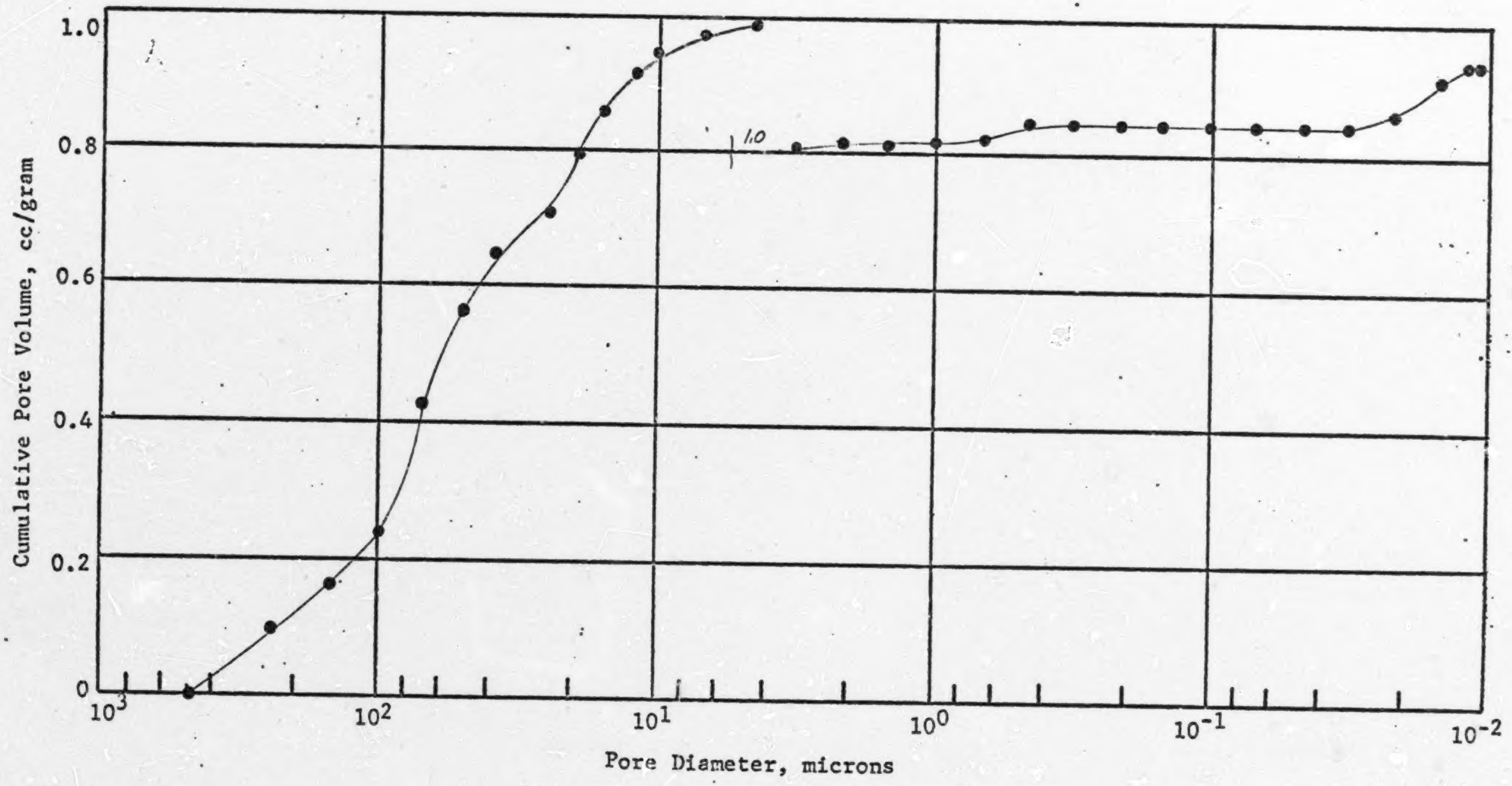

FIGURE C-2 PORE SIZE DISTRIBUTION

Sample No. - 925-C

Surface Area - 31.8 m^2/g

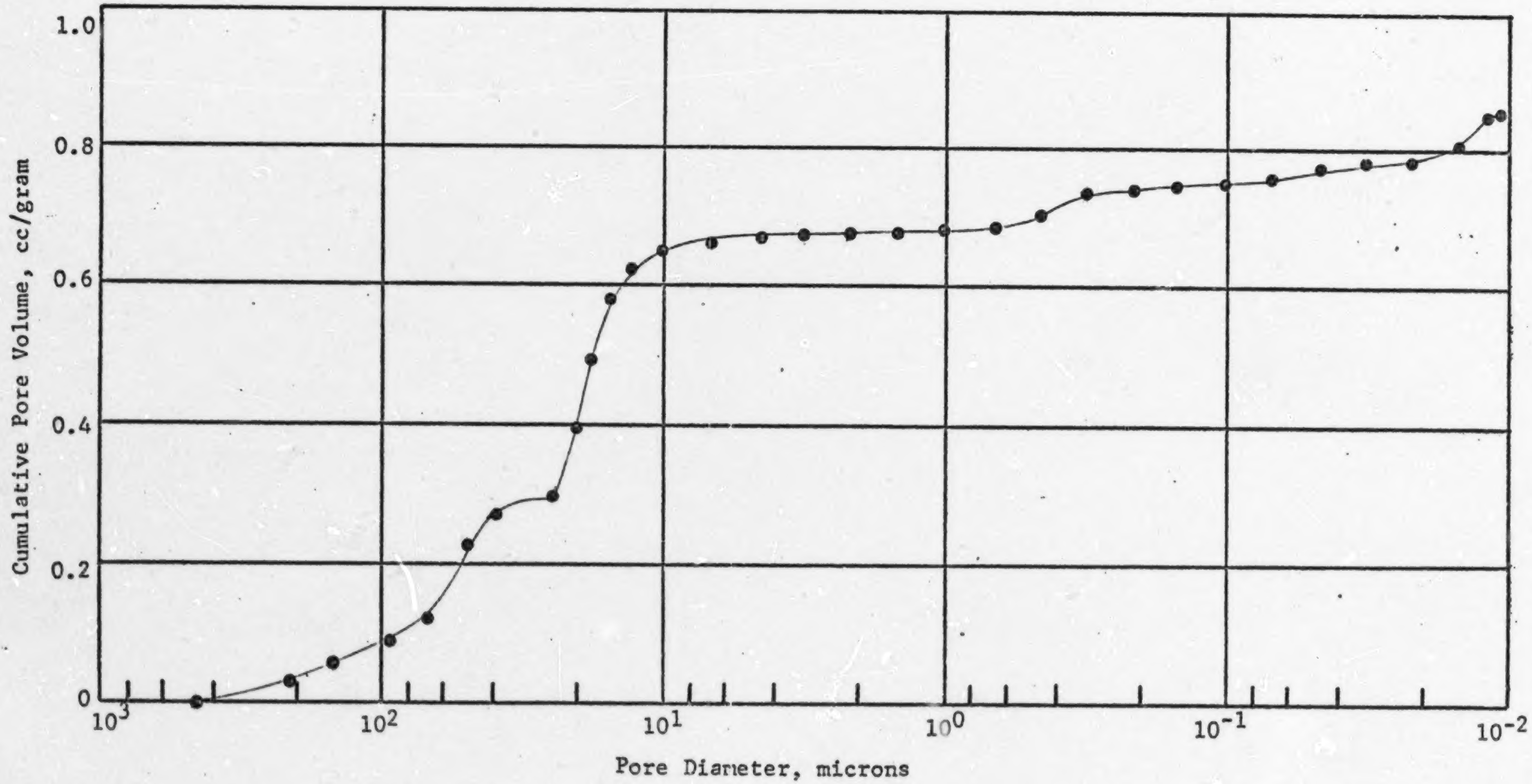

FIGURE C-3. PORE SIZE DISTRIBUTION

Sample No. - 925-D

Surface Area - 5.0 m^2/g

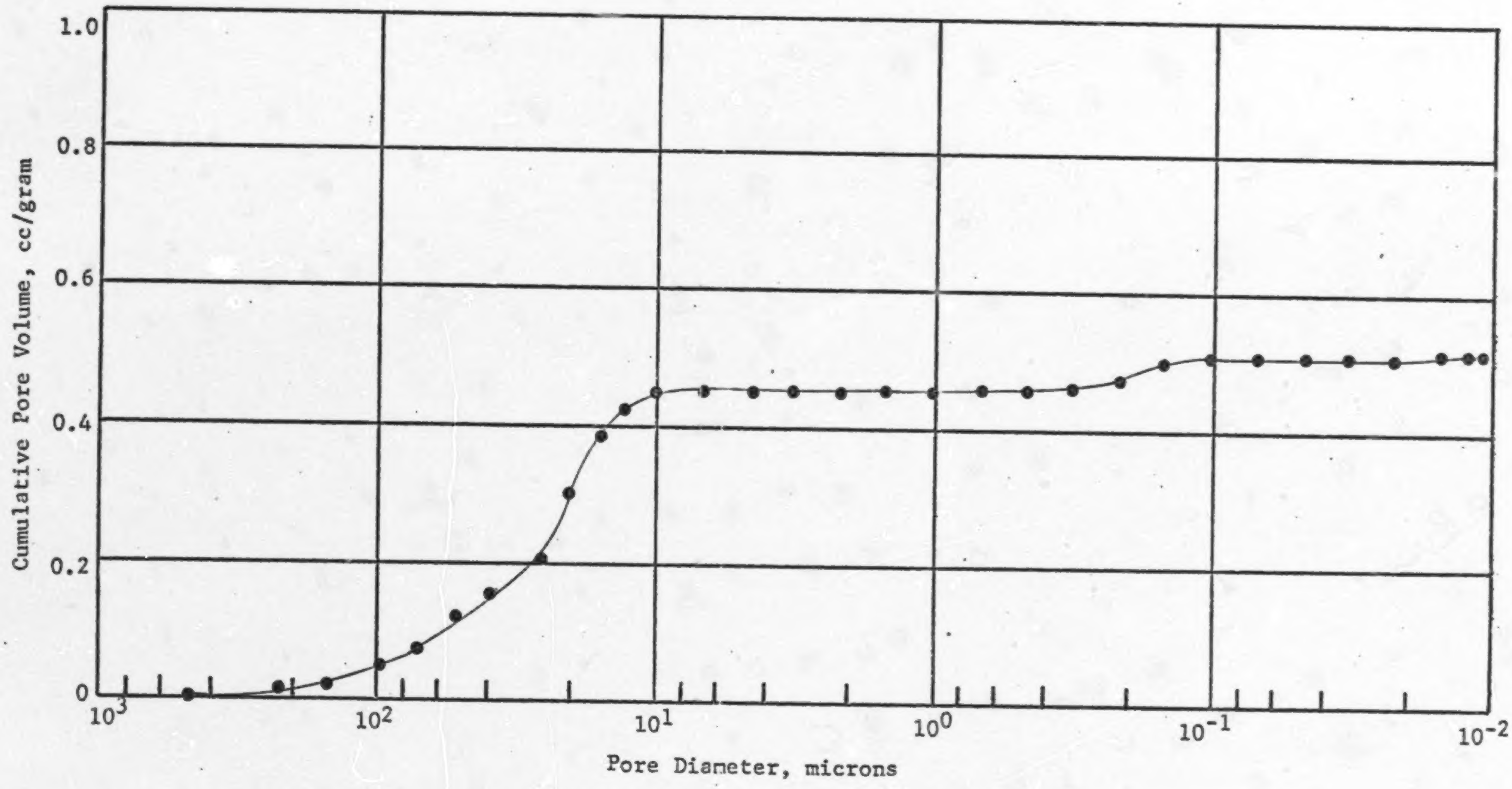

FIGURE C-4. PORE SIZE DISTRIBUTION

Sample No. - 106-A

Surface Area - 13.1 m^2/g

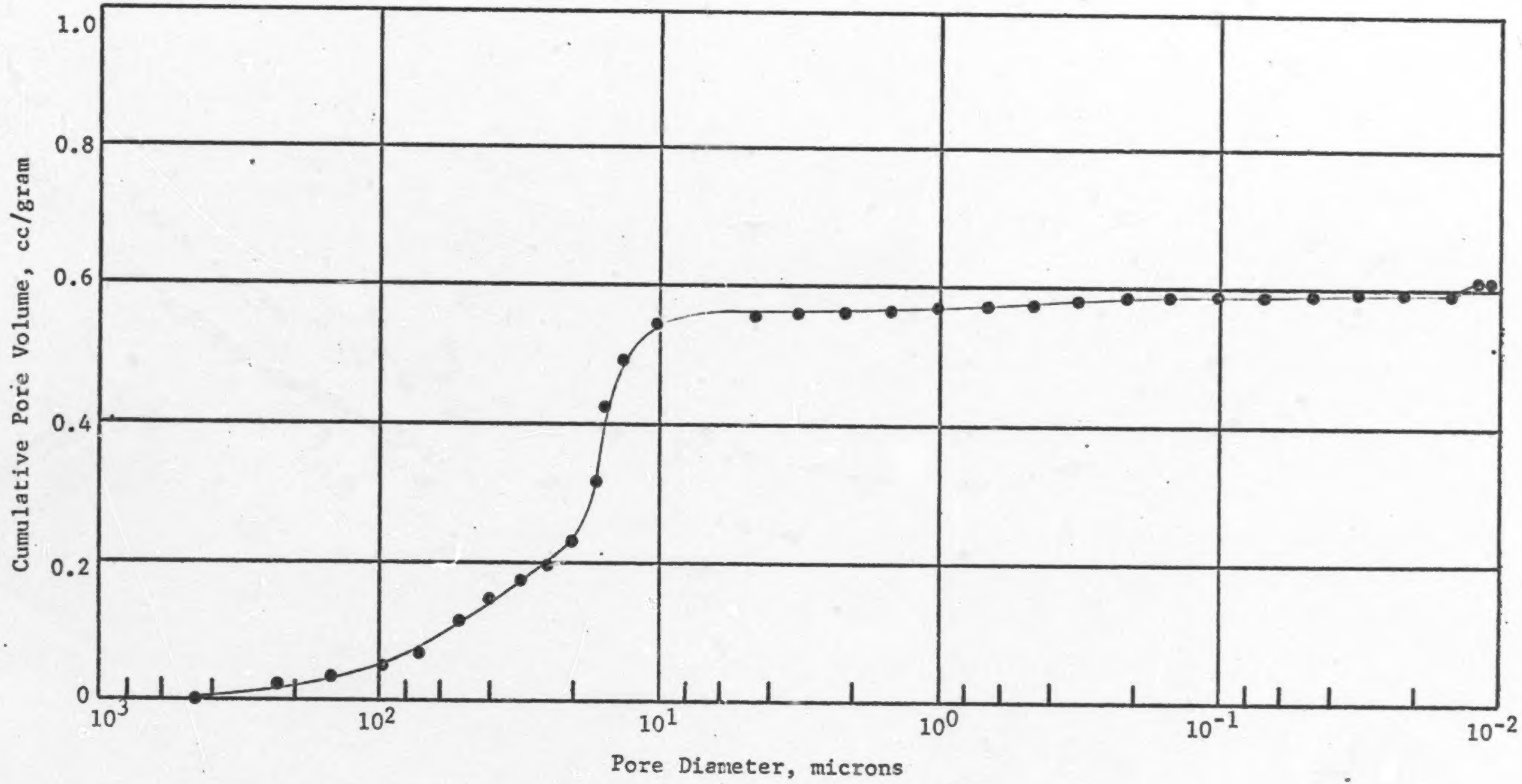

FIGURE C-5. PORE SIZE DISTRIBUTION

Sample No. - 106-B

Surface Area - 18.9 m^2/g

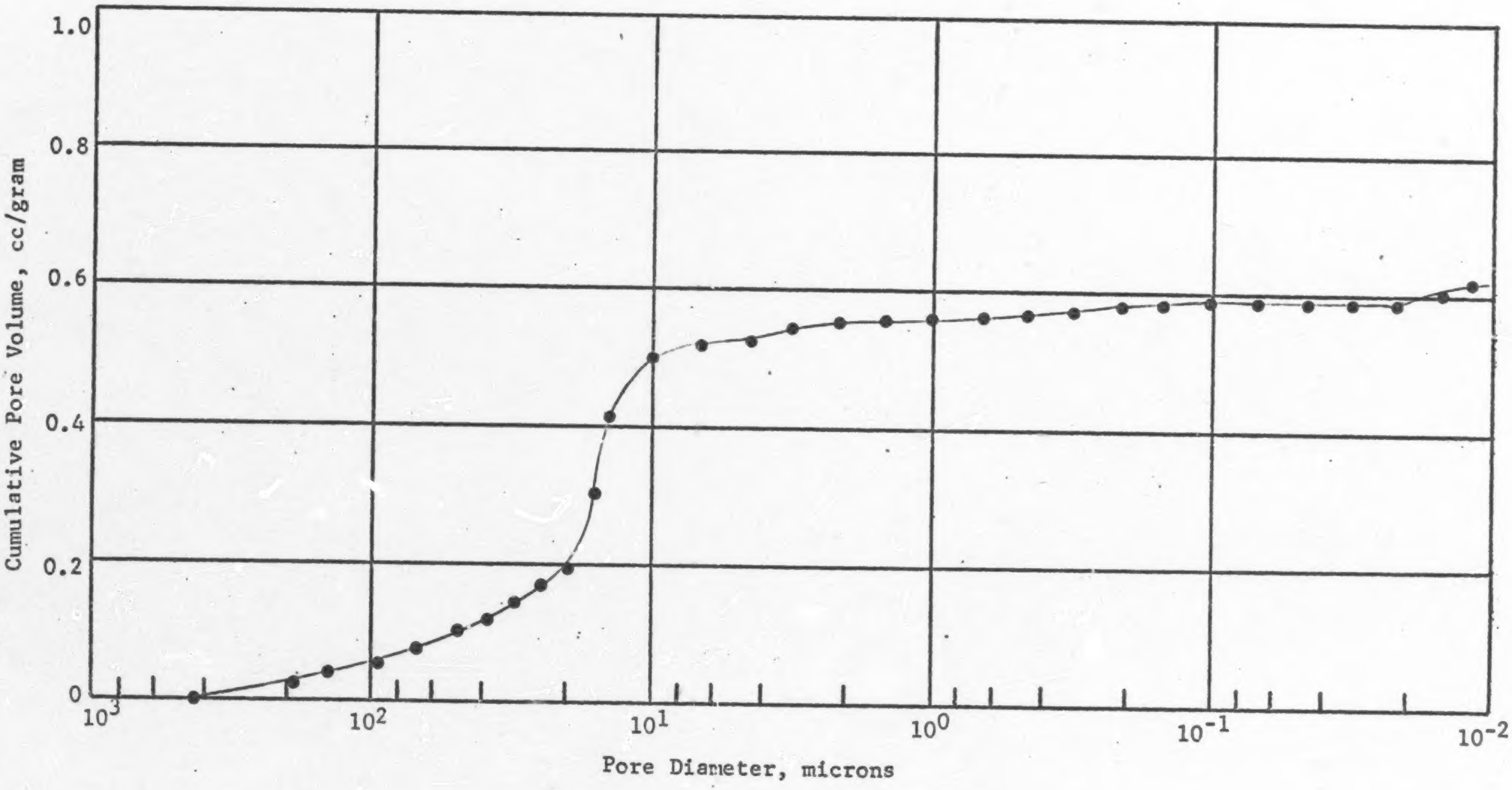

FIGURE C-6. PORE SIZE DISTRIBUTION

Sample No. 106-C

Surface Area - 11.4 m^2/g

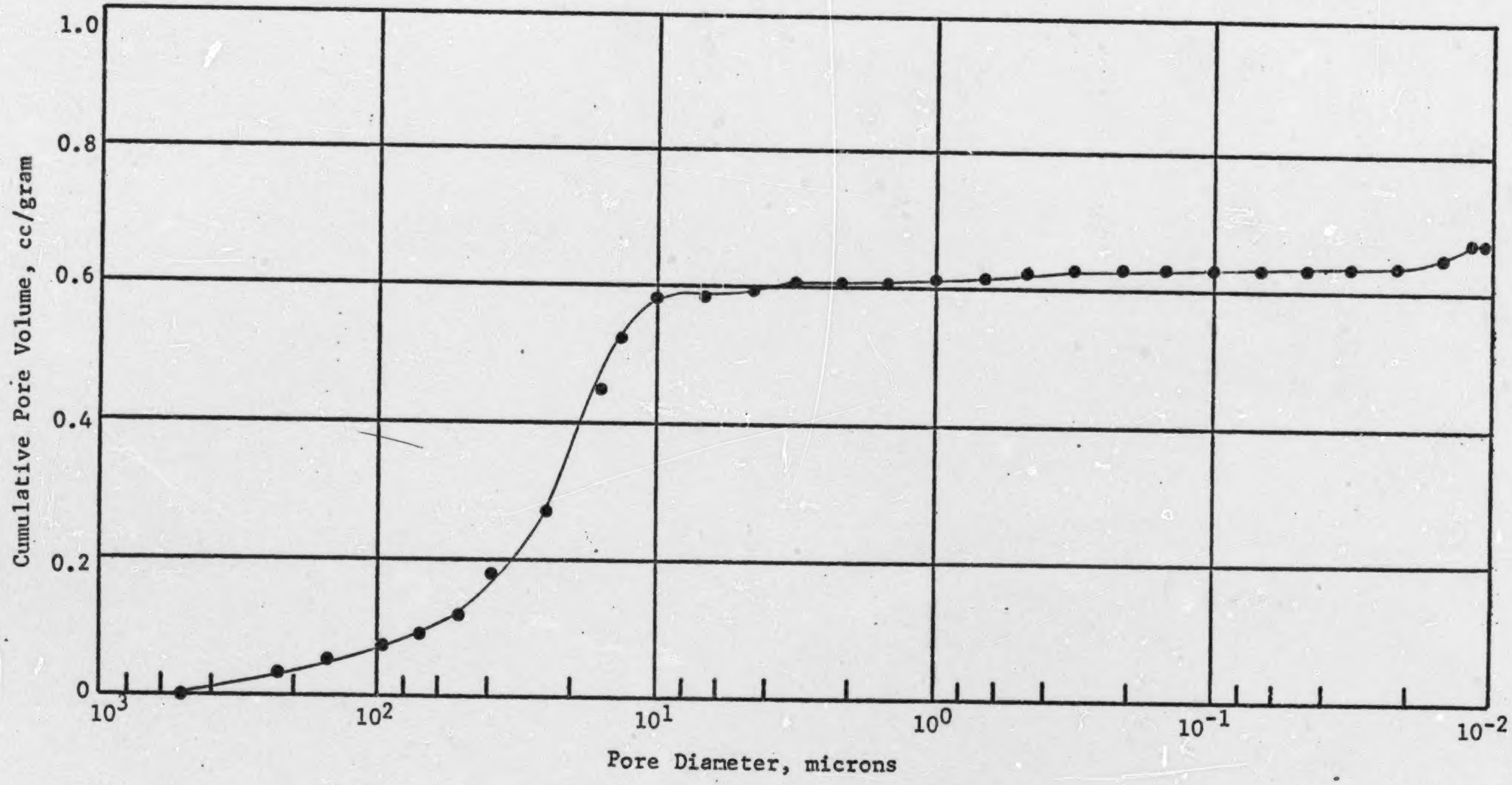

FIGURE C-7. PORE SIZE DISTRIBUTION

Sample No. - 106-D

Surface Area - 20.8 m^2/g

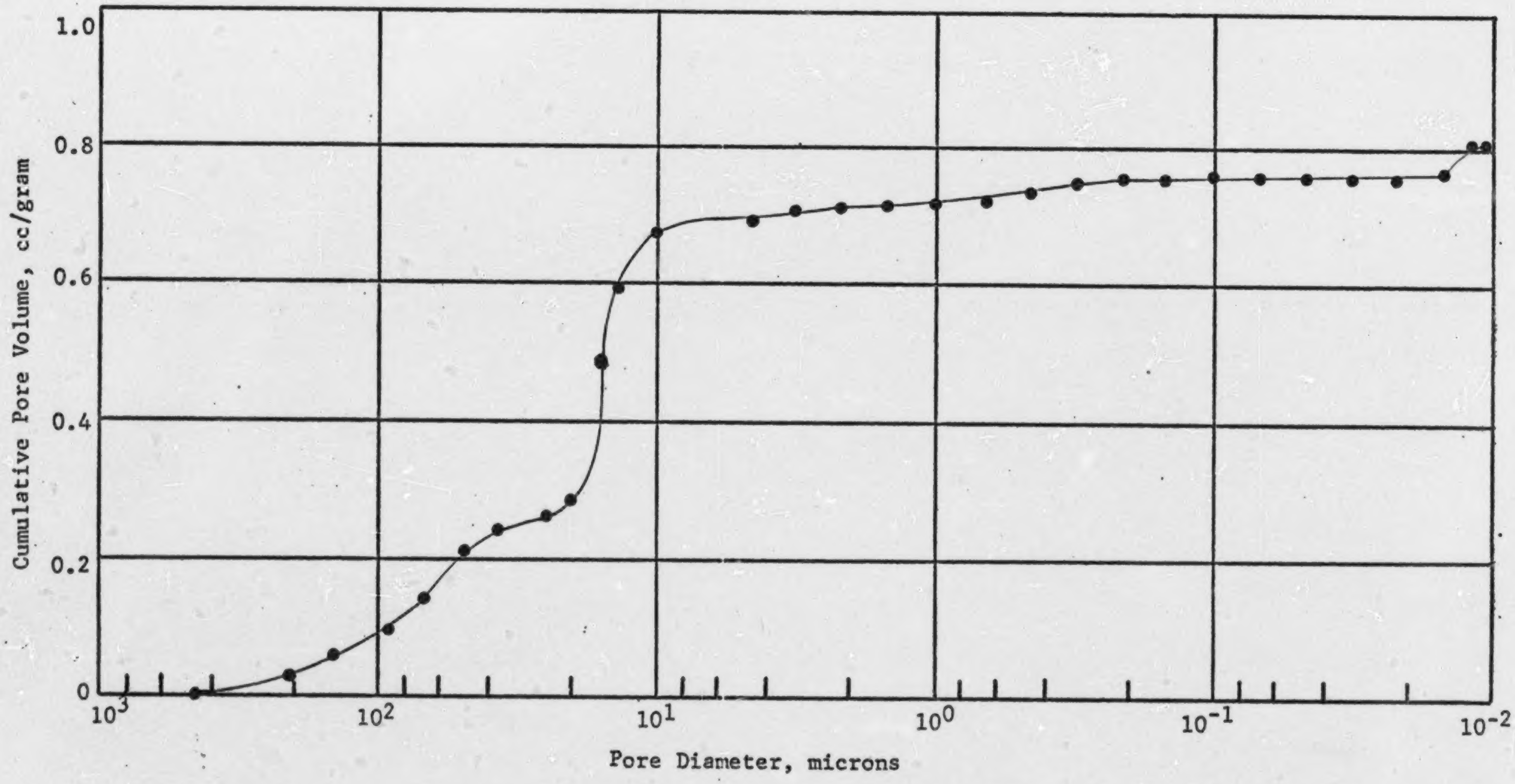

FIGURE C-8. PORE SIZE DISTRIBUTION

Sample No. - 106-E

Surface Area - 12.4 m^2/g

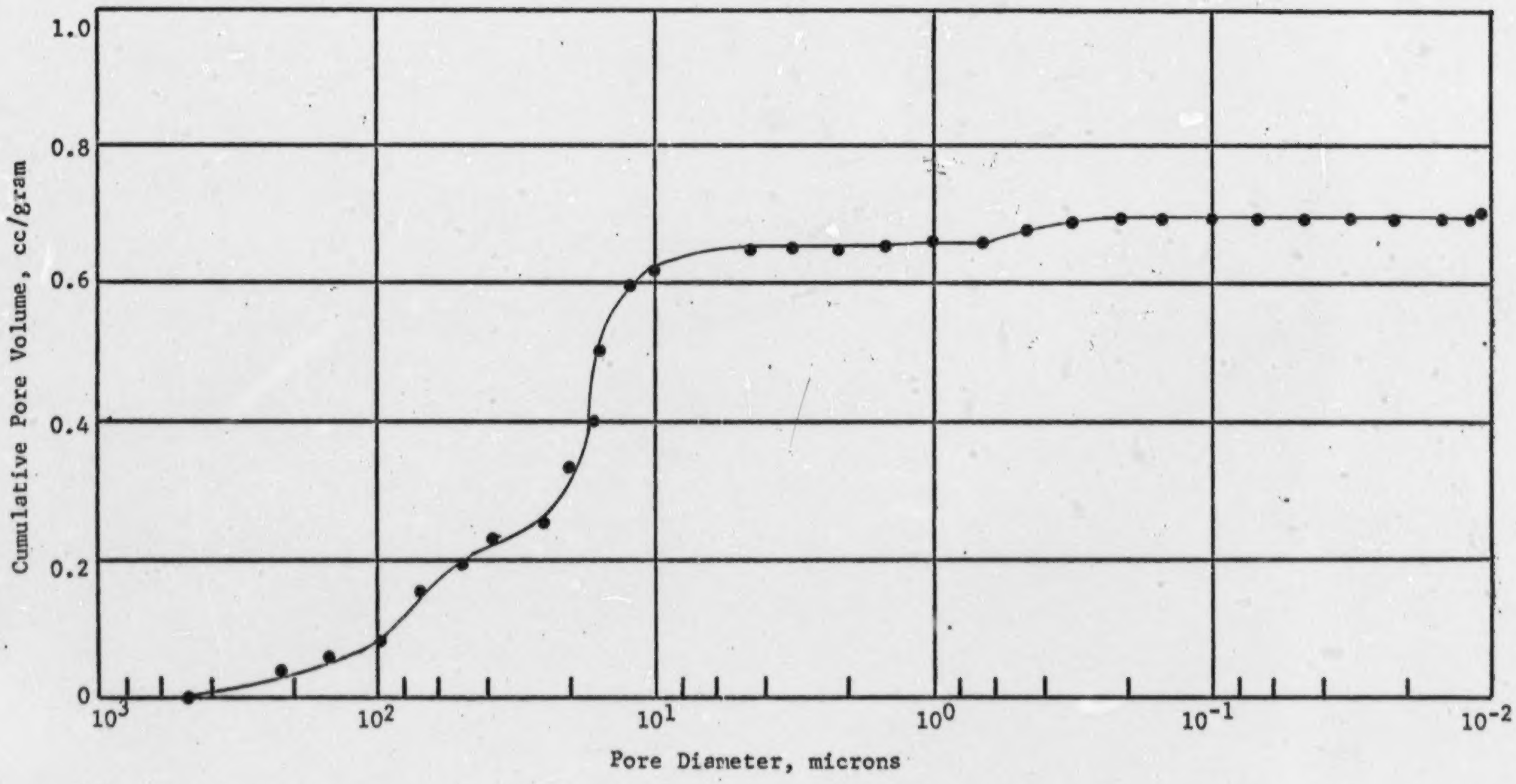

FIGURE C-9. PORE SIZE DISTRIBUTION

Sample No. - 106-F

Surface Area - 3.8 m^2/g

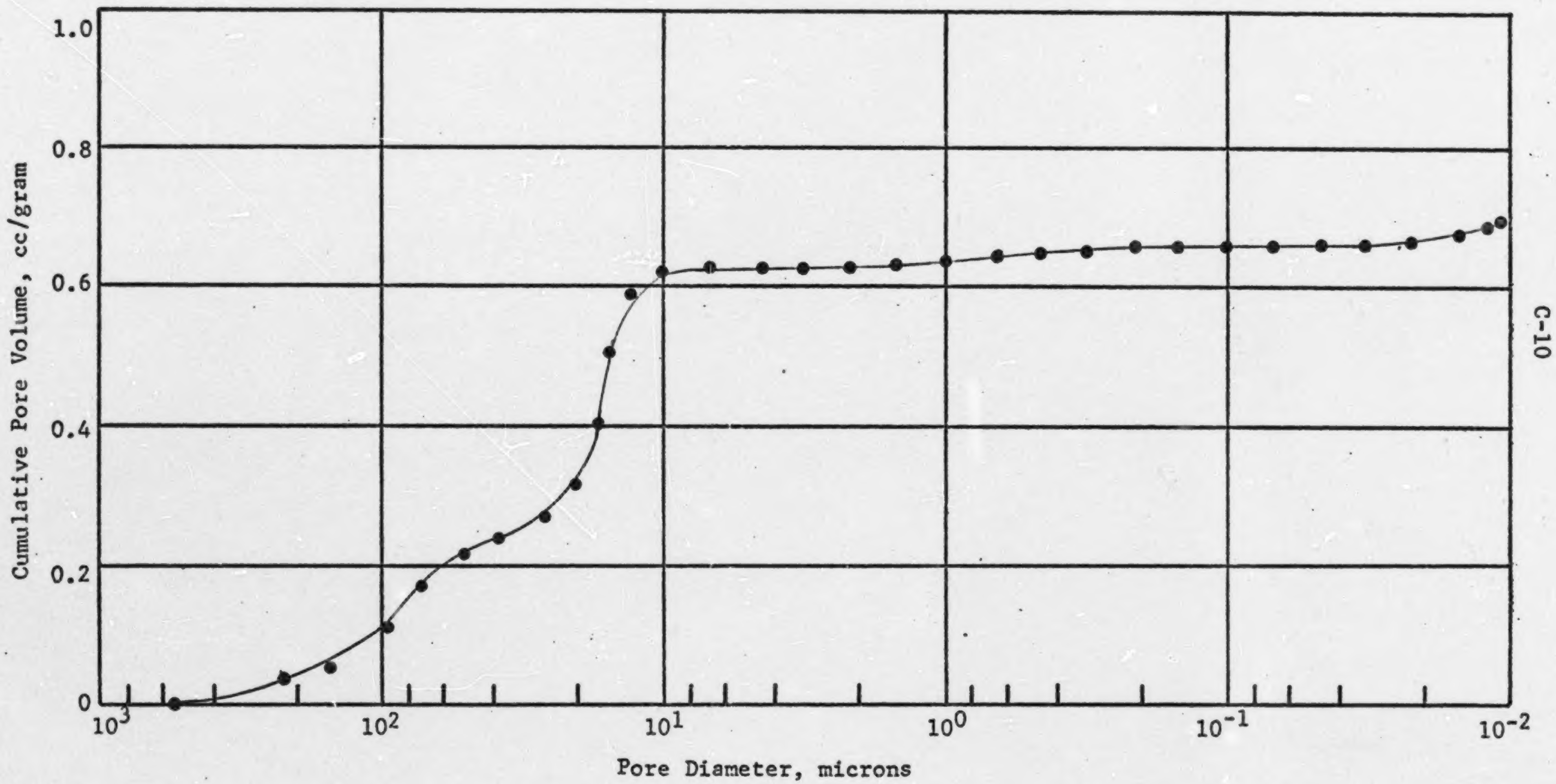

FIGURE C-10. PORE SIZE DISTRIBUTION

APPENDIX D

COMPUTER PROGRAM - CALNOW

Calcination of Limestone Under Simulated Boiler Conditions

```
00100  REAL L,M,MC,NUMT,NUMF
00110  DIMENSIØN PZ(21),PA(21),PB(21),FZ(21),FA(21),FB(21),R(21)
00120  DIMENSIØN ICØUNT(21)
00130  DØUBLE PRECISIØN TZ(21),TA(21),TB(21),TB1,TBI,TBJ1,TC,FUNCTC
00140  CØMMØN L,M,MC,THK,RH02,S2,RHØ1,S1,GASC,PØR,ETA,A,RCDA
00150  FUNCD(PF,TF)=A*(A*PF/8/ETA*3.22E05+2/3.*SQRT(1.5708*3.22E05
00160 & *GASC*(TF+460)/M))
00170  FUNCTC(PF)=(40.4E03/1.987/(24.195-ALØG(PF))-273.)*1.8+32.
00180  FUNCTG(PF)=40.4E03/1.987*1.8/(24.195-ALØG(PF))**2/PF
00190  FUNCSG(TF)=.156+.194E-03*TF-.056E-06*TF**2
00200  FUNCTD(GR,GR2,RF,TE,R1)=(THK*(GR2+2*GR/R1)-GR*RF*FUNCSG(TE))
00210 & /S1/RHØ1
00220  FUNCG2(GR,TD,RF,TE,R1)=-2*GR/R1+(S1*RHØ1*TD+RF*GR*FUNCSG(TE))/THK
00230  FUNCH(T1,T2)=HKG*(.015+.7E-05*(T1+T2))+EPS*SIG*(T1+T2+920.)
00240 & *((T1+460.)**2+(T2+460.)**2)
00250  FUNCPG(RE,RF,TE,PE,RFD,RFG)=-GASC/M/PØR*(TE+460)*RF/FUNCD(PE,TE)
00260 & -(RFD+GASC/M*(TE+460)/PE*RF*(RFG+2*RF/RE))/PØR/3.22E05
00270  FUNCINT(Z1,Z2,Y1,Y2,Y3,X1,X2)=Z1*((Y3*X1/X2-Y1*X2/X1)/(X1+X2)
00280 & -Y2*(X1-X2)/X1/X2)+Z2*((Y3/X2+Y1/X1)/(X1+X2)-Y2/X1/X2)
00290  DATA MULT,TERR,RERR,TGERR,FERR
00300 & /100,1.E-04,1.E-06,1.E-04,1.E-05/
00310  DATA RNE,S2,RHØ2,S1,RHØ1,TØ,EPS,SIG
00320 & /.06,.2,169.,.2,95.,70.,.3,.173E-08/
00330  DATA GASC,ETA,PGAS,THK,RØ,A,L,M,MC
00340 & /555.,.1,76.,.4,1.48E-04,3.28E-08,710.,44.,100./
00350  A=26.24E-08
00360  PRINT,' TNØM,C '
00370  ACCEPT, TNØM,C
00380  HKG=.5/R0*(2.+.37*RNE**.6)
00390   C=C/3600
00400  PØR=RHØ1/RH02
00410  X1=5.5
00420   X2=5.5
00430   TC=FUNCTC(PGAS)
00440  DØ 1000 IX=1,12
00450  X1=X1-MØD(IX+1,2)
00460   X2=X1+IX
00470  TEMP1=TNØM+50*(6-X1)
00480  TEMP2=TNØM+50*(6-X2)
00490  PRINT 3, X1,TEMP1,X2,TEMP2
00500  3 FØRMAT(///' X1=',F4.1,', TGAS=',F9.3,' TØ X2=',F4.1,', TGAS=',
00510 & F9.3/)
00520  IF (X1-5.5) 5,7,7
00530  5 IF (X1+X2-11.5) 7,1000,6
00540  6 DELT=AMIN1(1.2*DTINT,DETC/ABS(TCDB))
00550  GØ TØ 130
00560  7 TIME=0.
00570   XA=X1
00580   TAØ=TØ
00590  TGAS=TNØM+50*(6-XA)
00600   H=FUNCH(TAØ,TGAS)
00610  TDAØ=H*(TGAS-TAØ)*3/RØ/S2/RHØ2
00620  DELT=(TC-TØ)/TDAØ/10
00630  10 TBØ=TAØ+TDAØ*DELT
00640   TIME=TIME+DELT
00650  XB=XA+DELT/C
00660   TGAS=TNØM+50*(6-XB)
```

```
00670  IF (XB-X2) 40,20,20
00680  20 T3600=TIME*3600
00690  PRINT 30, TC,T3600,TBØ
00700  30 FØRMAT(' CALC TEMP(F)=',F9.3,' NØT REACHED AT X2.'/
00710 & ' TIME(SEC)=',F8.4,' PARTICLE TEMP(F)=',F9.3/)
00720  GØ TØ 1000
00730  40 H=FUNCH(TBØ,TGAS)
00740  TDBØ=H*(TGAS-TBØ)*3/RØ/S2/RHØ2
00750  TBT=TAØ+(TDAØ+TDBØ)/2*DELT
00760  IF (ABS(TBT-TBØ)-.001) 60,60,50
00770  50 TBØ=TBT
00780   GØ TØ 40
00790  60 IF (TBT-TC) 70,80,80
00800  70 TAØ=TBT
00810   XA=XB
00820   TDAØ=TDBØ
00830   GØ TØ 10
00840  80 DT=DELT*(TBT-TC)/(TBT-TAØ)
00850  TIME=TIME-DT
00860   XA=XB-DT/C
00870  TGAS=TNØM+50*(6-XA)
00880  R(1)=RØ
00890  KC=1
00900  TCØR=1.
00910  FCØR=1.
00920   J=0
00930   N=0
00940   NØ=0
00950  HA=FUNCH(TC,TGAS)
00960   SHGAS=FUNCSG(.5*(TC+TGAS))
00970  TGJ=HA/THK*(TGAS-TC)/(1.+M/MC*FUNCSG(TC)/L*(TGAS-TC))
00980  FDA=0.
00990   PDA=0.
01000  100 CALL FRØNT(PGAS,PGJ,PDA,PCDA,TC,TGJ,TG2J,TDA,TCDA,FC,FGJ,
01010 & FDA,FCDA,RØ,RCDA)
01020  H=HA-FC*SHGAS
01030  TGST=H/THK*(TGAS-TC)
01040  CALL CØMP(TGST/TGJ-1,TGERR,IND)
01050  GØ TØ (105,120,110), IND
01060  105 TGJ=TGST
01070   GØ TØ 100
01080  110 TGRAT=TGST/TGJ
01090  PRINT 115, TGRAT
01100  115 FØRMAT(' PØØR INIT. CØND. SØLUTIØN, TEMP. GRAD. RATIØ=',F7.4/
)
01110  120 TGJ=TGST
01120   PRINT 125
01130  125 FØRMAT(14X,'AT CALCINATIØN FRØNT:'//'   TIME     X      TGAS'
,
01140 & '     RAD  CALC       TEMP    PRESS   STRESS'/)
01150  PGJRØ=PGJ*RØ/2/51.715
01160  T3600=3600*TIME
01170  PRINT 295, T3600,XA,TGAS,1.,0.,TC,PGAS,PGJRØ
01180  DØ 127 I=1,21
01190  TZ(I)=TC
01200   TA(I)=TC
01210   TB(I)=TC
01220   PZ(I)=PGAS
01230   PA(I)=PGAS
```

```
01240    PB(I)=PGAS
01250   FZ(I)=FC
01260    FA(I)=FC
01270   127 FB(I)=FC
01280   DELT=-RØ/RCDA/MULT
01290    DTB=DELT
01300    DETC=DELT*TCDA
01310   130 TIME=TIME+DELT
01320   IF (RCDA) J=J+1
01330    J1=J+1
01340   KC=KC+1
01350   FCØR=(KC-1.)*FCØR/KC
01360   IF (TIME+.1*DELT-C*(X2-X1)) 133,132,132
01370   132 DTINT=DELT
01380   DELT=DELT-TIME+C*(X2-X1)
01390    TIME=C*(X2-X1)
01400   133 XB=XA+DELT/C
01410    TGAS=TNØM+50*(6-XB)
01420   135 IF (J-2) 136,137,137
01430   136 TB(1)=TA(1)+TDA*DELT
01440   GØ TØ 1383
01450   137 JM1=J-1
01460   QP=1+DELT/DTB
01470   QM=1-DELT/DTB
01480   DØ 138 I=1,JM1
01490   TB(I)=TZ(I)+QP*(QM*(TA(I)-TZ(I))+DELT/JM1*((J-I)*TDØ+(I-1)*TDA))
01500   FB(I)=FZ(I)+QP*(QM*(FA(I)-FZ(I))+DELT/JM1*((J-I)*FDØ+(I-1)*FDA))
01510   PB(I)=PZ(I)+QP*(QM*(PA(I)-PZ(I))+DELT/JM1*((J-I)*PDØ+(I-1)*PDA))
01520   138 CØNTINUE
01530   TB(J)=TA(J)+TDA*DELT
01540   FB(J)=FA(J)+FDA*DELT
01550   PB(J)=PA(J)+PDA*DELT
01560   1383 IF (J-2) 1385,139,139
01570   1385 TDI=2*(TB(1)-TA(1))/DELT-TDA
01580   FDI=2*(FB(1)-FA(1))/DELT-FDA
01590   GØ TØ 1387
01600   139 TDI=FUNCINT(1.,2*DELT,TZ(1),TA(1),TB(1),DTB,DELT)
01610   FB(1)=AMAX1(0.,FB(1))
01620   FDI=FUNCINT(1.,2*DELT,FZ(1),FA(1),FB(1),DTB,DELT)
01630   1387 PDI=0.
01640   140 TB1=TB(1)
01650   H=FUNCH(TB(1),TGAS)-FB(1)*FUNCSG(.5*(TB(1)+TGAS))
01660   TGI1=H/THK*(TGAS-TB(1))
01670   TG2I1=FUNCG2(TGI1,TDI,FB(1),TB(1),R(1))
01680   PØTDØT=(PDI-PB(1)*TDI/(TB(1)+460))/(TB(1)+460)
01690   FGI1=-PØR*M/GASC*PØTDØT-2*FB(1)/R(1)
01700   PGI1=FUNCPG(R(1),FB(1),TB(1),PB(1),FDI,FGI1)
01710   PGØ=PGI1
01720   TDØ=TDI
01730   FDØ=FDI
01740   PDØ=PDI
01750   IF (J-1) 189,189,181
01760   181 DØ 188 I=2,J
01770   TGI=TGI1+TG2I1*(R(I)-R(I-1))
01780   1815 IF (I-J) 182,183,183
01790   182 TDI=FUNCINT(1.,2*DELT,TZ(I),TA(I),TB(I),DTB,DELT)
01800   FDI=FUNCINT(1.,2*DELT,FZ(I),FA(I),FB(I),DTB,DELT)
```

```
01810  PDI=FUNCINT(1.,2*DELT,PZ(I),PA(I),PB(I),DTB,DELT)
01820  GO TO 184
01830  183 TDI=2*(TB(I)-TA(I))/DELT-TDA
01840  FDI=2*(FB(I)-FA(I))/DELT-FDA
01850  PDI=2*(PB(I)-PA(I))/DELT-PDA
01860  184 POTDOT=(PDI-PB(I)*TDI/(TB(I)+460))/(TB(I)+460)
01870  FGI=-POR*M/GASC*POTDOT-2*FB(I)/R(I)
01880  FB(I)=FB(I-1)+(FGI+FGI1)/2*(R(I)-R(I-1))
01890  TG2I=FUNCG2(TGI,TDI,FB(I),TB(I),R(I))
01900  TGI=TGI1+(TG2I1+TG2I)/2*(R(I)-R(I-1))
01910  TBI=TB(I-1)+(TGI+TGI1)/2*(R(I)-R(I-1))
01920  PGI=FUNCPG(R(I),FB(I),TB(I),PB(I),FDI,FGI)
01930  PB(I)=PB(I-1)+(PGI+PGI1)/2*(R(I)-R(I-1))
01940  CALL COMP(TBI-TB(I),TERR,IND)
01950  GO TO (185,187,186),IND
01960  185 TB(I)=TBI
01970   GO TO 1815
01980  186 TMPDIF=TBI-TB(I)
01990  PRINT 1865, I,J,TMPDIF
02000  1865 FORMAT(' POOR SOLUTION AT I=',I5,' J=',I5,
02010 & '  TEMP ERR(F)=',F8.5/)
02020  187 TB(I)=TBI
02030   TG2I1=TG2I
02040  TGI1=TGI
02050  PGI1=PGI
02060  FGI1=FGI
02070  188 CONTINUE
02080  189 IF (RCDA) R(J1)=R(J)+RCDA*DELT
02090  TGJ1=TGI1+TG2I1*(R(J1)-R(J))
02100  TB(J1)=TB(J)+(TGJ1+TGI1)/2*(R(J1)-R(J))
02110  PB(J1)=PB(J)+PGI1*(R(J1)-R(J))
02120  CALL FRONT(PB(J1),PGJ1,PDI,PCDB,TB(J1),TGJ1,TG2J1,TDB,TCDB,
02130 & FB(J1),FGJ1,FDI,FCDB,R(J1),RCDB)
02140  IF (RCDA) R(J1)=R(J)+(RCDA+RCDB)/2*DELT
02150  190 TGJ1=TGI1+(TG2I1+TG2J1)/2*(R(J1)-R(J))
02160  TB(J1)=TB(J)+(TGJ1+TGI1)/2*(R(J1)-R(J))
02170  PB(J1)=PB(J)+(PGJ1+PGI1)/2*(R(J1)-R(J))
02180  PDB=2*(PB(J1)-PA(J))/DELT-PCDA-RCDB*PGJ1
02190  FDB=2*(FB(J1)-FA(J))/DELT-FCDA-RCDB*FGJ1
02200  CALL FRONT(PB(J1),PGJ1,PDB,PCDB,TB(J1),TGJ1,TG2J1,TDB,TCDB,
02210 & FB(J1),FGJ1,FDB,FCDB,R(J1),RCDB)
02220  IF (RCDA) RJ1=R(J)+(RCDA+RCDB)/2*DELT
02230  CALL COMP((RJ1-R(J1))/R(1),RERR,IND)
02240  GO TO (191,192,1915), IND
02250  191 R(J1)=RJ1
02260  GO TO 190
02270  1915 NO=NO+1
02280  192 FBJ1=FB(J)+(FGJ1+FGI1)/2*(R(J1)-R(J))
02290  FDIF=FBJ1-FB(J1)
02300  IF (RCDA) 193,196,196
02310  193 TDIF=TB(J1)-FUNCTC(PB(J1))
02320  GO TO 198
02330  196 TBJ1=TA(J1)+(TDB+TDA)/2*DELT
02340  197 TDIF=TBJ1-TB(J1)
02350  198 IF (ABS(TDIF)-TERR) 1985,1985,199
02360  1985 IF (ABS(FDIF)-FERR*FC) 260,260,199
02370  199 N=N+1
```

```
GØ TØ (1992,1994,1996,1998), MØD(N-1,4)+1
1992 TDIF1=TDIF
FDIF1=FDIF
TB(1)=TB(1)-TDIF1*TCØR
GØ TØ 1383
1994 TDIF2=TDIF
FDIF2=FDIF
TB(1)=TB(1)+TDIF1*TCØR
FB(1)=FB(1)-FDIF1*FCØR
GØ TØ 1383
1996 TDIF3=TDIF
FDIF3=FDIF
DENØM=(TDIF2-TDIF1)*(FDIF3-FDIF1)-(TDIF3-TDIF1)*(FDIF2-FDIF1)
NUMT=TDIF3*FDIF1-TDIF1*FDIF3
NUMF=TDIF1*FDIF2-TDIF2*FDIF1
TB(1)=TB(1)-NUMT/DENØM*TDIF1*TCØR
FB(1)=FB(1)+(1-NUMF/DENØM)*FDIF1*FCØR
GØ TØ 1383
1998 IF (N-20) 199,200,200
200 IF (NØ-10) 202,202,220
202 IF (RCDB+.01*RCDA) 210,203,203
203 DELT=DELT*(-RCDA)/(RCDB-RCDA)
TIME=TIME+RCDB/RCDA*DELT
 GØ TØ 215
210 DELT=DELT/1.4
TIME=TIME-.4*DELT
215 NØ=NØ+1
 N=0
GØ TØ 133
220 T3600=3600*TIME
PRINT 225, T3600,TDIF,RCDA,RCDB
225 FØRMAT(' PØØR SØLUTIØN, TIME=',F7.4,' TEMP ERR=',F7.4/
& ' RCDA=',E10.3,' RCDB=',E10.3)
TICØ=3600*C*(X2-X1)
PRINT 298, TICØ
GØ TØ 1000
260 N=0
NØ=0
273 DTB=DELT
 XA=XB
IF (TCDB) 275,277,275
275 DELT=AMIN1(1.4*DELT,DETC/ABS(TCDB))
GØ TØ 280
277 DELT=1.4*DELT
280 PCDA=PCDB
 TCDA=TCDB
 FCDA=FCDB
RCDA=AMIN1(RCDB,0.)
TDA=TDB
FDA=FDB
PDA=PDB
DØ 290 I=1,J1
TZ(I)=TA(I)
 TA(I)=TB(I)
 PZ(I)=PA(I)
 PA(I)=PB(I)
 FZ(I)=FA(I)
 290 FA(I)=FB(I)
 293 PGR=PGJ1*R(J1)/2/51.715
 RJR=100*(1.-(R(J1)/RO)**3)
 RJRO=R(J1)/RO
 T3600=3600*TIME
 PRINT 295,T3600,XB,TGAS,RJRO,RJR,TB(J1),PB(J1),PGR
 295 FORMAT(F7.4,F6.2,F10.3,F8.4,F6.2,F10.3,F9.1,F9.1)
 IF (ABS(RCDB)-.01*RCDA) 297,297,299
 297 TICO=3600*C*(X2-X1)
 PRINT 298, TICO
 298 FORMAT(' CALCINATION COMPLETED. TIME AT X2=',F7.4,' SEC')
 GO TO 300
 299 IF (TIME-C*(X2-X1)) 410,300,300
 300 PRINT 302
 302 FORMAT(/'      RAD       TEMP     PRESS   STRESS'/)
 IRO=0
 DO 308 I=1,J1
 IR=5*(R(1)-R(I))/(R(1)-R(J1))
 IF (IR-IRO) 308,306,306
 306 RIRO=R(I)/RO
 IF (I-2) 3062,3066,3064
 3062 STRESS=PGO*RO/103.43
 GO TO 3068
 3064 IF (I-J) 3066,3066,3065
 3065 STRESS=PGJ1*R(J1)/103.43
 GO TO 3068
 3066 STRESS=FUNCINT(1.,0.,PB(I+1),PB(I),PB(I-1),R(I)-R(I+1),
& R(I-1)-R(I))*R(I)/103.43
 3068 PRINT 307, RIRO,TB(I),PB(I),STRESS
 307 FORMAT(F8.4,F10.3,F9.1,F9.1)
 IRO=IRO+1
 308 CONTINUE
 GO TO 1000
 410 IF (J1-20) 130,420,420
 420 IO=2
 DO 440 I=2,17
 IR=10*(R(1)-R(I))/(R(1)-R(18))
 IF (IR-IO+1) 440,430,430
 430 ICOUNT(IO)=I
 IO=IO+1
 440 CONTINUE
 DO 450 I=18,J1
 450 ICOUNT(I-8)=I
 J=J-8
 J1=J+1
 DO 460 I=2,J1
 IO=ICOUNT(I)
 PZ(I)=PZ(IO)
 PA(I)=PA(IO)
 FZ(I)=FZ(IO)
 FA(I)=FA(IO)
 TZ(I)=TZ(IO)
 TA(I)=TA(IO)
 460 R(I)=R(IO)
 GO TO 130
 1000 CONTINUE
 STOP
```

```
03520 END
03530 SUBRØUTINE CØMP(RT,ERR,IND)
03540 IF (ABS(RT)-ERR) 50,50,20
03550 20 IF (I-20) 40,40,30
03560 30 IND=3
03570  I=0
03580  RETURN
03590 40 IND=1
03600  I=I+1
03610  RETURN
03620 50 IND=2
03630  I=0
03640 RETURN
03650  END
03660 SUBRØUTINE FRØNT(P,PG,PD,PCD,T,TG,TG2,TD,TCD,F,FG,FD,FCD,R,RD)
03670 REAL L,M,MC
03680 CØMMØN L,M,MC,THK,RHØ2,S2,RHØ1,S1,GASC,PØR,ETA,A,RCDA
03690 TABS=T+460.
03700  TST=0.
03710 D=A*(A*P/8/ETA*3.22E05+2/3.*SQRT(1.5708*3.22E05*GASC*TABS/M))
03720 DTCDP=40400/1.987*1.8/(24.195-ALØG(P))**2/P
03730 SG=.156+.194E-03*T-.056E-06*T**2
03740 5 C1=(RHØ2*GASC*TABS/MC/PØR-P)/D*(1+TST)
03750 C3=(3*L/R/S2/DTCDP+FD/3.22E05/PØR)/C1
03760 C4=(3*THK*TG/R/S2/RHØ2/DTCDP-PD)/C1
03770 C5=(C3/2)**2+C4
03780 IF (C5) 10,20,20
03790 10 RD=0.
03800 GØ TØ 30
03810 20 RD=C3/2-SQRT(C5)
03820 IF (RCDA) 30,25,25
03830 25 RD=AMIN1(0.,RD)
03840 30 F=RD*(-M/MC*RHØ2+PØR*M/GASC*P/TABS)
03850 PG=RD/D*(GASC*TABS*RHØ2/MC/PØR-P)*(1+TST)-FD/PØR/3.22E05
03860 TCD=3/R/S2*(THK*TG/RHØ2+L*RD)
03870 TD=TCD-RD*TG
03880 PCD=PD+RD*PG
03890 FG=-2*F/R-PØR*M/GASC/TABS*(PD-P*TD/TABS)
03900 TSTA=D/P*(FG+2*F/R)/3.22E05
03910 IF (ABS(TSTA-TST)-.0001) 50,50,40
03920 40 TST=TSTA
03930  GØ TØ 5
03940 50 FCD=FD+RD*FG
03950 THD1=THK/RHØ1/S1
03960  THDG=THK/RHØ2/SG*MC/M
03970 TG2=TD/THD1-TG*(2/R+RD/THDG)
03980 RETURN
03990  END
```